Upgrading of bioethanol: kinetic modeling of the catalytic conversion on zeolites

Brecht Laforce

Promotoren: dr. Vladimir Galvita, prof. dr. ir. Joris Thybaut
Begeleider: Kristof Van der Borght

Masterproef ingediend tot het behalen van de academische graad van
Master in de ingenieurswetenschappen: chemische technologie

Vakgroep Chemische Proceskunde en Technische Chemie
Voorzitter: prof. dr. ir. Guy Marin
Faculteit Ingenieurswetenschappen en Architectuur
Academiejaar 2012-2013

UNIVERSITEIT
GENT

UNIVERSITEIT GENT

Laboratorium voor Chemische Technologie

Vakgroep Chemische Proceskunde en Technische Chemie

Laboratorium voor Chemische Technologie

Directeur: Prof. Dr. Ir. Guy B. Marin

Verklaring in verband met de toegankelijkheid van de scriptie

Ondergetekende, Brecht Laforce.....

afgestudeerd aan de UGent in het academiejaar 2012-2013 en auteur van de scriptie met als titel: Upgrading of bio-ethanol: kinetic modeling of the catalytic conversion on zeolites .....

.....

.....

De auteur(s) geeft(geven) de toelating deze masterproef voor consultatie beschikbaar te stellen en delen van de masterproef te kopiëren voor persoonlijk gebruik.

Elk ander gebruik valt onder de beperkingen van het auteursrecht, in het bijzonder met betrekking tot de verplichting de bron uitdrukkelijk te vermelden bij het aanhalen van resultaten uit deze masterproef.

(Datum)

(Handtekening)

Dankwoord

Aan het slot van dit thesis jaar, is het juiste moment gekomen om de mensen door wie dit werk mogelijk gemaakt is te bedanken voor hun steun en ondersteuning tijdens deze drukke, maar vooral boeiende maanden.

Vooreerst wens ik professor Marin te bedanken voor het opvolgen van mijn thesiswerk.

Next, my acknowledgements go to Vladimir Galvita for the valuable moments of discussion throughout the year, which each time led to new insights.

Ook professor Thybaut heeft mijn dankbaarheid verdiend. Meermaals hadden we interessante en leerrijke gesprekken over de reactie mechanismen en het kinetisch modelleren. Telkens weer zorgde dit voor de nodige inspiratie om verder te gaan.

Ik wil ten zeerste mijn begeleider, Kristof Van der Borght, bedanken. Het volledige jaar stond hij er steeds wanneer ik technische of theoretische ondersteuning nodig had. Met zijn nooit afnemende energie en enthousiasme hielp hij mee de uitdagingen tot een goed einde te brengen.

Speciale vermelding verdienen Kenneth Toch en Julie Timmerman, wiens kinetisch model voor ethyleen oligomerizatie een uitgangspunt vormde voor het SEMK model.

Ik wens ook de technische staf van het LCT te bedanken voor de ondersteuning bij het sleutelen aan de meetopstelling.

Heel wat doctoraatstudenten en mede-thesisstudenten hebben geholpen door het bieden van nieuwe invalshoeken en standpunten ten opzichte van het thesisonderzoek. Om zeker niemand te vergeten en zo onrecht aan te doen, waag ik me er niet aan iedereen hier op te sommen.

Ook moet ik mijn ouders uit de grond van mijn hart bedanken voor de steun gedurende het jaar. Dankzij hen was het mogelijk mijn studies aan te vatten en tot een goed einde te brengen.

Tot slot een woord van dank voor mijn vrienden bij wie ik steeds terecht kon om even te ontspannen. De boog kan ten slotte niet altijd gespannen staan.

Overzicht

Upgrading of bioethanol: kinetic modeling of the catalytic conversion on zeolites

Brecht Laforce

Promotoren: dr. Vladimir Galvita, prof. dr. ir. Joris Thybaut
Begeleider: Kristof Van der Borght

Masterproef ingediend tot het behalen van de academische graad van Master in de ingenieurswetenschappen: chemische technologie

Vakgroep Chemische Proceskunde en Technische Chemie
Voorzitter: prof. dr. ir. Guy Marin
Faculteit Ingenieurswetenschappen en Architectuur
Academiejaar 2012-2013

Kernwoorden: Micro-kinetic modeling, zeolite catalysis, conversion of ethanol

Upgrading of bio-ethanol: Kinetic Modelling of the Catalytic Conversion on Zeolites

Brecht Laforce

Coach: ir. Kristof Van der Borght

Supervisor(s): dr. Vladimir Galvita, prof. dr. ir. Joris Thybaut

Abstract: In this article, a study of the catalytic conversion of ethanol on zeolites is performed. This process has two reaction regimes: dehydration of ethanol and further conversion to higher hydrocarbons. Several zeolitic catalysts and post-synthesis modification methods are evaluated. For the best catalyst, HZSM-5 (Si/Al=15), an experimental dataset (263 data points) is constructed on a lab-scale tubular reactor which is used for (single-event) micro-kinetic modeling. The dehydration model yields significant parameters and an accurate calculation of the outlet flow rate. A model for conversion to higher hydrocarbons is constructed.

Keywords: zeolite catalysis, ethanol, micro-kinetic modeling, single-event

I. Introduction

Declining oil-reserves (often located in politically unstable regions) triggered the search for alternative sources for fuels and chemicals. Environmental considerations focussed this research on renewable sources. In the field of renewable chemistry, ethanol is an interesting compound. It is a platform molecule for many bio-based chemicals and fuels and can be produced from a multitude of crops. Several authors have reported on the conversion of ethanol over zeolitic catalysts. [1-3] In this work, experiments on HZSM-5 will be performed and used to construct a micro-kinetic model for the conversion of ethanol on zeolites for both ethanol dehydration and further conversion to higher hydrocarbons.

II. Procedures

A. *Experimental work*

The HZSM-5 catalysts are from Zeolyst. These zeolites are calcinated in air at 550°C to bring them in the protonated form. The modified HZSM-5 catalysts are synthesized by the Centre for Surface Chemistry and Catalysis (KU Leuven) and the Solid State Sciences department of Ghent University.

The catalysts are characterized using NH_3-TPD and N_2-adsorption. The zeolite properties are given in Table 1.

Table 1 Zeolite properties (modified zeolites based on Si/Al=40)

	Brøndsted acid site density (mmol/g)	BET surface area (m^2/g)	Pore volume (ml/g)	
			Micro	Meso
ZSM-5 (Si/Al=15)	0.433	336	0.130	0.111
Parent ZSM-5 (Si/Al=40)	0.264	361	0.162	0.066
Desil. ZSM-5	0.219	370	0.132	0.363
Al-ALD ZSM-5	0.179	336	0.116	0.317

Experiments are performed on a lab-scale, packed bed, tubular reactor. Thermal mass flow controllers are used to regulate the gas flows and a coriolis mass flow controller for the liquid feed, which is vaporized before being fed to the reactor. Tracing prevents condensation in the setup. A Chrompack CP-9003 gas chromatograph is used to analyze the reactor outlet. The absence of transport limitations is verified. [4]

B. *(Single-event) Micro-kinetic modelling*

Parameter estimation is performed with the commercially available program *AthenaVisualStudio*. Outlet flow rates for the packed bed reactor are computed via a pseudo-homogeneous, 1D isothermal and isobaric plug flow reactor model with neglected radial and axial diffusion. The axial flow profile for component j through the reactor can then be expressed as:

$$\frac{dF_j}{dW} = R_j$$

With W the catalyst weight, F_j the molar outlet flow of component j and R_j the production rate of j. Parameter estimation is done via non linear regression using the least-squares methodology.

The model for the conversion to higher hydrocarbons uses the single event approach to limit the number of parameter estimations. [5] In-house developed software will be used for reaction network generation, simulation and parameter estimation of this model.

III. Catalyst Screening

The experimental study shows HZSM-5 with Si/Al=15 has the highest activity towards ethanol dehydration. Desilication of HZSM-5 has no effect on the dehydration reaction (Figure 1).

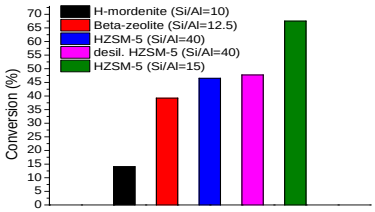

Figure 1 X_{EtOH} on different catalysts (230°C, 6.5$kg_{cat} \cdot s \cdot mol_{EtOH}^{-1}$ 20 kPa EtOH)

A clear distinction between the dehydration regime and the conversion to higher hydrocarbons exists (Figure 2). All ethanol is converted to ethylene before the offset of conversion to higher hydrocarbons. Based on this observation, ethylene is considered as reactant for the latter reaction.

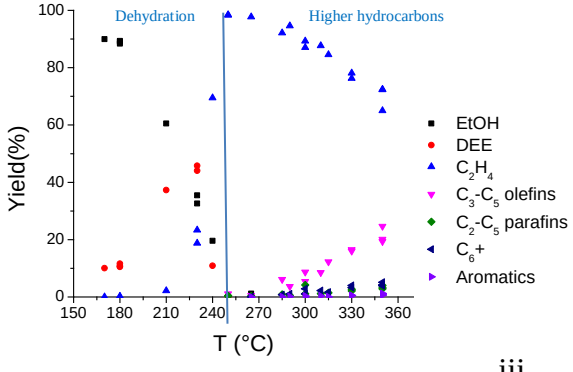

Figure 2 Hydrocarbon yield as a function of T at 20kPa EtOH and 10$kg_{cat} \cdot s \cdot mol_{EtOH}^{-1}$

IV. ETHANOL DEHYDRATION

Reaction with DEE yields EtOH and ethylene, co-feeding ethylene and water did not cause ethylene conversion. Reaction from DEE to ethylene and ethanol is added to the reaction network.

Several micro-kinetic models are constructed. A Langmuir-Hinschelwood mechanism proved to yield the best model prediction. Four adsorption steps and three surface reactions are considered:

$$EtOH^* \xrightarrow{k_1} C_2H_4{}^* + H_2O_g$$
$$2EtOH^* \xrightarrow{k_2} DEE^* + H_2O^*$$
$$DEE^* \xrightarrow{k_3} C_2H_4{}^* + EtOH_g$$

Parameter estimation is performed for the adsorption coefficient of DEE and the three reaction rate coefficients. The model shows a good fit to the experimental results (Figure 3).

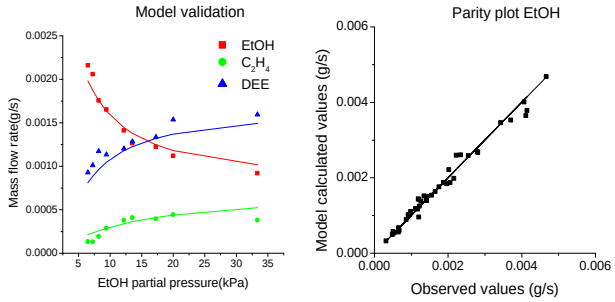

Figure 3 Experiments and model at 230°C and 6.5$kg_{cat} \cdot s \cdot mol^{-1}_{EtOH}$

V. CONVERSION TO HIGHER HYDROCARBONS

Between 300°C and 350°C, light olefins are the main products from the conversion of ethanol on zeolites. In the light olefins lump, butenes are the most abundant components, followed by propylene and pentene. Paraffin and aromatic formation is negligible under these conditions (Figure 4).

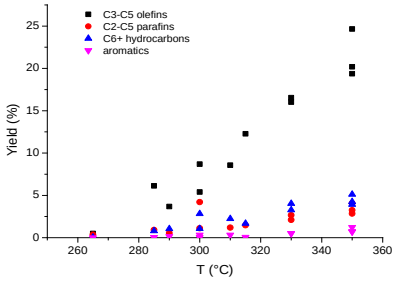

Figure 4 Product yield as function of T (W_{cat}/F^0=10 $kg_{cat}.s.mol_{EtOH}^{-1}$, p_{EtOH}=20kPa)

The olefins are formed in thermodynamic equilibrium within their lump (Figure 5). This indicates the reactions forming these species have a larger time scale than the isomerization reactions.

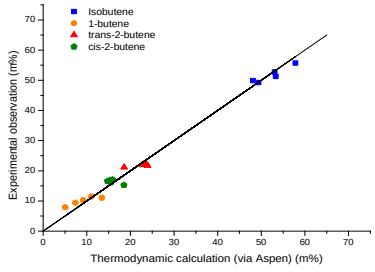

Figure 5 Butene-lump in thermodynamic equilibrium: EtOH conversion 5-50%

The total reactor outlet composition is not in thermodynamic equilibrium. This is demonstrated in Figure 6, where the light olefin lumps are plotted in the thermodynamic and experimental ratio. Propylene is formed to a larger and pentene to a smaller extent than thermodynamically calculated.

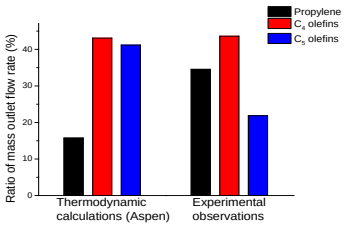

Figure 6 Thermodynamic calculation of the equilibrium and experimental observations

Feeding ethylene to the reactor at the same reaction conditions as ethanol ($p_{ethylene}$, W/F and T) gives a higher conversion. Adding water to the ethylene feed has no effect on the reaction.

A reaction network for the conversion to higher hydrocarbons is constructed. Based on the experimental observations, paraffin and aromatic formation are omitted from the model.

In literature, it is debated whether the ethyl carbenium- or ethoxy-ion is the active species for the reaction. In this work, carbenium ions are considered. Due to the high stability of ethoxy ions, they are presumably not very reactive. Primary carbenium ions are less stable than secondary or tertiary. The primary ethyl- and butyl-carbenium ions are added to the reaction network. The generation of the complete reaction network is performed with ReNeGeP, in-house developed software of the LCT. A maximal carbon number of 9 is implemented. The generated reaction network (Table 2) shows good resemblance to the experimentally obtained reaction products.

Table 2 Reaction network generated by ReNeGeP

Elementary Reaction type/Component	*Number*
Protonation /deprotonation	149
Hydride shift	389
Methyl shift	62
PCP branching	304
Oligomerization	41
β-scission	21
Olefins	104
Carbenium ions	80

The SEMK model is constructed based on the reaction network. At the LCT, codes on the oligomerization of ethylene over bifunctional metal/acid catalysts exist. Adaptations to these codes are performed. Primary carbenium ions and their reactions are added. The alkylation reaction between a primary carbenium ion and a primary olefin is important, since the reaction between an ethyl carbenium ion and ethylene is the first step in the formation of higher hydrocarbons.

VI. CONCLUSIONS

A kinetic dataset is obtained on the conversion of ethanol over zeolites. HZSM-5 with Si/Al=15 has the highest ethanol conversion of the tested catalysts. Desilication of HZSM-5 does not alter its catalytic properties at the experimental conditions of this study. A micro-kinetic model for dehydration is constructed, which gives good model calculations.

The single-event micro-kinetic model for the conversion of ethylene has been constructed. Further improvement to the computer code is necessary.

REFERENCES

1. Madeira, F.F., et al., *Ethanol transformation over HFAU, HBEA and HMFI zeolites presenting similar Brønsted acidity.* Applied Catalysis A: General, 2009. **367**(1–2): p. 39-46.
2. Gayubo, A.G., et al., *Kinetic Modelling of the Transformation of Aqueous Ethanol into Hydrocarbons on a HZSM-5 Zeolite.* Industrial & Engineering Chemistry Research, 2001. **40**(16): p. 3467-3474.
3. Stevens, S., *Transformation of bioethanol into hydrocarbons on modified ZSM-5*, in *Laboratory of Chemical Technology*2012, University of Ghent: Ghent. p. 98.
4. Berger, R.J., et al., *Eurokin. Chemical Reaction Kinetics in Practice.* CATTECH, 2001. **5**(1): p. 36-60.
5. Froment, G.F., *Kinetic modeling of acid-catalyzed oil refining processes.* Catalysis Today, 1999. **52**(2–3): p. 153-163.

Upgraden van bio-ethanol: Kinetisch Modelleren van de katalytische omzetting door zeolieten

Brecht Laforce

Coach: ir. Kristof Van der Borght

Supervisor(s): dr. Vladimir Galvita, prof. dr. ir. Joris Thybaut

Abstract: ***In dit artikel wordt een studie over de katalytische conversie van ethanol door zeolieten uitgevoerd. Bij het proces zijn er twee reactie-regimes: dehydratie van ethanol en de verdere omzetting naar hogere koolwaterstoffen (KWS). Verscheidene zeoliet katalysatoren en post-synthese modificatie technieken worden geëvalueerd. Met de beste katalysator, HZSM-5 (Si/Al=15), wordt op een labo- buisreactor een experimentele dataset (263 meetpunten) opgebouwd voor (single-event) micro-kinetisch modelleren. Het dehydratie model geeft significante parameters en een accurate berekening van de uitlaat stromen. Er is tevens een model opgebouwd voor de conversie naar hogere KWS.***

Sleutelwoorden: ***zeoliet katalyse, ethanol, micro-kinetisch modelleren, single-event***

I. Inleiding

De afnemende oliereserves (vaak in politiek onstabiele streken) hebben een zoektocht naar alternatieve bronnen voor chemicaliën en brandstoffen op gang gebracht. Door milieubewuste overwegingen ligt de focus op hernieuwbare bronnen. Ethanol is een interessante verbinding op het vlak van hernieuwbare chemie. Het vormt een platform molecule voor heel wat verbindingen en kan via heel wat methodes geproduceerd worden. Meerdere auteurs rapporteerden over de katalytische omzetting van ethanol met zeolieten. [1-3] In dit werk worden experimenten uitgevoerd op ZSM-5. Deze zullen gebruikt worden om een micro-kinetisch model op te stellen voor dehydratie van ethanol en de verdere omzetting naar hogere KWS.

II. Procedures

A. *Experimenteel luik*

De HZSM-5 katalysatoren van Zeolyst worden gecalcineerd in lucht op 550°C om de geprotoneerde vorm te verkrijgen. De gemodificeerde HZSM-5 katalysatoren zijn gesynthetiseerd door het Centre for Surface Chemistry and Catalysis (KU Leuven) en het Solid State Sciences departement van de Universiteit Gent.

De katalysatoren worden gekarakteriseerd via NH_3-TPD en N_2-adsorptie. Hun eigenschappen worden gegeven in Tabel 1.

Tabel 1 Zeoliet eigenschappen (de gemodificeerde vormen zijn gebaseerd op Si/Al=40)

	Densiteit Brøndsted zure sites (mmol/g)	BET oppervlakte (m^2/g)	Porie volume (ml/g)	
			Micro	Meso
ZSM-5 (Si/Al=15)	0.433	336	0.130	0.111
Parent ZSM-5 (Si/Al=40)	0.264	361	0.162	0.066
Desil. ZSM-5	0.219	370	0.132	0.363
Al-ALD ZSM-5	0.179	336	0.116	0.317

De experimenten gebeuren op een labo-buisreactor met gepakt bed. Thermische massadebietregelaars regelen de gasstromen en een coriolis massadebietregelaar de vloeistoffen. Deze worden verdampt voor ze de reactor binnentreden. Tracing voorkomt condenseren in de setup. De reactieproducten worden geanalyseerd met een Chrompack CP-9003 gas chromatograaf. Er is gecontroleerd dat geen transportlimiteringen optreden. [4]

B. *(Single-event) Micro-kinetisch modelleren*

Parameter schatting wordt uitgevoerd met het commercieel beschikbare programma *AthenaVisualStudio*. Uitstroomdebieten van de reactor worden berekend via een pseudo-homogeen, 1D isotherm en isobaar propstroom reactor model, met verwaarloosde radiale en axiale diffusie. Het axiale stromingsprofiel voor component j in de reactor kan dan als volgt uitgedrukt worden:

$$\frac{dF_j}{dW} = R_j$$

Met: W katalysator massa, F_j molair uitlaatdebiet van component j en R_j productiesnelheid van j. Parameter schatting gebeurt via niet-lineaire regressie m.b.v. de kleinste kwadraten methode.

Het model voor de vorming van hogere KWS gebruikt de single-event benadering om het aantal parameters te verkleinen. [5] In-house ontwikkelde software wordt gebruikt voor het opstellen van het reactie netwerk, het simuleren en de parameterschatting van dit model.

III. Katalysator screening

De experimentele studie toont aan dat HZSM-5 met Si/Al=15 de hoogste activiteit heeft voor dehydratie. Desilicatie van HZSM-5 heeft geen effect op de dehydratie reactie (Figuur 1).

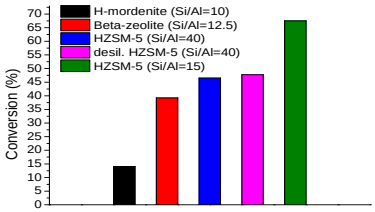

Figuur 1 X_{EtOH}, verschillende katalysators (230°C, 6.5kg_{kat} · s · mol^{-1}_{EtOH} 20 kPa EtOH)

Er bestaat een duidelijk onderscheid tussen het dehydratie regime en de verdere omzetting naar hogere KWS (Figuur 2). Alle ethanol is omgezet naar ethyleen voor de reactie naar hogere KWS begint. Gebaseerd op deze waarneming wordt ethyleen beschouwd als het reactant voor de omzetting naar hogere KWS.

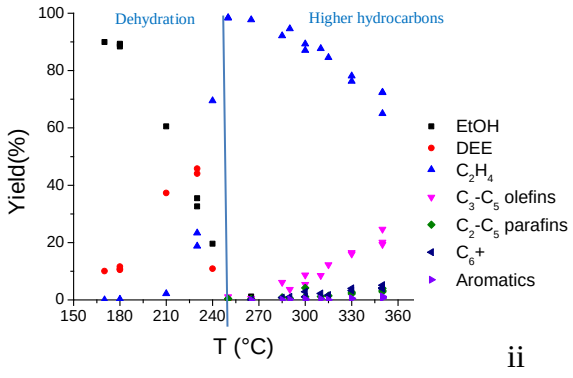

Figuur 2 KWS opbrengsten als functie van T bij 20kPa EtOH en 10kg_{cat} · s · mol^{-1}_{EtOH}

IV. ETHANOL DEHYDRATIE

Reactie van DEE geeft EtOH en ethyleen. Voeden van ethyleen en water veroorzaakt geen reactie. Door deze waarneming wordt een reactie van DEE naar EtOH en ethyleen in het netwerk opgenomen.

Meerdere micro-kinetische modellen worden opgesteld. Een Langmuir-Hinshelwood mechanisme geeft de beste resultaten. Er worden, naast adsorptie, drie oppervlakreacties beschouwd:

$$EtOH^* \rightarrow C_2H_4{}^* + H_2O_g$$
$$2EtOH^* \rightarrow DEE^* + H_2O^*$$
$$DEE^* \rightarrow C_2H_4{}^* + EtOH_g$$

De parameters voor DEE-adsorptie en de drie oppervlakreacties worden geschat. Het model geeft een goede fit ten opzichte van de experimentele resultaten (**Error! Reference source not found.** 3).

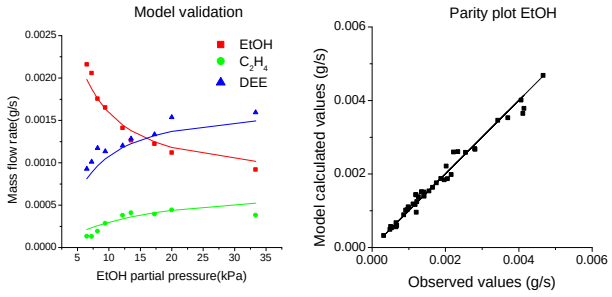

Figuur 3 Experimenten en model bij 230°C en 6.5$kg_{cat} \cdot s \cdot mol_{EtOH}^{-1}$ en pariteitsplot

V. OMZETTING NAAR HOGERE KOOLWATERSTOFFEN

Tussen 300°C en 350°C zijn lichte olefinen de voornaamste producten van de omzetting van ethanol door zeolieten (>90% etheen inbegrepen). Bij deze lichte olefinen komen butenen het meeste voor, gevolgd door propyleen en penteen. De vorming van alkanen en aromaten is verwaarloosbaar bij deze reactie condities (Figuur 4).

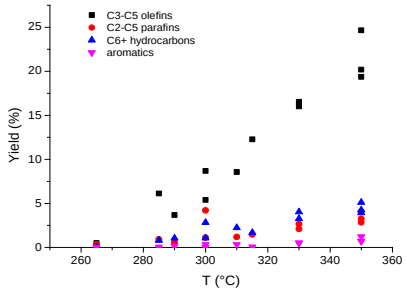

Figuur 4 Product opbrengst als functie van T (W_{cat}/F^0=10 $kg_{cat}.s.mol_{EtOH}^{-1}$, p_{EtOH}=20kPa)

C_4 en C_5 olefinen met eenzelfde koolstofgetal worden gevormd in thermodynamisch evenwicht. (Figuur 5). Dit wijst erop dat de vormingsreacties voor deze verbindingen doorgaan op een grotere tijdschaal dan hun omleggingsreacties.

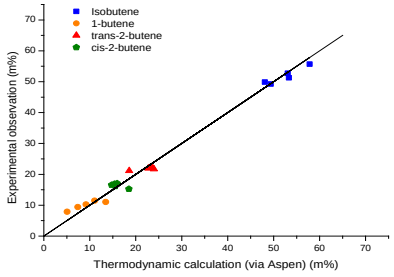

Figuur 5 Butenen in thermodynamisch evenwicht: EtOH conversie 5-50%

Het volledige productmengsel wordt niet gevormd in de evenwichtssamenstelling. Dit is aangetoond in Figuur 6, waar de verhouding van de lichte olefinen geplot zijn in de thermodynamische en experimentele ratio. Er wordt experimenteel meer propyleen en minder penteen opgemeten dan berekend is.

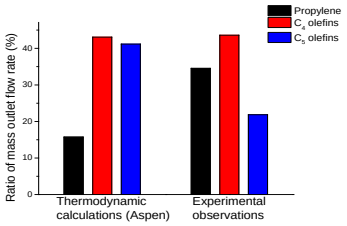

Figuur 6 Thermodynamische berekening evenwicht en experimentele waarnemingen

Het voeden van etheen onder dezelfde reactie conditie als ethanol (p_{etheen}, W/F en T) geeft een hogere conversie. Water toevoegen aan het etheen heeft geen invloed op de reactie.

Er wordt een reactie netwerk voor de omzetting naar hogere KWS opgesteld. De vorming van alkanen en aromaten wordt verwaarloosd, gebaseerd op de experimentele waarnemingen.

In de literatuur worden zowel het ethyl carbeniumion als het ethoxy ion als actieve verbinding voor de reactie vermeld. Hier wordt gewerkt met het carbenium ion, daar het stabiele ethoxy ion minder reactief is. Primaire carbenium ionen zijn minder stabiel dan secondaire of tertiaire. De primaire ethyl- en butyl-carbenium ionen worden aan het netwerk toegevoegd. De generatie van het complete netwerk gebeurt via ReNeGeP, een in-house ontwikkelde software van het LCT. De gegenereerde verbindingen hebben een maximaal koolstofgetal van 9. Het netwerk komt goed overeen met de experimenteel waargenomen resultaten (Tabel 2).

Tabel 2 Reactie netwerk gegenereerd via ReNeGeP

Soort elementaire reactie/component	*Aantal*
Protonering/deprotonering	149
Hydride shift	389
Methyl shift	62
PCP vertakking	304
Oligomerizering	41
β-scissie	21
Olefines	104
Carbenium ionen	80

Het SEMK model is gebaseerd op het reactienetwerk. Aan het LCT zijn codes beschikbaar betreffende oligomerizering van etheen op bi-functionele metaal/zuur katalysatoren. Primaire carbenium ionen en hun reacties worden toegevoegd aan deze codes. Alkylering tussen een primair carbenium ion en een olefine is belangrijk, want reactie tussen het ethyl carbenium ion en etheen is de eerste stap in de vorming van hogere KWS.

VI. CONCLUSIE

Er is een kinetische dataset omtrent de conversie van ethanol op zeolieten opgesteld. Onder de geteste katalysatoren geeft HZSM-5 (Si/Al=15) de hoogste ethanol conversie. Desilicatie van HZSM-5 wijzigt de katalytische eigenschappen niet binnen de geteste experimentele condities. Een micro-kinetisch model voor dehydratie is opgesteld. Dit model geeft goede berekeningen.

Het single-event micro-kinetisch model voor de omzetting van etheen is eveneens opgesteld, deze computer code dient nog verder geoptimaliseerd te worden.

REFERENTIES

1. Madeira, F.F., et al., *Ethanol transformation over HFAU, HBEA and HMFI zeolites presenting similar Brønsted acidity.* Applied Catalysis A: General, 2009. **367**(1–2): p. 39-46.
2. Gayubo, A.G., et al., *Kinetic Modelling of the Transformation of Aqueous Ethanol into Hydrocarbons on a HZSM-5 Zeolite.* Industrial & Engineering Chemistry Research, 2001. **40**(16): p. 3467-3474.
3. Stevens, S., *Transformation of bioethanol into hydrocarbons on modified ZSM-5*, in *Laboratory of Chemical Technology*2012, University of Ghent: Ghent. p. 98.
4. Berger, R.J., et al., *Eurokin. Chemical Reaction Kinetics in Practice.* CATTECH, 2001. **5**(1): p. 36-60.
5. Froment, G.F., *Kinetic modeling of acid-catalyzed oil refining processes.* Catalysis Today, 1999. **52**(2–3): p. 153-163.

Index

List of Figures

List of tables

List of Symbols

Abbreviations and acronyms

Al-ALD	aluminum atomic layer deposition
BET	Brunauer, Emmet and Teller (N_2-adsorption)
C_i	lump of hydrocarbon compounds with carbon number i
DEE	diethyl ether
DME	dimethyl ether
EPR	electric paramagnetic resonance
ER	Eley-Rideal
EtOH	ethanol
ETH	ethanol to hydrocarbons
FID	flame ionization detector
GC	gas chromatograph
LH	Langmuir-Hinschelwood
MTG	methanol to gasoline
MTH	methanol to hydrocarbons
MTO	methanol to olefins
NMR	nuclear magnetic resonance
NTP	normal temperature and pressure (20°C and 101,325kPa)
PE	polyethylene
PET	polyethylene terephthalate
PID	proportional-integral-derivative controller
SEMK	single-event micro-kinetic (modeling)
TCD	thermal conductivity detector
TOS	time on stream
TPD	temperature programmed desorption
XRD	X-ray diffraction

Roman symbols

A	pre-exponential factor reaction rate coef.	Depends on reaction
A_k	area on chromatogram corresponding to k	a.u.
a_p	number of C-atoms in a product species	-
a_r	number of C-atoms in the reactant	-
a_s	specific surface area	$m^2.kg^{-1}$
a_v	external catalyst surface	$m^2_p.m^{-3}_r$
$\underline{b}$	parameters estimations	-
b_{max}	maximal bed dilution	-
C_A	surface concentration of A	$mol.m^{-3}$
$C_{A,B}$	bulk concentration of A	$mol.m^{-3}$
CF_k	calibration factor of k	-
D_{eA}	effective diffusion coefficient of A	$m^3_f.m_r^{-1}.s^{-1}$
d_p	particle diameter	m
d_t	reactor diameter	m
E_0	intrinsic activation energy	$J.mol^{-1}$
$E_{a,i}$	activation energy for reaction i	$J.mol^{-1}$
F	F-distribution value	-
F_w	mass flow rate	$kg.s^{-1}$
h	Planck's constant	$6{,}626.10^{-34}$ J.s
$\Delta H^{0\neq}$	standard enthalpy change transition state	$J.mol^{-1}$
$\Delta_r H$	enthalpy of reaction	$J.mol^{-1}$
$\Delta_{ads} H$	enthalpy of adsorption	$J.mol^{-1}$
K	equilibrium coefficient	-
k'	rate coefficient for elementary step	Depends on reaction
k	single event rate coefficient	Depends on reaction
k_B	Boltzman's constant	$1{,}381.10^{-23}$ $J.K^{-1}$
$k_{f,A}$	mass transfer coefficient of A	$m^3_f.m^{-2}.s^{-1}$
k_L	mass transfer coefficient (liquid phase)	$m^3.m^{-2}.s^{-1}$
k_v	volumetric reaction rate coefficient	Depends on reactions
L_B	length of the catalyst bed	m

m_A	mass of a	kg
n_A	amount of A	mol
$\dot{n}_A$	molar flow of A	$mol.s^{-1}$
N_A	Avogadro's number	$6{,}022.10^{23}\ mol^{-1}$
n_e	number of single events	-
p	pressure	Pa
p^0	ambient pressure	Pa
p_A	partial pressure of A	Pa
R	ideal gas constant	$8{,}314\ J.mol^{-1}.K^{-1}$
R^2	multiple correlation coefficient	-
r_v	volumetric reaction rate	$mol.m^{-3}.s^{-1}$
r_w	specific reaction rate	$mol.\ kg^{-1}_{cat}.s^{-1}$
$R_{w,A}$	specific production rate of A	$mol.kg^{-1}_{cat}.s^{-1}$
S_A	selectivity towards A	%
$\Delta S^{0\neq}$	standard entropy change transition state	$J.mol^{-1}.K^{-1}$
t	t-distribution value	-
T	temperature	K
V	volume	m^3
V	variance matrix	-
V_{ii}	i^{th} diagonal element of the variance matrix	-
V_a	total adsorbed volume	m^3
V_m	theoretical monolayer capacity	m^3
W	catalyst mass	kg
$\underline{X}$	matrix of independent parameters	-
x_A	mass fraction of A	$kg.kg^{-1}$
X_A	fractional conversion of A	-
Y_A	yield of A	$kg.kg^{-1}$
$\underline{y}$	set of experimental values	-
$\underline{y}$	set of model calculated values	-

Greek symbols

α	transfer coefficient Polanyi expression	-
α_w	heat transfer coefficient	$W.m^{-2}.K^{-1}$
β	rate of temperature increase	$K.s^{-1}$
$\underline{\beta}$	set of model parameters	-
γ	Hatta-number ($= \frac{\overline{k_v D_A}}{k_L}$)	Depends on reaction
ε	experimental error	-
λ_{er}	Effective radial thermal conductivity	$W.m^{-1}K^{-1}$
ν_A	stoichiometric coefficient of A	-
ρ_A	density of A	$kg.m^{-3}$
σ	symmetry number	-
σ_{gl}	global symmetry number	-
θ_A	fraction of adsorption sites occupied by A	$mol.mol^{-1}$

Subscripts

g	species in the gas phase
av	average
_	matrix

Superscripts

*	adsorbed/activated species
0	initial value
^	estimated value
≠	transition state

Chapter 1

Biochemicals: the ethanol story

1.1 Ethanol as a versatile feedstock

During the past decades, the understanding has grown that the world's oil-reserves are not infinite. On top of that, much of these oil-reserves are located in politically unstable regions. These factors triggered the search for alternative sources of fuels and chemicals. In particular, renewable resources get a lot of attention due to environmental concerns and the phenomenon of global warming. Some examples of renewable resources are already used on relatively large scales, e.g. biodiesel. [1]

Ethanol is an interesting compound in the field of renewable chemicals. The strength of ethanol as resource for a bio-based chemical industry lies in the multiple crops from which bioethanol can be produced and the diversity of possible applications. In Figure 1-1, different options to convert biomass into value-added products using ethanol as a platform molecule are shown.

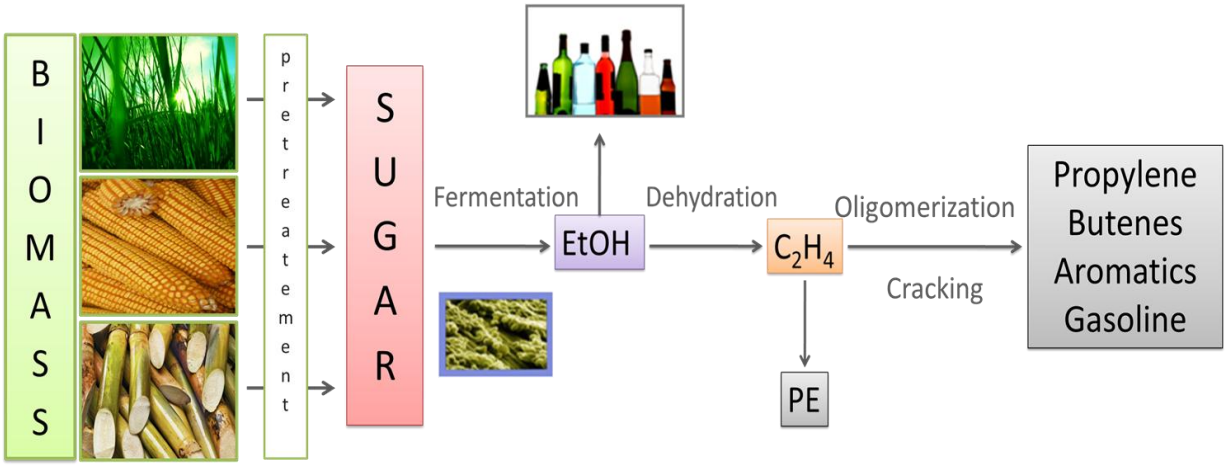

Figure 1-1 Possible routes of converting biomass into chemicals and fuels, using ethanol as platform molecule

Since centuries, sugars have been fermented to produce alcoholic beverages. Besides sugar, corn crops can be used, which is done in the US. Classically, sugars and starch are extracted from edible crops such as sugar cane and corn. Recently, the attention has shifted towards lignocellulosic biomass. [2-4] This term refers to biomass that is constituted from cellulose, hemicelluloses and lignin of which grasses or wood are well known examples. Although this resource needs to be pre-treated, which raises processing costs, it is an important alternative to sugar based ethanol. The main advantage of lignocellulosic biomass as an ethanol source is that it does not interfere directly with food production.

Gaining ethanol from sugar cane is more economical than gaining it from other crops such as e.g. corn. [5] Sugar cane is a tropical plant and can thus only be cultivated in a limited region. [6] Brazil is the lowest cost producer of sugar cane and consequently has an advantage on other countries in the commercialization of ethanol based processes.

Several other processes to produce bio-ethanol are possible, which are developed to allow for a far wider range of biomass to be used as feedstock. These processes mostly use gasification followed by ethanol synthesis from e.g. syngas or via DME. [7] Haro et al. discuss several options, but from these processes, only fermentation has been commercialized.

In some cases, ethanol is produced from ethylene. This reaction pathway has three important advantages over the fermentation reaction: it is faster, cheaper and it yields pure ethanol (instead of a ethanol/water mixture needing distillation and/or other separation techniques). Adding the need of pre-processing biomass before it can be fermented, gives some important reasons why ethylene is still used as reactant for ethanol. Due to the higher energy consumption of the ethylene process and the non-renewable character of the petroleum-based process, industry is focussing more and more on the fermentation process. The industrial importance of the fermentation reaction to produce ethanol is immediately clear when a study is made of the different possible facility lay-outs that are being used. An extensive review of these various plant lay-outs can be found in Ullmans encyclopaedia of industrial chemistry. [8]

Ethanol can be used as a fuel. [9] The implementation of pure ethanol as a fuel for combustion engines has several drawbacks. Engines must be redesigned to work on ethanol. The lower heating value of ethanol compared to gasoline leads to a higher volumetric consumption, hence larger fuel tanks are needed. Due to the hydrophilic character of ethanol, even the smallest amount of water will be absorbed. [10]

If the use of pure ethanol as a fuel is rather difficult, its implementation as a fuel additive is much more straightforward. [9] The ethanol concentration can be rather high, but again, the current design of combustion engines puts a limit on the ethanol/gasoline ratio. Also, water content should be near zero, because phase-separation phenomena could otherwise impose problems. Once these two considerations are taken into account, nothing hinders the addition of ethanol to regular car fuels. Brazil is an example of a country where a gasoline/ethanol mixture is implemented. However, mixing ethanol with gasoline means there's still need for a large amount of oil based fuels. The European Union has imposed its member-states to add 5,75% bioethanol to the gasoline in 2010 and 10% by 2020. Belgium has accordingly crafted legislations.

Converting ethanol into gasoline-like molecules could be an elegant solution to the problems encountered when using ethanol as a fuel. It would allow to use the biomass-based fuel directly in the current engines.

The concept of using an alcohol to produce relatively small hydrocarbons is not unique to ethanol. Methanol to Olefins (MTO) and Methanol to Gasoline (MTG) are working examples of this type of reaction. [11, 12] The ethanol to hydrocarbons process (ETH) would be a direct expansion of the principle.

Ethanol can be used as feedstock for several chemicals, e.g. ethylene, which is the primary chemical produced from ethanol. [13] In the fifties and sixties of the 20th century, ethanol was used for the production of ethylene in several countries, e.g. Brazil, India and Australia. After a short period of declining interest, ethanol saw a revival due to the energy crisis in the seventies.

According to *Chemical and Engineering News* [14], the world wide ethylene production in 2006 was 109 Mt/y. This figure makes ethylene the third most produced chemical, after sulfuric acid and nitrogen. As a comparison, according to the US Energy Information Administration, in 2011 the annual gasoline consumption in the United States of America amounted 134 billion gallons. [15] This is about 380 Mt/y of gasoline consumed in the US alone. Although ethylene is an important chemical, it consumes only a fraction of the resources that go to fuels.

In Brazil, the ethanol to ethylene process has been commercialized by Braskem in 2007. [16] The competition with petroleum based ethylene production still means only fully integrated ethanol-to-ethylene production sites can reduce the pricing disadvantage of the biomass based process. Such facility converts the biomass feedstock to high value end products, e.g. vinyl chloride monomer or high density polyethylene. [13]

The catalyst achieves a high selectivity towards ethylene and an ethanol conversion of about 99%. Because Braskem uses in-house developed catalysts, little is known about their exact composition. However, several patents describing acid catalysts for the ethanol dehydration can be found. [17, 18]

The dehydration reaction takes place in the vapour phase, in a fluidized- or a fixed-bed reactor. In the fixed-bed setup the process can be conducted on two types of reactor: an isothermal or an adiabatic reactor. [13]

Figure 1-2 gives a possible flow diagram of a facility producing polymer grade ethylene from ethanol. [19]

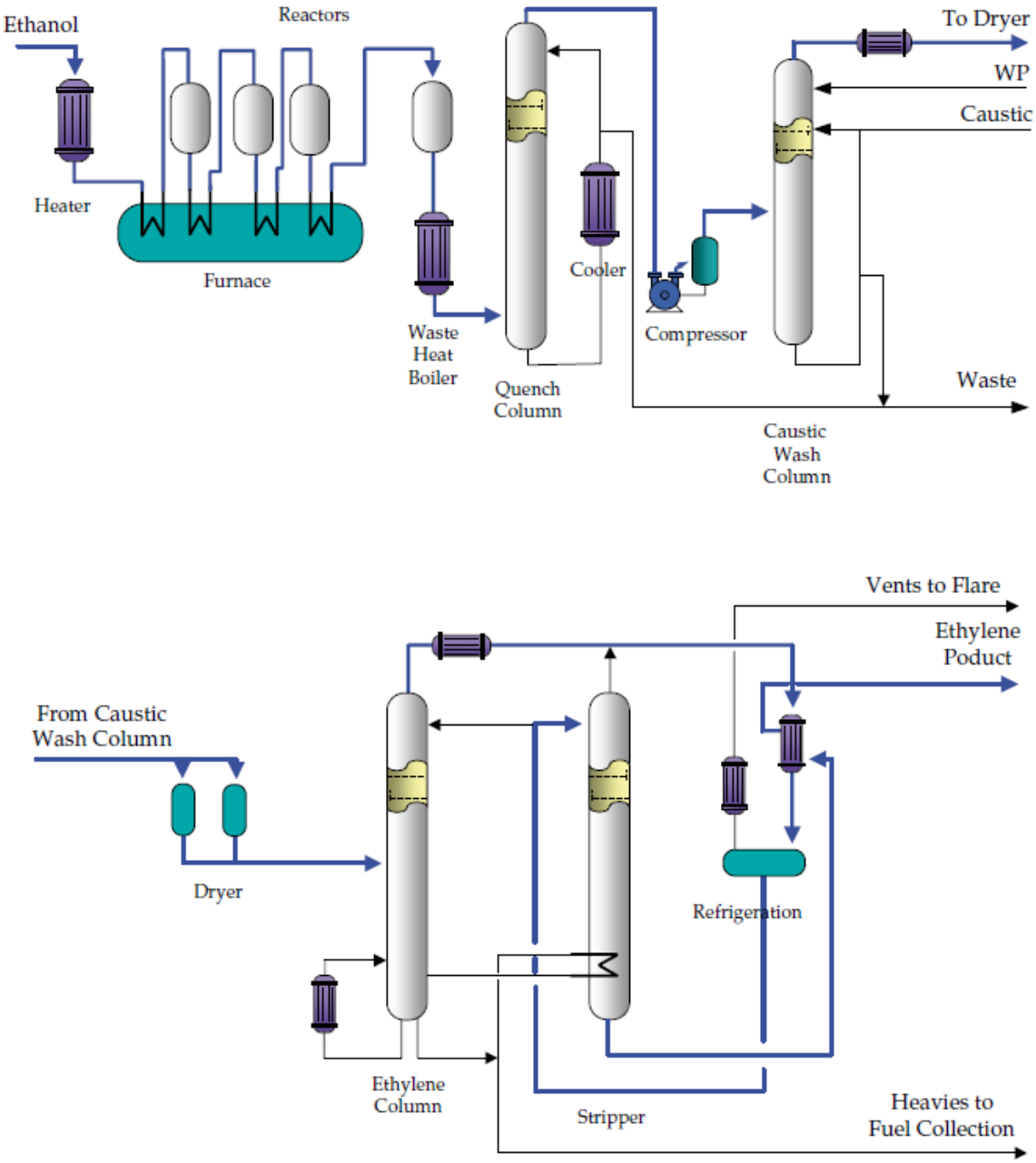

Figure 1-2 Flow sheet of a facility to produce polymer grade ethylene from (bio-)ethanol (by Chematur Engineering Group, Sweden) [19]

Haro et al performed a techno-economic assessment of several potential processes to produce bio-ethylene. [7] according to these authors, several routes to bio-ethylene can be economic viable. The fermentation and subsequent dehydration route is a good option in Brazil (based on sugar cane) and could be feasible in the USA (based on corn). Dependent on the price for sequestrated CO_2, several routes via gasification of biomass can be economic viable too, while gasification followed by ethanol formation from DME and subsequent dehydration to ethylene is the most promising process under all circumstances. This process is still under development. Based on the scarce literature on the subject, the viability is questionable.

Recently, several industrial companies have taken patents on the upgrading of ethanol. Some processes combine ethanol and methanol conversion [20], while others concentrate on upgrading pure ethanol (e.g. IFP and Total) [21-23]. These reactions not only yield ethylene, but also higher olefins, alkanes and aromatics.

Next to the direct use of ethanol and the catalytic conversion to ethylene or higher hydrocarbons, there are still other possible applications of ethanol. An example of such alternative process is the steam reforming of ethanol over cobalt-based catalysts, as discussed by Batista et al. [24] Steam reforming is used to produce syngas, which serves as intermediate in various reactions, e.g. the Fischer-Tropsch synthesis. However, syngas production is possible with any kind of organic compound, ranging from natural gas and coal to biomass. Since ethanol is a valuable chemical as such and can be upgraded without the energy intensive syngas production, this route seems excessive.

1.2 Solid acid catalysts

Catalysis is of great importance for most industrial employed chemical reactions. Much of the catalysed production processes use heterogeneous catalysis, which means the catalyst and the reaction mixture are present as separate phases, e.g. a solid catalyst and a gas- or liquid phase reaction mixture.

There are numerous ways of dividing solid catalysts into categories. One of the possibilities is based on the active sites. The main types to be found are acid, basic and metal or metal oxide sites. Each type has its own applications and particularities.

1.2.1 Zeolite materials

According to Guisnet and Gilson [25], zeolites are crystalline aluminosilicate materials. This definition has been broadened so that materials containing other elements (such as phosphorus in SAPO) are also covered by this term.

Since they occur in nature, zeolites have been known for a long time. The name ‘zeolite’ is given to these materials by the Swedish mineralogist Axel Fredrik Crönsted. It is derived from the Greek words zeo and lithos, which mean to boil and stone respectively. Their use as catalysts is more recent, originating in the 1950’s from researchers of Mobil. Other uses for these materials are molecular sieving, drying and ion exchange. Natural zeolite minerals are of little use as catalysts because of the inevitable impurities and their non-ideal structure and composition. Nonetheless, these minerals are the models on which the modern day synthetic zeolite materials are based. Synthetic zeolites are widely used as industrial catalysts. Their importance is due to their high activity and the possibility of shape selective reactions. [26]

1.2.1.1 Composition, structure and production

Zeolites consist mainly of two building blocks, SiO_4 and AlO_4 tetrahedra, joined by common oxygen atoms. They contain alkali and alkaline-earth metals. Because of the tetrahedral linkage of silica and alumina units, every aluminum atom induces a negative charge in the zeolite. These negative charges are compensated by cations. The constitution of a zeolite has some rules to abide. The most important is perhaps Löwenstein's rule. This rule states that tetrahedra containing aluminum as central atom cannot be linked. This puts a limit to the Si/Al-ratio in the zeolite structure. The minimal value of this ratio is one. In this extreme case, each tetrahedron would be linked to a tetrahedron of the other type. In practice, this configuration cannot be obtained. [25]

The constituting elements of a zeolite can be combined in many ways, each variation resulting in a specific framework structure. The zeolite framework consists of channels, intersections and cages. The dimension of these structures vary between 0,2 and 1nm. According to IUPAC, materials with pore sizes below two nanometers are called micro-porous materials. Typically, zeolites follow this definition. Between zeolites, there is still a wide variation in pore sizes following the differences in framework composition. Depending on the exact structure and the magnitude of the pores and cages, a wide range of applications is possible.

Classification of zeolites is based on the structure of the material. Some possible conformations are shown with their void systems and pore sizes in Figure 1-3, adapted from Weitkamp. [26] Zeolites with the same structure can still differ through their respective Si/Al ratio, but they will carry the same name. At the time of writing, 206 zeolite framework types are recognized by the International Zeolite Association (IZA). Of course, not all of these materials are equally well suited for catalysis purposes.

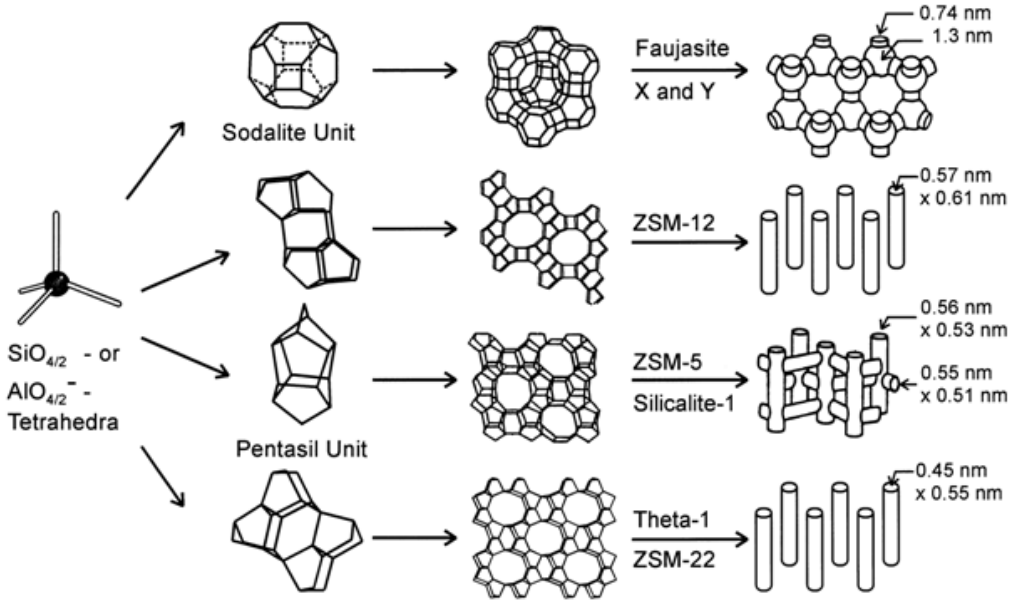

Figure 1-3 Framework structure, voids systems and pores sizes for a selection of zeolite materials [26]

The synthesis of zeolites occurs in an aqueous solution. Alumina, silica and a template-molecule are mixed. The formation of the framework can be compared to a polymerization. Zeolite-monomers combine to form oligomers, which are ring-shaped structures. The oligomers react to form linear structures, who in their turn combine to form the zeolite three dimensional framework. The produced zeolite still has the monomer counter-ions, often this is a sodium cation. Ion exchange replaces these with protons. A method to achieve this, is aqueous ion exchange with an ammonium salt, thus replacing the counter ion by a ammonium-cation. Next, the ammonium is thermally decomposed to ammonia. This ammonia is vacated from the zeolite to leave a Brønsted acid site. Other possibilities are ion exchange with a salt of a multivalent metal cation followed by thermal dehydration or direct ion exchange with mineral acids. [26]

The production scheme can be influenced in many ways. Changing the reaction mixture composition, the acidity of the aqueous solution, the temperature, the template molecule, etc. will yield different zeolite structures.

1.2.1.2 Zeolite materials as catalysts

The surface acidity of zeolites, which is created by the methodology described above, has gained them an important place in catalysis. Many reactions are catalysed by this kind of materials, the most important example being catalytic cracking. [27-29]

The zeolite acid sites are identified by four characteristics: the type of site (Brønsted or Lewis acid), their strength and the location and density of the sites in the zeolite framework.

Brønsted-sites are hydroxyl groups, formed by an oxygen from a framework AlO_4 tetrahedron and a proton. Mostly, Brønsted-sites are introduced into to framework by cation exchange: the small counter-cation of a negative charged site is exchanged for a proton. The Lewis acid sites originate from non-framework aluminum species. [30] They are formed by degradation of Brønsted-sites during thermal treatment. The nature of these sites is less obvious. Although they are weaker than the Brønsted-sites, Lewis acid sites can play a role in catalysis.

The density of acid sites in a zeolite material is related to the Si/Al ratio, since they only occur at tetrahedra with aluminium atoms at the centre. Identically, the location of the acid sites is defined by the position of the aluminium atoms in the framework. It is more difficult to get a distribution of the strengths of the acid sites. An idea of this distribution can be obtained using temperature programmed desorption of ammonia or pyridine. However, this method only gives information about the acid sites available to these molecules. It has been proven both experimentally [31] and from ab initio calculations [32, 33] that the strongest acid sites occur when the aluminum-tetrahedron is surrounded by silicon-tetrahedra. This is explained by the higher electronegativity of silicon atoms when compared to aluminum. An electron abstraction effect causes a weaker oxygen-hydrongen bond, thus making the Brønsted-site more acidic.

Another important aspect of zeolites is the possibility of shape selective catalysis. [34] Because zeolite pores can have dimensions comparable to molecule sizes, the interactions between the catalyst and the reaction compounds has unique characteristics. There are three categories of shape selectiveness: reactant shape selectivity, product shape selectivity and transition state shape selectivity. [35]

In reactant shape selectivity, there are several reactants with different molecular measurements. The zeolite pore size may hinder the diffusion of some of the bigger molecules, the smaller reactants will reach the active sites preferentially and convert to the reaction products to a larger extent than the bulkier reactants. In the extreme case of reactant shape selectivity, the diffusion of the biggest molecules to the active sites is impossible and only the small compounds react. Illustrations of reactant shape selectivity are dehydration of butanol [36] or the exclusion of branched paraffins in a dewaxing reaction over ZSM-5. [37]

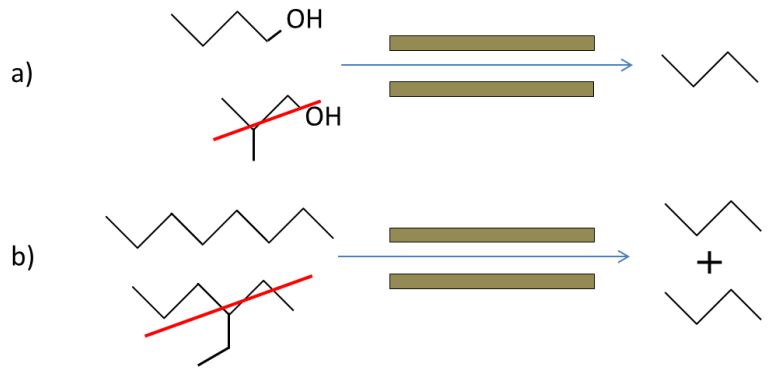

Figure 1-4 Reactant shape selectivity: a) dehydration of butanol and b) dewaxing

To allow product shape selectivity, there should be products with different dimensions. Although the products may be produced in equal measures in the catalyst framework, the bulky products will be hindered in their diffusion out of the zeolite material. As a result, the effluent of the reacting system will be composed mainly of the smaller product molecules.

An example of product shape selectivity is the isomerization of xylene. The only reaction product which diffuses out of the catalyst pores with relative ease, is the para-isomer. [38, 39]

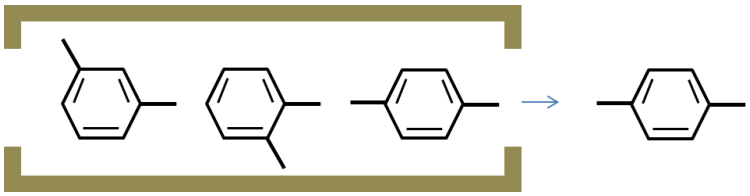

Figure 1-5 Product shape selectivity: isomerization of xylene

In the last case, transition state shape selectivity, it is not diffusion of either reactants or products which causes the selectivity. At least one of the possible transition states must be too large to fit in the zeolite framework. Only the reactions going over transition states that do fit in the pore structure will happen.

Transition state selectivity can be demonstrated by the alkylation reaction of aromatics, where the size of the transition state prevents the formation of multi-alkylated species. [40]

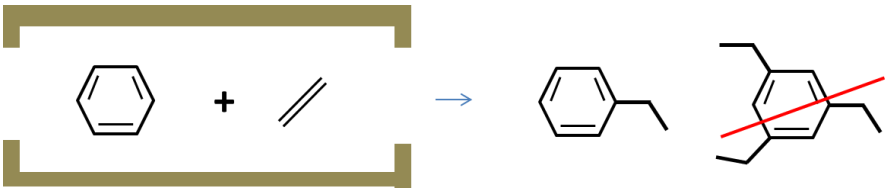

Figure 1-6 Transition state shape selectivity: alkylation of aromatics

Because reactant and product shape selectivity are based on diffusion limitations, increasing the path length in the zeolite will amplify the selectivity effect. This can be achieved, for example, by increasing the zeolite crystal size. Transition state selectivity on the other hand, is an intrinsic chemical effect and will not be affected by the crystal size. [26]

1.2.2 HZSM-5 zeolite

HZSM-5 is a zeolite with the MFI structure. A representation of this material can be found in Figure 1-3. HZSM-5 is the focus of this research since previous studies showed a good reactivity of this zeolite towards the catalytic conversion of ethanol. [20, 41-43]

Using a well-know and commercially available catalyst during the investigations eases the introduction of the findings into industrial application. To demonstrate the importance of HZSM-5 in the chemical industry a few examples of its applications will be given.

1.2.2.1 Isomerization of n-butene

A reaction performed on zeolite materials, more specific on HZSM-5, is the isomerization of hydrocarbons. The intermediate state is a carbenium ion. The formation and stabilization of these ions is facilitated by acid catalysts.

Being one of the important reactions in catalytic cracking, isomerization plays a key role in the production of e.g. liquid fuels. In the petrochemical industry, it is also used in other processes. An example is the upgrading of n-butene to the more valuable isobutene.

Because this reaction is prone to side reactions, it is important to find a selective catalyst. This can be achieved through micro-porous zeolites like HZSM-5. [44] The small pore size of the zeolitic material limit the formation of the oligomeric side-products, while the strong acidity yields high conversions. These factors make HZSM-5 an ideal catalyst for this reaction. [45]

1.2.2.2 Xylene production and isomerization

An important aspect of zeolite catalysts is the possibility of shape selectivity. This property is applied when producing xylenes. There are three isomers of xylene: ortho-, meta- and para-xylene. Since para-xylene is a reactant for tereftalic acid, the monomer for PET, it is consumed in much larger quantities than the other isomers. Catalysts with a high selectivity towards para-xylene are needed. The shape selectivity of zeolites offers a solution.

The disproportionation of toluene towards xylene is executed on HZSM-5 catalysts. This reaction yields primarily p-xylene and to a lesser extend o-xylene. The production of the meta isomer is small. The product distribution is very different from the thermodynamic equilibrium calculations. When a feed mixture of xylenes is reacted over HZSM-5, a very similar product mixture is achieved. [38] According to Mirth et al, the shape selectiveness is purely due to the diffusion rate of the molecules (p-xylene > o-xylene > m-xylene). [39] Liang et al state that the shape selectiveness is caused by product diffusion limitations and different surface reactivities. [46] In both explanations, the micro-porosity of the zeolite framework plays a crucial role in reaching the product distribution.

1.2.2.3 Aromatization of light alkanes

Aromatization of light hydrocarbons has a great interest. This reaction type allows converting natural gas and light refinery fractions to more valuable aromatic compounds. In industry, the aromatization uses MFI zeolite catalysts (HZSM-5) impregnated with gallium species. The industrial process is called the Cyclar-process and is developed in a co-operation between UOP and BP.

The aromatization reaction is in competition with a cracking reaction. When using pure HZSM-5, cracking predominates at high n-butane conversion, necessitating the use of gallium modified catalysts. [47]

1.2.3 Modifications of HZSM-5

Zeolites can be modified in numerous ways. Some examples are incorporation of metals, dealumination and desilication. These modifications take place during the zeolite synthesis or by post-synthesis techniques. Table 1-1 gives an overview of the different modification techniques for zeolitic materials as cited by Rahimi et al. [27] The methods used during this Master Thesis are written in bold and a larger font size. These techniques are discussed more extensively later on.

Table 1-1 Overview of the zeolite modification techniques

	Technique		Description	Effects
Synthesis	**Si/Al ratio**		Varying the ratio of silica and alumina changes the zeolite composition	Changes the number of acid sites and acid strength
	Isomorphous substitution		Substituting Si or Al in the framework by other elements (e.g. B, Fe, Ga) during the synthesis [48]	Alters the acidity (effects depending the introduced hetero atom)
Post-synthesis	Steaming/acid extraction		Partly dissolving or restructuring the zeolite	Creates a mesoporous system
	Cation exchange		Exchanging the zeolites' counter-ion	Changes the acid-base properties
	Impregnation (with metal oxides)	Alkali and alkaline earth metals	Occlusion of metal oxide clusters	Acidity diminishes
		Transition metals	Occlusion of metal oxide clusters	Creates Lewis acid sites, stabilizes zeolite alumina
		Rare earth	Occlusion of metal oxide clusters	Enhances hydrothermal stability Creates new Lewis sites and basic character
	Removing framework elements	**Desilication**	Removing framework silica	Gives stronger acid sites mesopores
		Dealumination	Removing framework alumina	Less but stronger acid sites and creates mesopores
	Atomic layer deposition		Adding a thin layer, a few atoms thick, to the zeolite (pore-)surface	Creates extra (types of) active sites
	Phosphorus		Impregnating the zeolite with phosphor (which may take the place of framework elements)	Enhances the hydrothermal stability (improved Al retention)

1.2.3.1 Metal-modified HZSM-5

According to several authors [27, 49-52], incorporating metal compounds into the zeolite gives more suitable catalysts, i.e. with higher yield of olefins and better stability. S. Stevens [53] investigated the effect of impregnating HZSM-5 with metal oxides. The research of Stevens indicated the selectivity of the zeolite catalyst, when linked to the conversion, is not altered significantly by these modifications. Because of these findings, metal-modified zeolites will not be discussed in detail here.

1.2.3.2 Desilicated HZSM-5

Desilication is a post-synthesis modification of a zeolite: silicon is extracted from the framework using a basic solution. This process allows tailoring of the zeolite pore structure. [54, 55] When external aluminum species are present, they may fill the gaps left by extracted silicon. The zeolite structure is changed: the Si/Al ratio decreases, making the zeolite more acid and a mesoporous structure arises. [56] The result of desilication depends on the Si/Al ratio of the starting material. For ratios smaller than 15, the high aluminum concentration prevents silicon extraction, thus limiting mesopore formation. On the other hand, ratios above 200 allow unselective and excessive solution of silicon and large pores arise. An intermediate ratio yields optimal results and gives a zeolite material with mesopores, while preserving the overall structure. These effects are illustrated in Figure 1-7 based on representations by Tao et al. [54]

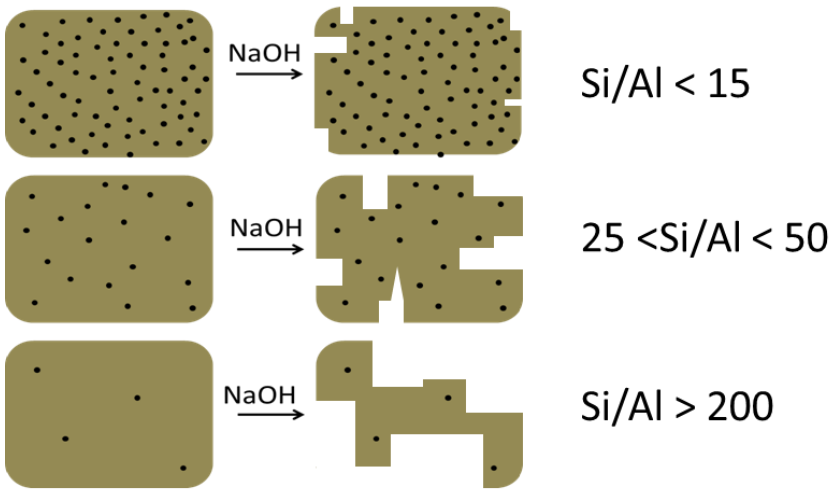

Figure 1-7 Desilication of ZSM-5: representation of the effect of the Si/Al ratio

According to Tao and co-workers, Brønsted acid sites disappear during the desilication, due to treatment with basic solution. These sites are restored by ion exchange with NH_4NO_3.

A study by Gil et al [56] focusses on the effects of desilication of ZSM-5 and ZSM-12 on the texture, the acidic and the catalytic properties of these zeolites. They use a catalyst with a Si/Al ratio of approximately 45, therefore, the zeolite falls within the optimal category for mesopore formation. To test the catalytic characteristics, the isomerization of α-pinene is used as reference reaction. This reaction has little resemblance to the ethanol conversion and primarily gives information on altered diffusion behaviour. XRD measurements by these authors show a significant loss of cristallinity (30%) upon treatment with a 1M NaOH solution. This effect is due to the formation of extra-framework amorphous phase.

1.2.3.3 Aluminum atomic layer deposition (ALD)

As noted by Toa et al, the acidity of desilicated zeolites is lower than the acidity of the parent zeolite. To restore the original acid sites, these authors propose ion exchange with NH_4NO_3.

Another way to (re-)introduce acidity to mesoporous catalysts is atomic layer deposition (ALD). The ALD technique improves acidity and acidic catalytic activity of the mesoporous material. [57, 58]

ALD is a technique to deposit films with heights on the nanometer scale. Figure 1-8 gives a schematic representation of this technique. Precursor molecules chemisorb to the surface of the treated material, followed by reaction. The support is exposed to pulses of $Al(CH_3)$ precursor and pulses of water. Because the reaction needs both components and chemisorption only proceeds until all active sites are occupied, the alternating exposure allows control of the layer thickness. Other advantages are the possibility of selective coverage of specific sites, the good ability to cover the topology of the support and the industrial scalability.

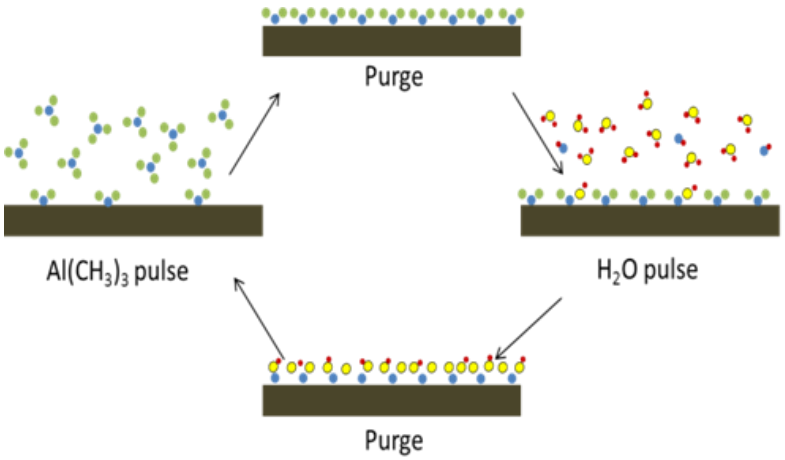

Figure 1-8 Atomic layer deposition of aluminum: schematic representation of the procedure

Sree et al investigated the acidity of zeolite after ALD treatment via pyridine adsorption and FTIR spectroscopy. The number of acid sites increased with about 17%. They also noted the deposit of extra-framework aluminum phase reduces the pore volume. [57]

The ability to tailor catalyst structures and acidity to suffice specific needs opens interesting opportunities. This thesis will incorporate a study on the behaviour of desilicated ZSM-5, with and without ALD treatment.

1.3 Reaction mechanism

A heterogeneously catalysed reaction always involves some kind of adsorption step, next there will be one or several reaction steps involving adsorbed or gas phase molecules. Finally, the products must desorb to free the active site and enable a new reaction sequence to start.

The main steps in the ethanol to hydrocarbons process can be divided into three groups: adsorption and desorption of ethanol and reaction products, dehydration of ethanol and further conversion of ethylene to hydrocarbons. In the following discussion, the emphasis will be on adsorption and dehydration of ethanol and on the conversion of ethylene to hydrocarbons. Since the presumed adsorption mode has a major impact on the possible dehydration mechanisms, adsorption and dehydration will be discussed together. A separate paragraph will be devoted to the formation of hydrocarbons.

1.3.1 Adsorption and dehydration

Most of the research performed on the conversion of ethanol on HZSM-5 focusses experimental results. Few articles giving a clear reaction mechanism are found. The way ethanol adsorbs to the zeolite helps explaining how dehydration occurs. Hence, adsorption and dehydration are discussed together.

Golay et al propose a mechanism with two kinds of adsorption modes: a strong irreversible and a weak reversible adsorption. [59, 60] This implies there are multiple types of adsorption sites in a HZSM-5 zeolite. According to Golay, a simultaneous adsorption to both sites is necessary for the formation of ethylene. Diethyl ether formation is described as a quasi-homogeneous reaction, without catalyst interaction, thus equivalent to a simple gas phase reaction. Although the authors are able to simulate their experimental results using this mechanism the latter assumption seems unlikely, because this would imply that ethanol reacts to DEE when heated.

Several authors use a two-step adsorption mechanism. [61-63] The first step is physisorption of ethanol to a Brønsted-site, followed by the formation of a protonated chemisorbed complex. Nguyen et al investigated this adsorption sequence by quantum mechanical

calculations for both small alcohols [63] and hydrocarbons [62], yielding good results for sorption enthalpies.

Saito et al. use a physisorption/chemisorption model to generate a dehydration reaction mechanism. [61] According to these authors, gas phase ethanol first physisorbs to the zeolite surface. Next, this physisorbed molecule can chemisorb on an acid site or it can react with a chemisorbed molecule, thus forming diethyl ether (DEE) and water. Ethylene is formed by decomposition of chemisorbed ethanol into ethylene and water.

Chiang et al present several possible reaction mechanisms. [64] They describe four possible schemes of DEE-formation and one for ethylene formation.

The first DEE mechanism starts with physisorption of ethanol to the catalyst surface. When a second ethanol molecule adsorbs to a neighboring site, an ethanol dimer is formed using a framework proton as bridging element. To finalize the reaction scheme, water is eliminated and DEE desorbs.

The second mechanism starts identically with the physisorption of ethanol. Elimination of water yields a chemisorbed ethyl group. This group reacts with a gas phase ethanol molecule by an Eley-Rideal mechanism, or it can yield ethylene by desorption.

The last two DEE reaction mechanisms involve ethylene as reactant, either by direct reaction of a physisorbed ethanol molecule with gas-phase ethylene, or by reaction of a chemisorbed ethylene and ethanol molecule.

According to these authors, the dimer mechanism is dominant because of the lower energy barrier compared to the other reaction pathways.

Chiang et al use a differential reactor. The temperatures and spacetimes are far lower than those that will be used during the experimental part of this Master Thesis. The experimental results of both studies cannot be compared.

1.3.2 Further conversion to hydrocarbons

Three main theories on the conversion of ethanol to higher hydrocarbons have been published in literature: a hydrocarbon pool model, the alkylation and cracking of ethylene and a radical mechanism.

1.3.2.1 Hydrocarbon pool

The upgrading of ethanol to higher hydrocarbons and the methanol-to-hydrocarbons (MTH)-process are very alike. Both reactions produce hydrocarbons starting from small alcohols using catalysts (e.g. HZSM-5). According to Johansson et al., the product distribution of both processes is essentially the same. [43] Considering this argumentation, it seems legitimate to

extrapolate the proposed MTH-reaction mechanism to the ethanol process as is done by Johansson et al.

The hydrocarbon pool model originates from the hard-to-explain first carbon-carbon link in the conversion of methanol to higher hydrocarbons. Because no such things as a methyl-radical or -carbocation are likely to exist, an alternative had to be found. In the hydrocarbon pool model, the actual catalytic sites are large organic species which are trapped within the zeolite framework. These compounds consist mainly of alkylated aromatic species. The reaction products come forth from these molecules by a cracking mechanism. This mechanism implies an inhibition period during which the hydrocarbon pool is building up before the products are formed to the fullest extent.

According to Johansson et al., the same mechanism works for the ethanol to hydrocarbons processes. To prove this hypothesis, a study of the molecules retained in the zeolite framework is made. According to this study, similar molecules can be found for both processes. Because the same species are present, the authors conclude the reaction mechanism is the same for the conversion of methanol and ethanol to higher hydrocarbons.

A detailed study of the hydrocarbon pool model in the MTH process can be found in the review by Olsbye et al. [12] These authors divide the hydrocarbon pool model into two cycles. Figure 1-9 shows a schematic representation of the model. The first cycle is the alkene methylation/cracking cycle. These reactions are responsible for alkane and alkene production. The only exception is ethylene, this alkene is produced by the second cycle, the hydrocarbon pool. According to this mechanism, the hydrocarbon pool is not strictly necessary when using ethanol as feed component. The main product of the hydrocarbon pool is ethylene, which can be directly produced from ethanol by dehydration.

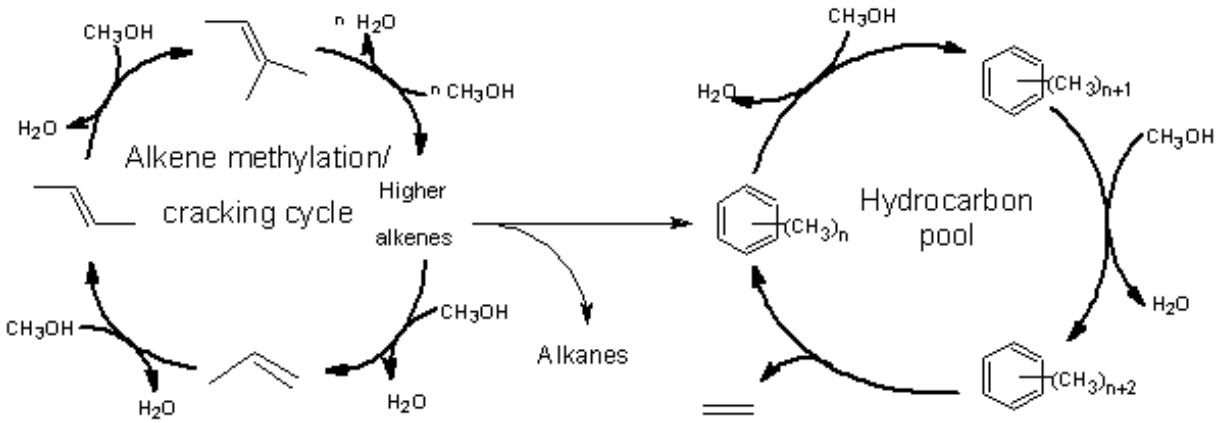

Figure 1-9 The hydrocarbon pool model for the MTH process

1.3.2.2 Alkylation and cracking of ethylene

A simple reaction network based on oligomerization reactions has been proposed by several authors. [65-68] A scheme of this reaction mechanism is represented in Figure 1-10. According to Costa et al [67], carbenium ions play a central role in the production of higher molecular weight compounds. These ions are thought to condensate with alkenes, thus forming longer chained molecules. Carbenium ions are known intermediates in zeolitic catalyzed reactions. Ermakov and coworkers [68] state another type of cations, oxonium ions, are the reacting species.

Next to oligomerization of ethylene, several other reactions proceed, e.g. hydride transfer and cracking. Prove of this is given by the occurrence of olefin isomers and compounds with odd carbon-numbers such as propylene and pentene. These small compounds stem from cracking reactions of higher hydrocarbons. [69] Using a lumped kinetic model, the oligomerisation mechanism can predict the product distribution, as shown by Gayubo et al. [66]. However, lumped kinetics alone are insufficient to evaluate a reaction mechanism. Therefore, a microkinetic model is necessary.

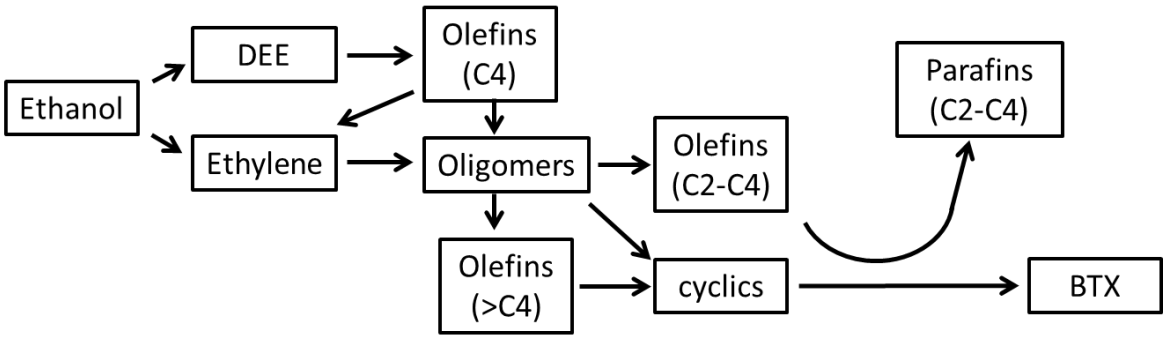

Figure 1-10 Reaction scheme of the ethanol to hydrocarbon reaction

The hydrocarbon pool and the alkylation/cracking of ethylene are two closely related reaction mechanisms. In fact, the latter reaction mechanism is part of the hydrocarbon pool model. For the hydrocarbon pool, heavy carbon components must be present in the catalyst. Without these species, no conversion would be noticed. The alkylation/cracking mechanism does not need these species. This is the main difference between the two models.

1.3.2.3 Radical model

Madeira et al proposed a reaction mechanism based on radical species. [42, 70] The radical model is based on observations concerning the deactivation of several zeolitic catalysts in the ethanol conversion process. [70] The authors note a retained activity when the acid active sites are claimed to be no longer accessible for the ethanol molecules because of pore blocking.

According to Madeira et al, radical species are the active compounds of the reaction. Measurements with electric paramagnetic resonance (EPR) revealed the presence of radical species in the hydrocarbon pool. The authors state that these radicals act as active species in the conversion of ethylene to higher hydrocarbons. The mechanism is very alike to radical polymerization. The measurements reveal a change in the nature of the radical species over time. With longer time on stream, more stable radicals are formed, thus diminishing reactivity. According to Madeira and co-workers, this phenomenon accounts for the deactivation of the catalyst.

Apart from the active species, the mechanism proposed by these authors does not differ by much with the oligomerization of ethylene. Both rely on a polymerization-like reaction to form higher hydrocarbons, while cracking is also incorporated into the mechanism.

An argument which counters this theory, is the need of acid catalysts for the reaction to take place. This radical mechanism does not use the catalyst functionalities and reduces its function to a mere reaction medium. Also, although radicals are present in the zeolite pores, the concentration is rather low and it seems unlikely these alone account for the reactivity.

K. Ben Tayeb et al support the theory that radicals are active species in the ethanol conversion. [71] EPR-measurements by these authors indicate some of the radical species are active. However, they do not exclude the acid sites from their proposed mechanism. According to these authors, there are two pathways towards the reaction products: one via acid-catalysis and one by radical reactions. The latter becoming more important when cokes deactivate the acid sites of the zeolite.

1.3.3 Deactivation

Catalysts deactivate in several ways. According to the specific deactivation mechanism, the process can be reversible or not. A well-known example of reversible deactivation is coking, whereby the formation of large hydrocarbon molecules block catalytic sites for the reagents. Irreversible deactivation can for example be due to the loss of active sites via chemical binding of components, or loss of atoms. In HZSM-5, dealumination could lead to irreversible deactivation, since the aluminum tetrahedra form the acid sites.

Studies show that for the ethanol to olefins process, the catalysts activity can be fully regenerated [72], indicating the loss of activity is caused by cokes deposit. Dealumination of HZSM-5 zeolites is insignificant under steam atmosphere up to temperatures well above 500K. [41, 73] Regenerative catalysts are interesting to the industry, because it avoids high operating costs by regular acquisition of fresh catalyst.

Several authors have investigated the nature of the cokes deposit in the ethanol to hydrocarbons [66, 72] and the methanol to hydrocarbons processes. [73, 74] Because of the similarities between these two reactions, the investigations on the methanol process can also yield insights into the deactivation mechanism of the ethanol process.

Däumer and coworkers [72] studied coking by means of ab initio calculations and experiments. They noticed the coking reactions and composition depend on the reaction conditions. An increased spacetime results in faster deactivation, because it promotes the formation of highly substituted aromatics. These kind of compounds are responsible for blocking the catalyst pores.

According to Madeirra et al, [42] cokes consists of polyaromatic compounds. These authors state the strong acid sites are quickly deactivated by cokes deposits. For HZSM-5, after 16h of reaction at 350°C, 55% of the microporosity is lost. Of the Brønsted acid sites, up to 94% is deactivated. The Meassurements by Ben Tayeb et al show similar results. [71]

Based on lumped kinetic models, Gayubo et al and Aguayo et al [66, 73, 74] study the reaction mechanism of cokes formation. According to these authors, coking proceeds parallel with the ethanol reactions and ethylene is the most important precursor for cokes deposit. [66]

1.4 Kinetic model

As with the reaction mechanism, the kinetic modelling will be split into two parts: the adsorption and dehydration of ethanol and the conversion to higher hydrocarbons. This paragraph will give an overview of the research that has been performed on the kinetic modeling of the ETH process. Overall, two techniques of modeling can be distinguished: lumped kinetic modeling and micro kinetic modeling. Both types will be discussed.

1.4.1 Lumped kinetic models

Lumped kinetic models are based on a simplified reaction mechanism. Instead of considering every molecule in the reaction mixture, they are subdivided into several families. The model uses these families to predict the composition of the product stream. Although lumped kinetic models can yield good results, they do not give detailed information on the reaction mechanism. They can be useful to predict the influence of reaction condition on the reaction outcome and the product distribution. For everyday industrial application, a lumped kinetic model sometimes suffices. These models should not be used outside the reaction conditions used for the parameter estimation.

Gayubo et al. constructed a lumped kinetic model for the conversion of ethanol to hydrocarbons. They claim to incorporate catalyst deactivation by coking. [66, 75] The mechanism these authors employ, uses four components: ethylene, a propylene and butene lump, a light paraffin lump and a gasoline lump that includes all compounds with five or more carbon atoms in their structure and also the aromatics. Ethylene is considered as the reacting species, so no dehydration is incorporated into the model.

The effect of cokes is introduced into the model by a deactivation term, which is fitted to experimental values. Although the idea to add a deactivation term stems from chemical considerations, the function itself has no fundamental physical meaning. The authors do investigate the interaction between reaction kinetics and deactivation. Different models are used for coking in parallel or in series with the ethanol conversion. The model also depends on which product lump causes the coking. It does not give fundamental information on the coking reaction mechanism, because no elementary reaction steps are used to build the model.

Another lumped kinetic model has been constructed by Chang and co-workers. [76] These authors include dehydration kinetics into the model. Their reaction network consists of seven reactions and eight components, of which five are individual compounds and three are product lumps. These components are ethanol, water, diethyl ether, ethylene, ethane, C_3-C_6 olefins, C_3-C_5 paraffins and C_{6+} aliphatics and aromatics. The seven reaction rates are based on Langmuir-Hinshelwood expressions. All reactions are considered irreversible and the rate determining step for every reaction is the surface reaction.

Kagyrmanova et al [77] have used a kinetic model based on elementary steps for the dehydration of ethanol to ethylene. They use this model in the simulation of a tubular fixed-bed reactor. The catalyst employed in the experimental work, is alumina based. Their reaction network includes five elementary reaction steps:

$$C_2H_5OH \rightarrow C_2H_4 + H_2O$$
$$2C_2H_5OH \rightarrow (C_2H_5)_2O + H_2O$$
$$(C_2H_5)_2O \rightarrow 2C_2H_4 + H_2O$$
$$C_2H_5OH \rightarrow C_2H_4O + H_2$$
$$2C_2H_4 \rightarrow C_4H_8$$

The rate equations of these five elementary steps are used to build the kinetic model. The reaction rate coefficients are estimated using an Arrhenius equation.

These authors have not included adsorption into the reaction network, so it is not micro-kinetic, even though the surface reactions are based on elementary steps.

1.4.2 Microkinetic modeling

Micro-kinetic modelling is different from lumped modelling. Micro kinetic models take into account every elementary reaction that occurs during the overall process. This makes parameter estimation much more complicated. Micro kinetic models give information on the reaction mechanism (e.g. the rate determining steps) and because they yield fundamental kinetic information (e.g. the activation energy of the elementary reactions) extrapolation of the obtained results to reaction conditions far beyond the experimental settings is possible.

Up until this date, no sources on the micro kinetic modelling of ethanol conversion are available.

S.K. Mondal [78] uses a kinetic model to study the dehydration of butyl alcohols and isopropyl alcohol over alumina, titania and a cation exchange resin. In this model, the author incorporates adsorption, reaction and desorption steps. Thus, all elementary reaction steps are considered. Since both reactants and catalyst are different of those used during this research, only the modeling procedures can be compared.

Park et al [79] have used a micro-kinetic model for the methanol to olefins reaction over a HZSM-5 catalyst. These authors rigorously modelled the formation of primary products, DME and ethylene, using the Hougen-Watson formalism, while carbenium ion mechanisms account for the higher olefins formation.

The same method these authors used will be implemented to construct the micro-kinetic model of the ethanol to hydrocarbons reaction.

1.5 Scope of the thesis

The focus of this Master thesis is the catalytic conversion of ethanol to hydrocarbons. This reaction proceeds on zeolite catalysts and is analogous to the methanol to hydrocarbons process. The methanol reactions have got a wide attention in literature, but the sources on the ethanol process are relatively limited. For example, no microkinetic model is available today. This thesis aims to close this gap, by working on the kinetic modelling of the catalytic conversion of bioethanol on zeolites.

Previous research at the *Laboratory of Chemical Technology* [53] has shown metal-modified zeolite catalysts do not exhibit great influence on the reaction selectivity. During this Master Thesis, mainly unmodified HZSM-5 will be used. Since this type of catalyst is commercially available, it means the results of this thesis could be readily implemented in industrial practice. To examine the effect of the zeolite topology, H-mordenite and beta-zeolite are employed too. Two post-synthesis modification techniques are investigated: desilication and desilication with subsequent Al-ALD-treatment.

Experiments are performed over a wide range of experimental conditions, since the dehydration reaction of ethanol starts at relatively low temperatures, while temperatures up to 400°C are reported for the further conversion to higher hydrocarbons. [53, 64, 75]

Different feeds will be used during the experiments. The bulk of the experimental work will be performed with pure ethanol, but ethanol water mixtures will be employed to assess the effect of using bio-ethanol with a certain fraction of water in the mixture, eliminating the energy intensive separation steps from the process. Some experiments with DEE feed are performed to gain further insight in the dehydration mechanism. Because ethylene originating from the dehydration reaction is considered to be the reactant in the formation of higher hydrocarbons, some experiments using ethylene as feed are performed too. In this context,

ethylene, ethylene-water and ethylene-ethanol mixtures are fed to the reactor to thoroughly examine the effects of each compound. The experiments are discussed in Chapter 3.

Next, a micro-kinetic model will be constructed for the conversion of ethanol into hydrocarbons. A single-event methodology will be employed. This modelling effort is split into two sections: the dehydration reaction and the conversion to higher hydrocarbons. This simplification is based on the experimental observation that all ethanol is dehydrated towards ethylene before the offset of the further conversion to higher hydrocarbons.

Chapter 4 is dedicated to the dehydration model. Several reaction networks are proposed, based on the experimental work performed within the context of this thesis. Starting from the reaction mechanism, the reaction rate equation are constructed. These are then implemented in a micro-kinetic model in the commercially available software *AthenaVisualStudio* for parameter estimation. A posteriori model discrimination is performed to selected the best model.

The SEMK model for higher hydrocarbon formation is discussed in Chapter 5. After elucidating the single-event methodology, an extensive reaction network is generated using ReNeGeP, an in-house developed computer program. Using the experimental observations, this model will first be simplified and then used to construct the single-event micro-kinetic model.

1.6 Bibliography

1. Administration, U.S.E.I., *Biofuels Issues and Trends*, 2012. p. 46.
2. Hamelinck, C.N., G.v. Hooijdonk, and A.P.C. Faaij, *Ethanol from lignocellulosic biomass: techno-economic performance in short-, middle- and long-term.* Biomass and Bioenergy, 2005. **28**(4): p. 384-410.
3. Abril, D. and A. Abril, *Ethanol from lignocellulosic biomass.* Ciencia e investigación agraria, 2009. **36**: p. 163-176.
4. Wyman, C.E., *Ethanol from lignocellulosic biomass: Technology, economics, and opportunities.* Bioresource Technology, 1994. **50**(1): p. 3-15.
5. Méjean, A. and C. Hope, *Modelling the costs of energy crops: A case study of US corn and Brazilian sugar cane.* Energy Policy, 2010. **38**(1): p. 547-561.
6. Rao, E.V.V.P. *Sugarcane*. Available from: http://www.sugarcanecrops.com/.
7. Haro, P., P. Ollero, and F. Trippe, *Technoeconomic assessment of potential processes for bio-ethylene production.* Fuel Processing Technology, 2013. **114**(0): p. 35-48.
8. Kosaric, N., et al., *Ethanol*, in *Ullmann's Encyclopedia of Industrial Chemistry*2000, Wiley-VCH Verlag GmbH & Co. KGaA.
9. Melo, T.C.C.d., et al., *Hydrous ethanol–gasoline blends – Combustion and emission investigations on a Flex-Fuel engine.* Fuel, 2012. **97**(0): p. 796-804.
10. Kyriakides, A., et al., *Evaluation of gasoline–ethanol–water ternary mixtures used as a fuel for an Otto engine.* Fuel, (0).
11. Keil, F.J., *Methanol-to-hydrocarbons: process technology.* Microporous and Mesoporous Materials, 1999. **29**(1–2): p. 49-66.
12. Olsbye, U., et al., *Conversion of Methanol to Hydrocarbons: How Zeolite Cavity and Pore Size Controls Product Selectivity.* Angewandte Chemie International Edition, 2012. **51**(24): p. 5810-5831.
13. Bruscino, M., *Biorefineries: Fact or Fiction?* Hydrocarbon Processing, 2009: p. 65-70.
14. News, C.a.E. *Production: growth is the norm*. Output of chemicals increased across most products and in most countries, 2006.
15. Administration, U.S.E.I. *How much gasoline does the United States consume?* 2012; Available from: http://www.eia.gov/tools/faqs/faq.cfm?id=23&t=10.
16. Braskem. *History*. 2013; Available from: http://www.braskem.com.br/site.aspx/History-USA.
17. Donald E. Pearson, C.C.N.T.N., *Process for catalytic dehydration of ethanol vapor to ethylene*, 1983, US 2220430 (Nov, 1940) Stanley 585/639; US 2569092 (Sep, 1951) Deering 585/639; US 3388181 (Jun, 1968) Anspon 585/639: US.
18. Kojima, M.N., JP), Aida, Takahiro (Niitsu, JP), Asami, Yukio (Yokohama, JP), *Catalyst for production of ethylene from ethanol*, 1981, Nikki Chemical Co., Ltd. (Tokyo, JP): United States.
19. Group, C.E., *Ethylene from Ethanol*.
20. Le Van, M.R.M., CA), Dao, Le H. (Montreal, CA), *Ethylene light olefins from ethanol*, 1987, Institut Nationale de la Recherche Scientifique (Sainte-Foy, CA): United States.
21. Ruziska, P.A.K., TX, US), Jenkins, Christopher D. W. (Houston, TX, US), Lattner, James R. (Seabrook, TX, US), Nicoletti, Michael Peter (Houston, TX, US), Veraa, Michael J. (Houston, TX, US), Van Egmond, Cor F. (Pasadena, TX, US), *Converting methanol and ethanol to light olefins*, 2006: United States.

22. Minoux, D.P.d.C.d.F., B-7181 Familleureux, BE), Nesterenko, Nikolai (Boîte 21, bât. 32Chaussée de Namur, B-1400 Nivelles, BE), Vermeiren, Walter (Winningstraat 4, B-3530 Houthalen, BE), Van Donk, Sander (Avenue de la Ramée 32, B-1180 Uccle, BE), Grasso, Giacomo (81 Rue Bosquet, B-1060 Bruxelles, BE),, *PROCESS TO MAKE OLEFINS FROM ETHANOL*, 2010, Total Petrochemicals Research Feluy (Zone Industrielle C, 7181 Seneffe (Feluy), BE).
23. Coupard, V.V., FR), Guillon, Emmanuelle (Vernaison, FR), Maury, Sylvie (Charly, FR), Cadran, Nicolas (Oullins, FR), *PROCESS FOR THE PRODUCTION OF LIGHT OLEFINS FROM ETHANOL IN THE PRESENCE OF A MACROPOROUS CATALYST THAT COMES IN THE FORM OF BALLS*, 2011, IFP ENERGIES NOUVELLES (Rueil-Malmaison Cedex, FR): United States.
24. Batista, M.S., et al., *High efficiency steam reforming of ethanol by cobalt-based catalysts.* Journal of Power Sources, 2004. **134**(1): p. 27-32.
25. Gilson, J.-P., et al., *Zeolites for cleaner technologies : [lectures presented at the Poitiers school - the meeting Zeolites for Cleaner Technologies, a pre-conference school held in early July 2001 in Poitiers and organized before the 13th International Zeolite Conference (Montpellier, July 2001)]*2002, London: ICP, Imperial College Press.
26. Weitkamp, J., *Zeolites and catalysis.* Solid State Ionics, 2000. **131**(1–2): p. 175-188.
27. Rahimi, N. and R. Karimzadeh, *Catalytic cracking of hydrocarbons over modified ZSM-5 zeolites to produce light olefins: A review.* Applied Catalysis A: General, 2011. **398**(1–2): p. 1-17.
28. Van Borm, R., *Single-event microkinetics of hydrocarbon cracking on zeotype catalysts: effect of acidity and shape selectivity*, in *Faculty of Engineering and Architecture*2011, Ghent University: Ghent.
29. Van Borm, R., M.-F. Reyniers, and G.B. Marin, *Catalytic cracking of alkanes on FAU: Single-event microkinetic modeling including acidity descriptors.* AIChE Journal, 2012. **58**(7): p. 2202-2215.
30. Staudte, B., et al., *Detection of Lewis acid sites using NO as probe molecule.* Microporous and Mesoporous Materials, 2000. **40**(1–3): p. 1-7.
31. Lercher, J.A., C. Gründling, and G. Eder-Mirth, *Infrared studies of the surface acidity of oxides and zeolites using adsorbed probe molecules.* Catalysis Today, 1996. **27**(3–4): p. 353-376.
32. Gale, J.D., et al., *Methanol in microporous materials from first principles.* Catalysis Today, 1999. **50**(3–4): p. 525-532.
33. Shah, R., J. D. Gale, and M. C. Payne, *Comparing the acidities of zeolites and SAPOs from first principles.* Chemical Communications, 1997(1): p. 131-132.
34. Mark M. Green, H.A.W., *Organic Chemistry, Principles and Industrial Practice*2003, Weinheim: Wiley-VCH. 341.
35. Bekkum, H.v. *Introduction to zeolite science and practice*. 2001; Available from: http://search.ebscohost.com/login.aspx?direct=true&scope=site&db=nlebk&db=nlabk&AN=207250.
36. Weisz, P.B., *Molecular shape selective catalysis.* Pure and Applied Chemistry, 1980. **52**(9): p. 2091-2103.
37. Degnan Jr, T.F., *The implications of the fundamentals of shape selectivity for the development of catalysts for the petroleum and petrochemical industries.* Journal of Catalysis, 2003. **216**(1–2): p. 32-46.
38. Young, L.B., S.A. Butter, and W.W. Kaeding, *Shape selective reactions with zeolite catalysts: III. Selectivity in xylene isomerization, toluene-methanol alkylation, and*

toluene disproportionation over ZSM-5 zeolite catalysts. Journal of Catalysis, 1982. **76**(2): p. 418-432.
39. Mirth, G., J. Cejka, and J.A. Lercher, *Transport and Isomerization of Xylenes over HZSM-5 Zeolites.* Journal of Catalysis, 1993. **139**(1): p. 24-33.
40. de Almeida, J.G., et al., *Effect of pore size and aluminium content on the production of linear alkylbenzenes over HY, H-ZSM-5 and H-ZSM-12 zeolites: Alkylation of benzene with 1-dodecene.* Applied Catalysis A: General, 1994. **114**(1): p. 141-159.
41. Aguayo, A.T., et al., *Study of operating variables in the transformation of aqueous ethanol into hydrocarbons on an HZSM-5 zeolite.* Journal of Chemical Technology and Biotechnology, 2002. **77**(2): p. 211-216.
42. Ferreira Madeira, F., et al., *Ethanol transformation into hydrocarbons on ZSM-5 zeolites: Influence of Si/Al ratio on catalytic performances and deactivation rate. Study of the radical species role.* Applied Catalysis A: General, 2012. **443–444**(0): p. 171-180.
43. Johansson, R., et al., *The Hydrocarbon Pool in Ethanol-to-Gasoline over HZSM-5 Catalysts.* Catalysis Letters, 2009. **127**(1): p. 1-6.
44. Gayubo, A.G., et al., *Kinetic modelling for selective deactivation in the skeletal isomerization of n-butenes.* Chemical Engineering Science, 1997. **52**(16): p. 2829-2835.
45. Houžvička, J. and V. Ponec, *Skeletal Isomerization of Butene: On the Role of the Bimolecular Mechanism.* Industrial & Engineering Chemistry Research, 1997. **36**(5): p. 1424-1430.
46. Liang, W., S. Chen, and S. Peng, *A model for highly para-selective reactions in HZSM-5 zeolite catalyst.* Chemical Engineering Science, 1995. **50**(15): p. 2391-2396.
47. Van Mao, R.L. and J. Yao, *Kinetic study of n-butane aromatization on ZSM-5 and gallium bearing ZSM-5 catalysts.* Applied Catalysis A: General, 1991. **79**(1): p. 77-87.
48. Tuan, V.A., J.L. Falconer, and R.D. Noble, *Isomorphous substitution of Al, Fe, B, and Ge into MFI-zeolite membranes.* Microporous and Mesoporous Materials, 2000. **41**(1–3): p. 269-280.
49. Bi, J., et al., *C2–C4 light olefins from bioethanol catalyzed by Ce-modified nanocrystalline HZSM-5 zeolite catalysts.* Applied Catalysis B: Environmental, 2011. **107**(1–2): p. 68-76.
50. Calsavara, V., M.L. Baesso, and N.R.C. Fernandes-Machado, *Transformation of ethanol into hydrocarbons on ZSM-5 zeolites modified with iron in different ways.* Fuel, 2008. **87**(8–9): p. 1628-1636.
51. Lu, J., Y. Liu, and N. Li, *Fe-modified HZSM-5 catalysts for ethanol conversion into light olefins.* Journal of Natural Gas Chemistry, 2011. **20**(4): p. 423-427.
52. Machado, N.R.C.F., et al., *Obtaining hydrocarbons from ethanol over iron-modified ZSM-5 zeolites.* Fuel, 2005. **84**(16): p. 2064-2070.
53. Stevens, S., *Transformation of bioethanol into hydrocarbons on modified ZSM-5*, in *Laboratory of Chemical Technology*2012, University of Ghent: Ghent. p. 98.
54. Tao, Y., et al., *Mesopore-Modified Zeolites: Preparation, Characterization, and Applications.* Chemical reviews, 2006. **106**(3): p. 15.
55. van Donk, S., et al., *Generation, Characterization, and Impact of Mesopores in Zeolite Catalysts.* Catalysis Reviews, 2003. **45**(2): p. 297-319.
56. Gil, B., et al., *Desilication of ZSM-5 and ZSM-12 zeolites: Impact on textural, acidic and catalytic properties.* Catalysis Today, 2010. **152**(1–4): p. 24-32.
57. Sree, S.P., et al., *Aluminium atomic layer deposition applied to mesoporous zeolites for acid catalytic activity enhancement.* Catalysis Science & Technology, 2011. **1**(2): p. 218-221.

58. Detavernier, C., et al., *Tailoring nanoporous materials by atomic layer deposition.* Chemical Society Reviews, 2011. **40**(11): p. 5242-5253.
59. Golay, S., R. Doepper, and A. Renken, *In-situ characterisation of the surface intermediates for the ethanol dehydration reaction over γ-alumina under dynamic conditions.* Applied Catalysis A: General, 1998. **172**(1): p. 97-106.
60. Golay, S., et al., *Influence of the catalyst acid/base properties on the catalytic ethanol dehydration under steady state and dynamic conditions. In situ surface and gas-phase analysis.* Chemical Engineering Science, 1999. **54**(15-16): p. 3593-3598.
61. Saito, Y. and H. Niiyama, *Reaction mechanism of ethanol dehydration on/in heteropoly compounds: Analysis of transient behavior based on pseudo-liquid catalysis model.* Journal of Catalysis, 1987. **106**(2): p. 329-336.
62. Nguyen, C.M., et al., *Physisorption and Chemisorption of Linear Alkenes in Zeolites: A Combined QM-Pot(MP2//B3LYP:GULP)–Statistical Thermodynamics Study.* The Journal of Physical Chemistry C, 2011. **115**(48): p. 23831-23847.
63. Nguyen, C.M., M.-F. Reyniers, and G.B. Marin, *Theoretical study of the adsorption of C1-C4 primary alcohols in H-ZSM-5.* Physical Chemistry Chemical Physics, 2010. **12**(32): p. 9481-9493.
64. Chiang, H. and A. Bhan, *Catalytic consequences of hydroxyl group location on the rate and mechanism of parallel dehydration reactions of ethanol over acidic zeolites.* Journal of Catalysis, 2010. **271**(2): p. 251-261.
65. Viswanadham, N., et al., *Catalytic performance of nano crystalline H-ZSM-5 in ethanol to gasoline (ETG) reaction.* Fuel, 2012. **95**(0): p. 298-304.
66. Gayubo, A.G., et al., *Kinetic modelling for the transformation of bioethanol into olefins on a hydrothermally stable Ni–HZSM-5 catalyst considering the deactivation by coke.* Chemical Engineering Journal, 2011. **167**(1): p. 262-277.
67. Costa, E., et al., *Ethanol to gasoline process: effect of variables, mechanism, and kinetics.* Industrial & Engineering Chemistry Process Design and Development, 1985. **24**(2): p. 239-244.
68. Ermakov, R.V. and V.A. Plakhotnik, *Conversion of lower alcohols into C2–C4 olefins over acid-base catalysts.* Petroleum Chemistry, 2008. **48**(1): p. 1-5.
69. Ingram, C.W. and R.J. Lancashire, *On the formation of C3 hydrocarbons during the conversion of ethanol using H-ZSM-5 catalyst.* Catalysis Letters, 1995. **31**(4): p. 395-403.
70. Madeira, F.F., et al., *Ethanol transformation over HFAU, HBEA and HMFI zeolites presenting similar Brønsted acidity.* Applied Catalysis A: General, 2009. **367**(1–2): p. 39-46.
71. Ben Tayeb, K., et al., *Ethanol transformation into higher hydrocarbons over HZSM-5 zeolite: Direct detection of radical species by in situ EPR spectroscopy.* Catalysis Communications, 2012. **27**(0): p. 119-123.
72. Däumer, D., K. Räuchle, and W. Reschetilowski, *Experimental and Computational Investigations of the Deactivation of H-ZSM-5 Zeolite by Coking in the Conversion of Ethanol into Hydrocarbons.* ChemCatChem, 2012. **4**(6): p. 802-814.
73. Aguayo, A.T., et al., *Catalyst deactivation by coking in the MTG process in fixed and fluidized bed reactors.* Catalysis Today, 1997. **37**(3): p. 239-248.
74. Gayubo, A.G., et al., *Kinetic model of the MTG process taking into account the catalyst deactivation. Reactor simulation.* Chemical Engineering Science, 1996. **51**(11): p. 3001-3006.
75. Gayubo, A.G., et al., *Kinetic Modelling of the Transformation of Aqueous Ethanol into Hydrocarbons on a HZSM-5 Zeolite.* Industrial & Engineering Chemistry Research, 2001. **40**(16): p. 3467-3474.

76. Chang, C.L., A.L. DeVera, and D.J. Miller, *A LUMPED KINETIC MODEL FOR DEHYDRATION OF ETHANOL TO HYDROCARBONS OVER HZSM-5.* Chemical Engineering Communications, 1990. **95**(1): p. 27-39.
77. Kagyrmanova, A.P., et al., *Catalytic dehydration of bioethanol to ethylene: Pilot-scale studies and process simulation.* Chem Eng J, 2011. **176-177**: p. 7-7.
78. Mondal, S.K., *Kinetics of dehydration of alcohols over different catalysts.* Journal of Chemical Engineering, 2005. **23**.
79. Park, T.Y. and G.F. Froment, *Kinetic modeling of the methanol to olefins process. 1. Model formulation.* Industrial & Engineering Chemistry Research, 2001. **40**(20): p. 4172-4186.

Chapter 2

Procedures

In this chapter, the procedures for synthesis and characterization of the catalysts, obtaining experimental data and microkinetic modeling are described.

The catalysts are synthesized and characterized partially at the Laboratory for Chemical Technology (LCT) of the University of Ghent and partially at the Centre for Surface Chemistry and Catalysis of the KU Leuven. The experimental testing is conducted in a tubular lab-scale reactor at the LCT. Analysis of the experimental data leads to the formulation of a kinetic model for the dehydration reaction. The kinetic parameters for this reaction are estimated using *AthenaVisualStudios*, a commercially available software program. Network generation for the conversion of ethanol into higher hydrocarbons uses in-house developed software of the LCT. The reaction network is implemented into regression software to obtain the kinetic parameters. This software uses a single event approach and is also created at the Laboratory for Chemical Technology.

2.1 Catalyst synthesis

The preparation of the HZSM-5 catalysts starts from commercially available NH_4-ZSM-5 precursor from Zeolyst, which is available at the laboratory with varying SiO_2/Al_2O_3 ratios (SiO_2/Al_2O_3=30 and 80). To transfer this material into the protonated form, calcination at high temperature is used. The zeolite is heated in air from room temperature to 550°C with a heating rate of 2°C per minute at ambient pressure. An isothermal period of 5h is foreseen. Gaseous NH_3 is released from the zeolite, replacing the ammonium-counterions by protons. It is important to employ a slow heating rate to avoid structural damage to the zeolite. H-mordenite and Beta-zeolite receive the same pre-treatment as the MFI zeolites.

The post-synthesis modified zeolites (desilicated and Al-ALD) are based on HZSM-5 with a SiO_2/Al_2O_3 ratio of 80. These catalysts (parent zeolite, desilicated ZSM-5 and ALD-treated desilicated ZSM-5) were delivered by the Centre for Surface Chemistry and Catalysis (KU Leuven) within the context of an cooperating FWO project.

2.2 Catalyst Characterization

Catalyst structure, the number of active sites and the strength of these sites all play a role in the catalytic properties of the material. Explaining experimental observations, certainly those concerning the comparison of different catalysts, is impossible without proper knowledge of the characteristics of the used materials.

2.2.1 Ammonia Temperature Programmed Desorption (NH_3-TPD)

NH_3-TPD can be used to identify the number of acid sites in a catalytic material as well as to measure the strength of these sites. Only sites that are accessible to ammonia can be studied by this technique. To perform the NH_3-TPD experiments, the Micromeritics Autochem 2910 setup is employed.

The catalyst is dried for 24h at 200°C. The dry catalyst mass is then determined using a balance with a 10^{-5}g precision.

The sample is loaded in a U-shaped tube (Figure 2-1) and placed in an oven. Quartz wool is used to prevent catalyst entrainment. All adsorbed molecules are removed by heating the sample to 520°C in a helium stream, the heating rate is 20°C.min^{-1}. The sample is kept at this temperature for 10min.

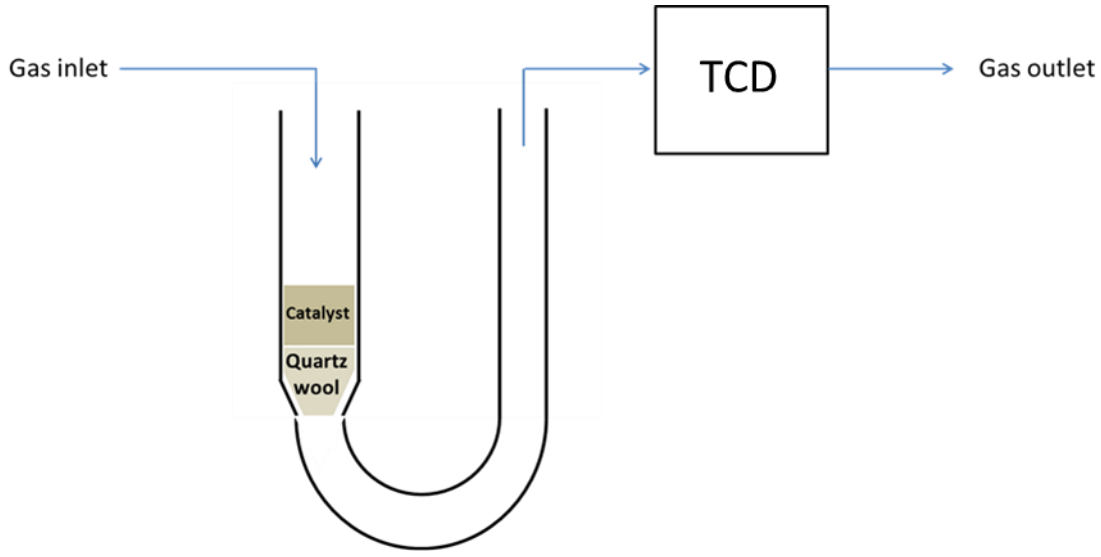

Figure 2-1 Schematic representation of the NH_3-TPD setup

The catalyst is cooled at 10°C.min^{-1} to 100°C using KwikCool, a cooling device employing an air flow through the oven. After cooling, diluted ammonia (4%NH_3 in He) is sent over the catalyst for a time span of 90min.The ammonia can both physisorb and chemisorb to the catalyst surface. Only the molecules which are chemisorbed to the acid sites of the catalyst are

of interest in the TPD-experiment. Before the desorption measurements start, non-adsorbed and physisorbed ammonia is purged from the catalyst pores by sending pure helium over the sample during 90min at 100°C.

Next, a temperature ramp is applied to the sample. The end-temperature of this step is 550°C, the heating rate can be varied if desired. Adsorption is entropic unfavorable, so at a specific temperature, the ammonia will start to desorb from the zeolite. This temperature depends on the interaction strength of ammonia and the acid site: the stronger the acidity of the site, the higher the temperature at which desorption initiates. A TCD-detector is used to analyze the outlet gas flow of the system, allowing detection of the ammonia.

The TCD-chromatogram of a HZSM-5 material has two distinct peaks (Figure 2-2). According to several authors [1-3] the first, low-temperature peak originates from ammonia that is weakly adsorbed to extra-framework structures. The second peak is caused by the Lewis and Brønsted acid sites.

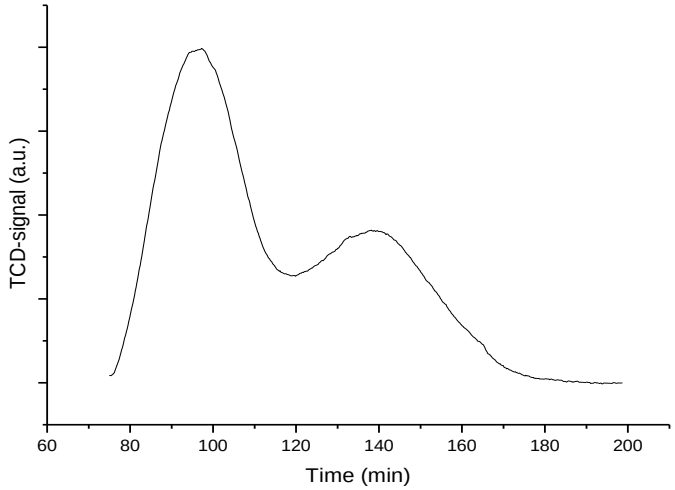

Figure 2-2 TCD chromatogram, experiment on HZSM-5 (SiO_2/Al_2O_3=30) heating rate of 5°C.min^{-1}

Niwa and Katada [3] used temperature programmed desorption to measure the acid properties of zeolites. They give several arguments for the identification of the low temperature peak as adsorption to extra-framework structures. It is removable by evacuation of the pores, while the high temperature peak is not. Also, in Na-type zeolites, only the low temperature peak is present. Since these zeolites have no acid sites, this identifies the low temperature peak as a non-acid peak. Topsøe et al [1] state that only the high temperature peak comes forth from acid sites with catalytic properties. Their observations are based on the MTH process. These authors observed that a decrease of the high temperature peak results in a comparable decrease in methanol conversion. From this, they deduce that the sites giving the high temperature desorption-peak are responsible for the methanol conversion.

Assuming each adsorption site is occupied by a single ammonia molecule, the number of acid sites can be determined by calculating the number of adsorbed ammonia molecules. This value can be computed from the peak-area in the TPD-profile. To correlate the area with a specified ammonia flow, a calibration experiment is conducted. During this calibration, a

known volume of an ammonia-helium mixture is sent over the TCD-detector. A factor correlating the amount of ammonia with the peak-area is calculated. Via this factor, the number of each type of acid sites in the catalyst sample will be determined. This number is then correlated to the mass of the sample to allow comparison of different catalysts. The calibration experiment is given in Appendix A.

2.2.2 Surface area and pore volume by N_2-adsorption/desorption

The specific surface area plays an important role in the number of molecules that can absorb on the catalyst surface. The total pore volume defines the maximal amount of components present in the catalyst pores. The volume of the different pore fractions (micro, meso and macro) are important when comparing the desilicated catalysts with the unmodified HZSM-5.

The catalyst specific surface area is measured via nitrogen-adsorption/desorption isotherms, using the assumptions proposed by Brunauer, Emmett and Teller in 1938. [4] These authors made five basic assumptions:

- ✓ Adsorption occurs on specific catalytic sites
- ✓ Surface (of the catalyst) is uniform
- ✓ No interaction between adsorbed molecules
- ✓ Multilayer adsorption is possible
- ✓ Only the first layer is influenced by the surface

Based on these hypotheses, the so-called B.E.T. equation is derived:

$$\frac{V_a}{V_m} = \frac{C(p\ \ p^0)}{(1-p\ \ p^0)(1-p\ \ p^0+C(p\ \ p^0))}$$

Where V_a is the total adsorbed volume, V_m the theoretical monolayer capacity, C a value indicating the surface-adsorbate interaction strength, p the pressure and p^0 the ambient pressure.

From this equation, V_m and C can be derived via regression. To simplify this regression, the expression is re-written in a linear form:

$$\frac{V_a}{V_m} = \frac{1}{V_m C} + \frac{C-1}{V_m C} \cdot \frac{p}{p^0}$$

From V_m, it is possible to calculate the specific surface area of the catalyst via:

$$a_s = \frac{V_m}{W} \cdot N_A \cdot \frac{1}{22414} \cdot a_m \quad [cm^2/g]$$

Where the units of V_m should be cm^3NTP and a_m is the area occupied by one gas molecule adsorbed to the surface in the closest packed order.

The experimental setup uses nitrogen as adsorbing gas at a temperature of 77K. Typical, the B.E.T. equation only gives satisfying regression results for relative pressures within the interval $0.05 < p/p° < 0.35$, hence the experiments are conducted in this range.

The equipment used for the experiments is the Micromeritics TriStar II. The software Micromeritics delivers with the experimental setup (Tristar) allows the analysis of a wide range of sorption isotherms and calculations. The B.E.T. equation is solely given as an example of perhaps the best known technique. Further techniques that are being used during this study are the t-plot to determine micro-pore volume and total volume and BJH for measuring the pore size distribution.

2.3 Experimental Setup

The experiments are conducted on a lab-scale tubular reactor. This reactor is located at the Laboratory for Chemical Technology of the University of Ghent. A flow scheme of the setup can be seen in Figure 2-3. The installation can be divided into three major parts: a feeding, a reaction and an analysis section.

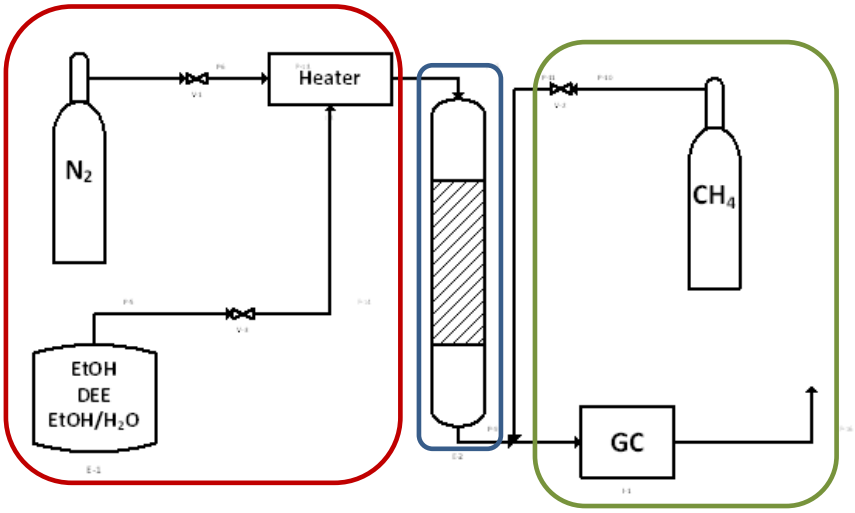

Figure 2-3 Schematic representation of the reactor setup: feeding section (red), reactor (blue) and analysis section (green)

2.3.1 Reactor feeding section

It is possible to connect gas cylinders with various gasses. Via thermal flow controllers (Brooks), these gasses are fed to the system. Four gas flows can be controlled simultaneously on the control panel. During the experiments the carrier gas (N_2) and in some cases ethylene as reactant are sent to the feeding section, while the internal standard (methane) is added in the analysis section. Calibration curves for the gas flow controllers are given in Appendix B.

Next to the gases, it is also possible to add liquid compounds to the feed stream. These are stored in a vessel. The liquid flow is controlled by a correolis controller (mini Cori-Flow, Bronkhorst). Liquid feeds are first sent to a vaporizer at a temperature above 190°C. Heating of the piping avoids condensation. This is accomplished via a tracing. Since this heating puts the piping at a temperature of about 130°C, any liquid with an atmospheric boiling temperature below this value could be used as feedstock. As liquid feed, pure ethanol, DEE and ethanol/water mixtures are used.

2.3.2 Reaction section

The reaction section consists of a tubular reactor made of stainless steel with a length of 0,2m, an external diameter of 0,01m and a wall thickness of 0,001m.

The reactor is placed in an electrically heated oven. The oven temperature is controlled by a PID-controller (Thermochem) regulated by a thermocouple. A second thermocouple is placed inside the reactor catalyst bed to measure the exact reaction temperature.

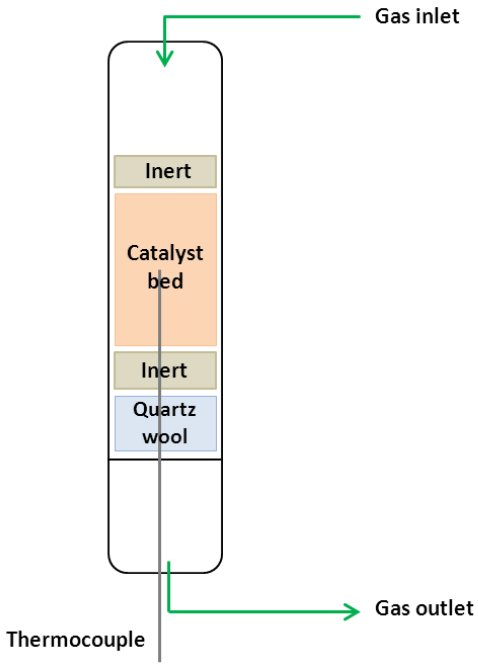

Figure 2-4 Representation of the catalyst bed layout

The catalyst is added to the reactor via a fixed sequence (Figure 2-4). First, quartz wool is added to avoid catalyst entrainment with the gas flow. On top of the quartz wool, inert is placed to make sure the catalyst bed is at the height of the thermocouple. A second function of this inert is eliminating the effect of the catalyst bed support on the flow pattern through the bed. Next, the bed itself is added. Above the catalyst, a second layer of inert material is positioned to ensure plug flow over the catalytic bed. The used inert material is α-alumina. Test runs showed no activity of this material to the conversion of ethanol at temperatures up to 450°C.

2.3.3 Analysis section

The analysis of the reactor effluent is performed online. Via a four-way valve, a sample of the product mixture can be sent over the gas chromatograph (Chrompack CP-9003). The GC uses an apolar capillary column (CP-SilPONA CB) to separate the components and is equipped with a flame ionization detector (FID).

Because of the small number and the easy-to-separate components in the product mixture, the dehydration reaction products can be separated at room temperature. To separate the hydrocarbons formed during the further conversion, especially ethane from ethylene and propane from propylene, cryogenic cooling to -50°C is employed, followed by a temperature ramp to 240°C. The pressure and the temperature programs for the dehydration and further conversion experiments are given in Table 2-1.

Table 2-1 Temperature programs of the GC-analyses

	Dehydration	**Conversion to higher hydrocarbons**
p	130kPa	130kPa
T_0	25°C	-50°C
Time on T_0	12min	4min
β	/	8°C.min^{-1}
T_{final}	/	240°C
Time on T_{final}	/	6min

2.4 Data gathering and analysis

2.4.1 Intrinsic kinetics

Doing experiments aiming at micro kinetic modeling, it is important to collect intrinsic kinetic data on the chemical reactions. The term intrinsic kinetics means no effect of transport phenomena may influence the measurements, so the measured reaction rates are purely determined by the fundamental chemical reaction parameters (e.g. activation energy).

Two types of transport limitations can appear in the reactor: energy (i.e. heat) and mass transport limitations. The experiments must be conducted in such way no problems arise.

To eliminate the effects of heat transport in the catalyst bed, the zeolite is diluted with α-alumina. This dilution ensures a good evacuation of reaction heat from the bed and guarantees good external and radial heat transport. Due to the small size of the catalyst pellets (300-500μm), internal heat transport doesn't cause problems either.

Mass transport must be considered on two scales: external transport from the bulk gas phase to the catalyst particle and internal mass transport inside the catalyst. The internal mass transport limitation can be kept small by using small catalyst particles. Care must be taken that the particle size is not too small or this might cause a too high pressure drop. The final choice on the particle size is thus a tradeoff between transport limitations and pressure drop. External mass transport is controlled by the flow rates.

Correlations from literature are used to check for plug flow, isothermal operation and transport limitations. [5, 6]

The first criterion assures the reactor operates in a plug flow regime. To achieve this, the effect of the reactor inlet, outlet and wall on the flow pattern must be limited. The criterion is:

$$\frac{d_t}{d_p} > 10 \;\; and \;\; \frac{L_B}{d_p} > 50$$

With d_t the reactor diameter, d_p the particle diameter and L_B the length of the catalyst bed.

The plug flow reactor is considered isothermal when the effect of the temperature gradient on the reaction rate is smaller than 5%. This criterion leads to correlations for both radial and axial conditions.

The axial condition is directly related to the dilution of the catalyst bed. A maximal bed dilution (b_{max}) is stipulated via the correlation:

$$b_{max} = \frac{0.004 L_B \, \varepsilon \;\; d_p}{1 + 0.004 L_B \, \varepsilon \;\; d_p}$$

L_B is the length of the undiluted catalyst bed. This correlation ensures the effect of diluting the catalyst bed on the conversion remains lower than 10% of the relative experimental error ε.

For radial isothermal conditions, the reaction is considered to be a stoichiometric singular reaction:

$$r_v = A e^{-E_a \;\; RT} f(C_A)$$

Under these conditions, the reactor is considered isothermal when following criterion is fulfilled:

$$\frac{|\Delta_r H| r_v^{obs} (1 - \varepsilon_B)(1 - b) d_t^2}{\lambda_{er} T_{wi}} < \frac{1.6 \frac{R T_{wi}}{E_a}}{1 + 8 \frac{\lambda_{er}}{\alpha_w d_t}}$$

In this inequality, α_w is the heat transfer coefficient between bed and reactor wall, λ_{er} the effective thermal conductivity of the catalyst bed, $1 - \varepsilon_B$ the fraction of the reactor volume occupied by the bed, $1 - b$ the fraction of the bed occupied by catalyst and T_{wi} the inner wall temperature.

After confirming the reactor is isothermal, the transport limitation on the particle scale are examined. Four criterions are used to check the absence of an external concentration and temperature gradient and of an internal diffusion limitation or temperature gradient respectively:

External

$$Conc.: \quad \frac{|R_{w,A}^{obs}|}{k_{fA} a_s C_{A,b}} < 0.03$$

$$Temp.: \quad \frac{|r_{w,s} - r_{w,b}|}{r_{w,b}} < 0.05$$

Internal

$$Dif.: \quad \frac{(n+1)\rho_p r_w^{obs}}{2a_v^2 D_{eA} C_{A,s}} \ll 1$$

$$Temp.: \quad \left|\frac{2E_a \gamma}{5RT_s^2}\right| < 0.05$$

Based on the criterions described in this paragraph, it is concluded the experiments will yield intrinsic kinetic data.

2.4.2 Mixture compositions

The GC-chromatograms have to be translated into mixture compositions. To achieve this, the calibration factors for the different compounds must be known. These factors link the area beneath the chromatogram with a certain mass of product. During this thesis, the factors defined by Dietz et al [7] en Van Borm et al [8] were used as a starting point. Although the definition of the two sets of factors is slightly different concerning reference component and application, the values do not differ by much. Calibration runs on the test reactor show good results with the Dietz factors, hence these will be used, which are listed in Appendix C. An example of a chromatogram with identified peaks is given in Appendix D.

The composition of the product mixture is calculated by normalization:

$$x_k = \frac{A_k \; CF_k}{\sum_{i=1}^{n} A_i \; CF_i}$$

With CF_k the calibration factor belonging to component k, A_k the area of this component on the chromatogram and x_k the mass fraction of the compound.

Because water cannot be detected with FID, elemental balances must be used to calculate the complete composition of the outlet stream. The available balances are the carbon, oxygen and hydrogen balance, each is assumed to be closed during the calculations. Combining the carbon balance with the oxygen balance allows determination of the amount of water in the product mixture, while the hydrogen balance can be used to check this value.

Calculation of the mass outlet via normalization uses the elemental balances. Starting from the calculated mass percentages of the carbon components, their molar fraction is determined. Based on the reaction equations, the amount of produced water is computed. From the molar flow rates, the mass flow is calculated using the molecular mass of the components.

The normalization method can only be applied when the mass balance of the experiments is closed. Several reasons could lead to a non-closed mass-balance: leaks in the setup, wrong calibration factors, bad separation on the column, etc. To check the mass-balance, an internal standard (IS) is added to the mixture. The IS should be a component that is not reactive under the conditions of the product stream and has no or very little overlap with other components on the chromatogram. The chosen internal standard is methane. Because the outlet stream of the IS equals its inflow, the total outlet flow rate can be calculated from the mass fraction of the IS in the product mixture:

$$F_{w,tot}^{out} = \frac{F_{w,IS}}{x_{IS}}$$

From the total outlet flow rate and the mass fraction of the different compounds in this stream, the outlet flow rate of the different components can be calculated. The total mass inlet flow rate must equal the total mass outlet flow rate. If the deviation is smaller than 5%, the balance is said to be closed.

$$deviation = \frac{F_{w,tot}^{in} - F_{w,tot}^{out}}{F_{w,tot}^{in}} \cdot 100\%$$

2.4.3 Calculating conversion, yield and selectivity

The fractional ethanol conversion, X_{EtOH} is calculated via the molar in- and outlet flow rate:

$$X_{EtOH} = \frac{F_{mol,EtOH}^{in} - F_{mol,EtOH}^{out}}{F_{mol,EtOH}^{in}}$$

The selectivity is calculated on carbon basis from the molar flow rates of the reagent r and the product of interest p by next formula:

$$S_i = \frac{a_r}{a_p} \cdot \frac{F_{mol,p}^{out} - F_{mol,p}^{in}}{F_{mol,r}^{in} - F_{mol,r}^{out}}$$

Where a_r and a_p are the number of carbon atoms in the reagent and the product respectively.

Yield of a certain compound is expressed as the conversion multiplied with the selectivity of that compound:

$$Y_i = X_{EtOH} \cdot S_i$$

In the higher hydrocarbon regime, the product mixture will be characterized using the mass percentage of the compounds. Since the chromatographic analysis gives the mixture composition in terms of mass percentages, this approach allows for faster computation, eliminating several calculation steps.

2.4.4 Spacetime

Spacetime combines catalyst mass and molar reagent inlet flow rate, hence the units of spacetime are not seconds. The definition is as follows:

$$W \quad F_{feed}^0 = \frac{m_{cat}}{n_{feed}^0} \quad [kg_{cat} \cdot s \cdot mol_{Feed}^{-1}]$$

The spacetime quantifies the timeframe an average molecule has available for reaction and thus influences the conversion and selectivity.

2.5 Network generation and kinetic parameter estimation

2.5.1 Overview

Figure 2-5 gives an overview of the procedure to calculate the optimal parameter estimations. The basic information can be subdivided into three categories. The experimental inputs are the operating conditions and the experimentally observed outlet flow rates. The model input comprises the model parameter values for both catalyst descriptors (the pre-exponential factors and adsorption coefficients) and kinetic descriptors (activation energies of the elementary reactions).The reaction network generation provides these elementary reactions and allow the constructing of reaction rate equations. Based on the gathered knowledge, model production rates are calculated. Via the reactor model, these yield the calculated outlet flow rates. By comparing experimental and modeled outlet flow rates, the parameters are optimized in an iterative process.

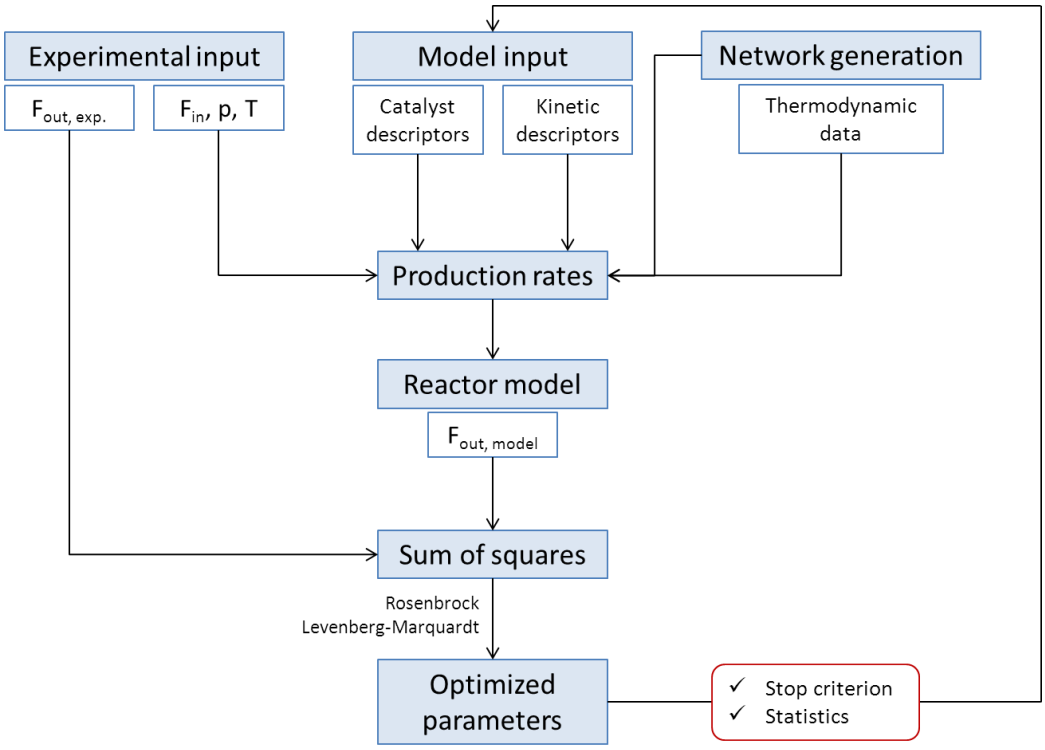

Figure 2-5 Schematic representation of the parameter estimation

2.5.2 Network generation

2.5.2.1 Dehydration

Network generation for the dehydration reaction is performed manually, based on experimental observations and literature articles. Since only one reagent (EtOH) and three products (DEE, ethylene and water) have to be considered, the reaction network has a rather limited number of elementary reactions. Hence manual network construction remains feasible. Reactions and reaction rate equations are given in Appendix E.

2.5.2.2 Further conversion to higher hydrocarbons

The large amount of reactions in the conversion of ethanol to higher hydrocarbons necessitates the use of a computer algorithm to build the reaction network and to generate the corresponding rate equations. The method is based on binary relation matrices, also known as Boolean relation matrices.

Every hydrocarbon is described by a binary matrix. A one means there is link between two carbon atoms, a zero indicates the absence of such linkage. An auxiliary vector defines the character of the carbon species, for example, the position of the charge on a carbocation.

An example of a molecule representation can be seen in Figure 2-6 for 3-methylheptane. Numbering is added to the structure of the molecule to ease identification of the matrix elements. In practice the sequence of the numbers can be randomly chosen, but within a program a standardized method should be used.

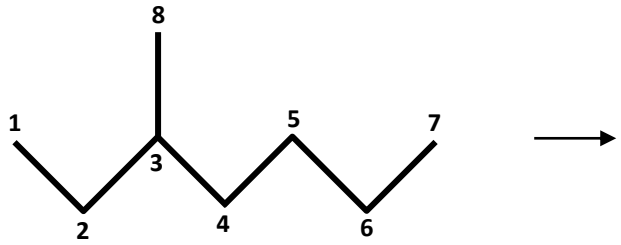

	1	2	3	4	5	6	7	8
1	0	1	0	0	0	0	0	0
2	1	0	1	0	0	0	0	0
3	0	1	0	1	0	0	0	1
4	0	0	1	0	1	0	0	0
5	0	0	0	1	0	1	0	0
6	0	0	0	0	1	0	1	0
7	0	0	0	0	0	1	0	0
8	0	0	1	0	0	0	0	0

Figure 2-6 Illustration of the translation of a hydrocarbon into a boolean matrix

The elementary step approach is employed while defining the reaction network. Reactions such as “cracking” are subdivided into several elementary reactions. These reactions can be common between different overall reactions. Although a huge number of elementary steps may be present in a reaction network, they belong to a limited set of reaction types. The network generated by the computer algorithm will use these elementary reactions, which are characterized by matrices in a similar way as the hydrocarbon species. Every type of elementary reaction has its own descriptors. Definitions and detailed methodology can be found in literature. [9, 10]

The in-house developed network generation software *ReNeGeP* is based on the above described procedure. The program needs some specifications as input, such as the maximum carbon number and the types of elementary reactions allowed in the network. The maximal carbon number is determined by experimental observations and set to be nine. It is used to create a stopping criterion for the generation algorithm. The elementary reactions are defined by the catalysts active sites. Acidic and metallic sites each catalyze specific elementary reaction steps. Since only acidic sites are available on the catalysts employed during the experiments, only carbocation chemistry is allowed in the program. The enabled elementary reactions are (de)protonation, hydride shift, hydride abstraction and donation, methyl shift, PCP branching, oligomerization, β-scission, cyclization and aromatization. When a reaction can yield several products, only the most stable one will be introduced in the network.

2.5.3 Parameter estimation

The kinetic parameters are estimated by minimizing an objective function: [11]

$$S\ \underline{\beta}\ = \underline{\varepsilon}^T \underline{\varepsilon}\ \overset{\underline{\beta}}{Min}$$

In this expression, $\underline{\beta}$ is the set of model parameters and ε the experimental error. This minimization corresponds to searching the model parameters that yield the minimal squared error between model calculations and observed values.

For the dehydration, the parameter estimation is performed with the commercially available software *AthenaVisualStudio*, where the kinetic model must be entered using Fortran code language. The program then minimizes the objective function and yields parameter estimations. Some statistical tests are computed by the program too. These tests will be discussed in the paragraph on statistical testing. *AthenaVisualStudio* uses the DDAPLUS algorithm for parameters estimation and sensitivity analysis. This algorithm is based on work by Petzold et al [12] and Caracotsios et al [13, 14].

The enormous amount of elementary reaction steps in the reaction network of the conversion to higher hydrocarbons makes the estimation of every individual parameter non-feasible. That is why the single event methodology is applied to reduce the number of parameters. This methodology will be addressed in detail in the chapter on the micro kinetic modeling of the conversion to higher hydrocarbons.

2.5.4 Statistical testing

Statistical tests are computed for the estimated model parameters to evaluate the results. The quality of the regression is evaluated via the multiple correlation coefficient, the significance of the global regression is tested via a F-test and the individual parameters via a Student's t-test. [11]

The multiple correlation coefficient is the ratio of the regression sum of squares and the sum of squares of the observed values:

$$R^2 = \frac{\underline{\hat{y}}^T \underline{\hat{y}}}{\underline{y}^T \underline{y}}$$

Where $\underline{y}$ stands for the observed values and $\underline{\hat{y}}$ for the model predicted values. R^2 is a number between zero and one. The closer to one, the better the overall quality of the regression.

The significance test is calculated through the ratio of the regression's sum of squares and the residual sum of squares, each divided by its respective degrees of freedom, under the hypothesis that all model parameters are equal to zero. This ratio suffices the definition of a F-distribution:

$$F_C = \frac{\frac{\underline{\underline{y}}^T \underline{\underline{y}}}{p}}{\frac{\underline{\underline{y}}^T \underline{\underline{y}} - \underline{b}^T \underline{X}^T \underline{\underline{y}}}{n-p}} \sim F(p, n-p)$$

With n the number of experiments, $\underline{b}$ the model parameter estimations $\underline{X}$ the matrix of independent variables and p the number of different experimental settings. If the value of F_C is sufficiently larger than the tabulated value of F(p,n-p) the hypothesis can be discarded and not all model parameters are equal to zero at the same time. This test is usually calculated for a probability value of 95%.

The significance test on the individual parameter estimations is based on following formula:

$$t = \frac{b_i - \beta_i}{s(b_i)} = \frac{b_i - \beta_i}{\sqrt{V_{ii}}} \sim t(n-p)$$

This value is calculated for the i^{th} estimated model parameter b_i, β_i is the exact parameter value, $s(b_i)$ is the estimated standard deviation and V_{ii} is the i^{th} diagonal element of the variance matrix. The t-value is calculated under the hypothesis that the exact parameter is equal to zero. If the value is sufficiently larger than the tabulated value, the parameter is not zero. The test is also mostly performed with a probability of 95%.

2.6 Bibliography

1. Topsøe, N.-Y., K. Pedersen, and E.G. Derouane, *Infrared and temperature-programmed desorption study of the acidic properties of ZSM-5-type zeolites.* Journal of Catalysis, 1981. **70**(1): p. 41-52.
2. Anderson, J.R., et al., *Reactions on ZSM-5-type zeolite catalysts.* Journal of Catalysis, 1979. **58**(1): p. 114-130.
3. Niwa, M. and N. Katada, *Measurements of acidic property of zeolites by temperature programmed desorption of ammonia.* Catalysis Surveys from Asia, 1997. **1**(2): p. 215-226.
4. Brunauer, S., P.H. Emmett, and E. Teller, *Adsorption of Gases in Multimolecular Layers.* Journal of the American Chemical Society, 1938. **60**(2): p. 309-319.
5. Berger, R.J., et al., *Eurokin. Chemical Reaction Kinetics in Practice.* CATTECH, 2001. **5**(1): p. 36-60.
6. Marin, G.B., *Cursus chemische reactoren*. 2011.
7. Dietz, W.A., *Response Factors for Gas Chromatographic Analyses.* Journal of Chromatographic Science, 1967. **5**(2): p. 68-71.
8. Van Borm, R., *Single-event microkinetics of hydrocarbon cracking on zeotype catalysts: effect of acidity and shape selectivity*, in *Faculty of Engineering and Architecture*. 2011, Ghent University: Ghent.
9. Clymans, P.J. and G.F. Froment, *Computer-generation of reaction paths and rate equations in the thermal cracking of normal and branched paraffins.* Computers & Chemical Engineering, 1984. **8**(2): p. 137-142.
10. Baltanas, M.A. and G.F. Froment, *Computer generation of reaction networks and calculation of product distributions in the hydroisomerization and hydrocracking of paraffins on Pt-containing bifunctional catalysts.* Computers & Chemical Engineering, 1985. **9**(1): p. 71-81.
11. Thybaut, J., *Kinetische Modelbouw en Simulatie*. 2011: Ghent. p. 176.
12. Petzold, L.R., *A description of DASSL: a differential/algebraic system solver.* 10th IMACS World Congress on System Simulation and Scientific Computation, 1982: p. 430-2 vol.12 vol.1.
13. Caracotsios, M. and W.E. Stewart, *Sensitivity analysis of initial value problems with mixed odes and algebraic equations.* Computers & Chemical Engineering, 1985. **9**(4): p. 359-365.
14. Caracotsios, M. and W.E. Stewart, *Sensitivity analysis of initial-boundary-value problems with mixed pdes and algebraic equations: Applications to chemical and biochemical systems.* Computers & Chemical Engineering, 1995. **19**(9): p. 1019-1030.

Chapter 3

Experimental results

From the different catalysts available at the laboratory, ZSM-5 with a SiO_2/Al_2O_3 ratio of 30 is chosen as reference catalyst. The effects of several parameters on the conversion and selectivity are evaluated. The most important are the catalyst and the reaction conditions: temperature, space-time and partial pressure. Other effects such as water content of the feed mixture and co-feeding ethylene and water are also investigated.

3.1 Catalyst Characterization

A good knowledge of the properties of the catalytic material is important when comparing different catalysts or explaining experimental observations. The characterization techniques will also give an image of the effect of the catalyst modifications. Relating catalyst activity to the properties of the zeolite will yield valuable information that can be used when developing new catalysts.

For the specific case of acid catalysis using zeolites, two types of characteristics are important: acid properties and characteristics of the zeolite structure. Both surface area and porosity are important factors for the occurring reactions. The surface area is a vital measure when it comes to adsorption of reagents and reaction products, while the porosity –certainly the micropore distribution– gives an indication of the shape selectiveness of the material. Although shape selectivity is no specific aim in the ethanol to higher hydrocarbons process, it may play a role it the product distribution.

3.1.1 NH_3-TPD

The catalytic conversion of ethanol is an acid catalyzed process. The knowledge of the concentration of acid sites is important to compare different catalysts. When modified catalysts are used, the effects of this modification on the acid sites of the material are thus of interest. Table 3-1 gives the measured catalyst characteristics for each of the studied zeolites.

Table 3-1 Zeolite properties

	Brøndsted acid site density (mmol/g)	BET surface area (m^2/g)	Pore volume (ml/g)	
			Micro	Meso
ZSM-5 (SiO_2/Al_2O_3=30)	0.433	336	0.130	0.111
ZSM-5 (SiO_2/Al_2O_3=80) =parent	0.264	361	0.162	0.066
Desil. ZSM-5	0.219	370	0.132	0.363
Al-ALD ZSM-5	0.179	336	0.116	0.317
H-mordenite (SiO_2/Al_2O_3=20)	1.032	350	0.151	0.089
β-zeolite (SiO_2/Al_2O_3=25)	0.556	576	0.170	0.623

The acid sites in zeolites are positioned at the aluminum atoms. Hence, the catalyst with the largest alumina concentration is expected to have the highest concentration of acid sites. The measured values confirm the theory: the zeolites synthesized from commercial precursor show a decreasing acid site density with an increasing SiO_2/Al_2O_3 ratio. The obtained values correspond to those found in literature. [1-3]

According to the results of the NH_3-TPD, the desilication procedure leads to a small decrease in the number of Brøndsted acid sites. Although the only intension of the zeolite desilication is the removal of silicon atoms from the framework, a certain amount of aluminum atoms will inevitably be removed too. This drop in the number of aluminum atoms in the zeolite framework, will cause a similar drop in the number of acid sites, as is observed in Table 3-1.

The Al-ALD procedure aims at restoring the original catalyst acidity, or even raise the number of acid sites above that of the parent material. The measurements, however, show the contrary: a further decline in the number of acid sites. The Al-ALD catalyst also gives very low ethanol conversion when reactor experiments are performed.

An ^{27}Al-NMR is used to clarify these observations. Figure 3-1 shows the NMR-spectra of four catalysts: the parent material, the desilicated catalyst and two Al-ALD treated zeolites. The left-hand peak corresponds to 4-coordinated aluminum, i.e. aluminum in the zeolite framework, while the second peak is due to extra-framework Al_2O_3. Upon desilication, the framework aluminum decreases, as expected. A small amount of extra-framework aluminum compounds is formed in due course. The goal of Al-ALD is increasing the aluminum content in the zeolite framework. Apparently, something went wrong during the atomic layer deposition, leading to a catalyst with its pores largely blocked by alumina. After these observations, the Al-ALD catalyst is no longer used.

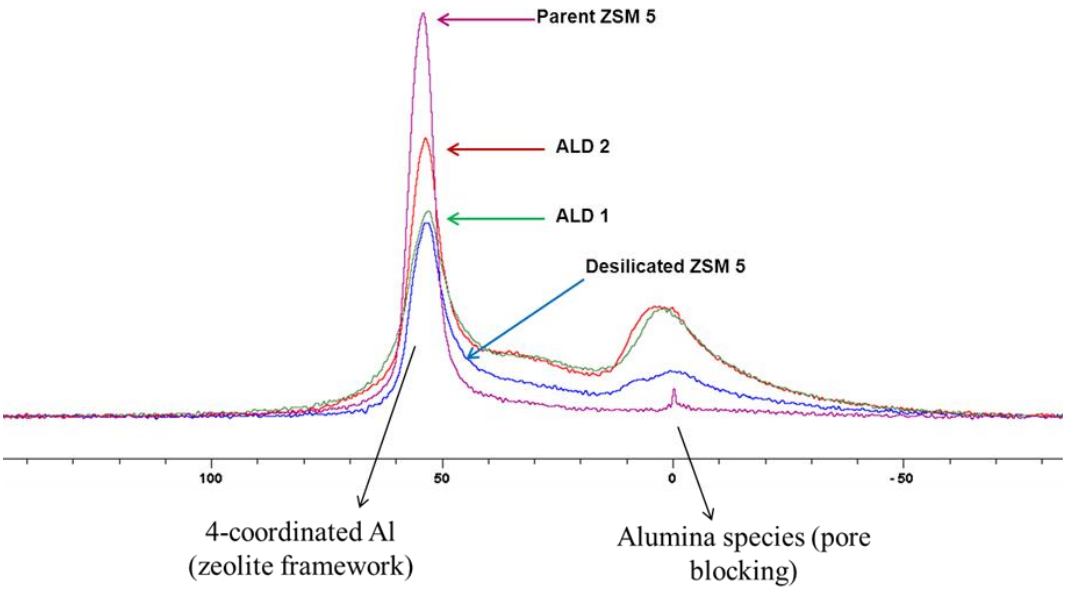

Figure 3-1 ^{27}Al-NMR spectrum of the parent ZSM-5 (SiO_2/Al_2O_3=80), the desilicated zeolite and the two Al-ALD treated catalysts

3.1.2 N_2-adsorption

Nitrogen adsorption can yield a lot of valuable information on the catalyst. In this work, the surface area and pore volume (both meso- and micro-pores) are of interest. Table 3-1 gives the results for the catalyst library. In literature, similar values are found. [3-7]

It is observed that the B.E.T. surface area and the pore volume are rather constant for the non-modified MFI-zeolites. Different ZSM-5 catalyst with a varying SiO_2/Al_2O_3 ratio have the same framework structure, even though the elemental composition of the framework differs. H-mordenite has similar values for B.E.T. surface and pore volume as HZSM-5, but β-zeolite has a far larger surface area and meso-pore volume.

Desilicating the MFI zeolite does not change the surface area significantly. Desilication alters the zeolite structure, so it is not obvious the area does not vary. An explanation is found by looking at the micro-pore volume. This is not changed much by desilication. An important part of the surface area is located in the micro-pores, so it remains rather constant.

To some extent, the previous argumentation also holds for the Al-ALD catalyst. The small decrease compared to the desilicated material is caused by a declining pore volume of both micro- and meso-pores. Smaller pores lead to a smaller surface area.

The effect of the modifications is mostly observed in the pore volume. The micro-pore volume decreases, while the meso-pore volume increases drastically. The pore volume is lowered by the ALD due to the deposition of extra material in the pores.

3.2 Different reaction regimes

To create an overview of the reaction regimes, experiments are conducted between 170°C and 350°C. The results are depicted in Figure 3-2 and are in accordance with previous work at the LCT on the catalytic conversion of ethanol on zeolites. [8]

The division between the dehydration regime and conversion to higher hydrocarbons can clearly be noticed on this figure. For temperatures up to 230°C, both the DEE and ethylene yield increase, while more and more ethanol is converted. At 240°C, a definite drop in the DEE yield occurs. At 250°C, ethylene is the sole reaction product. No ethanol or DEE are measured under these conditions, while the conversion of ethylene towards higher hydrocarbons is still insignificant. With increasing temperature, the ethylene yield decreases, producing mostly light olefins (propylene to pentene). The other product lumps still comprise less than 10% of the total product mixture at temperatures up to 350°C. The low yield of both paraffins and aromatics justifies their omission from the reaction network when building a simplified micro-kinetic model later on.

By considering ethylene as the reactant for the further conversion to higher hydrocarbons, the mass balance and selectivity are computed more straightforward, since only carbon and hydrogen have to be taken into account. Water, being a product of the dehydration, is only considered in calculating the partial pressures.

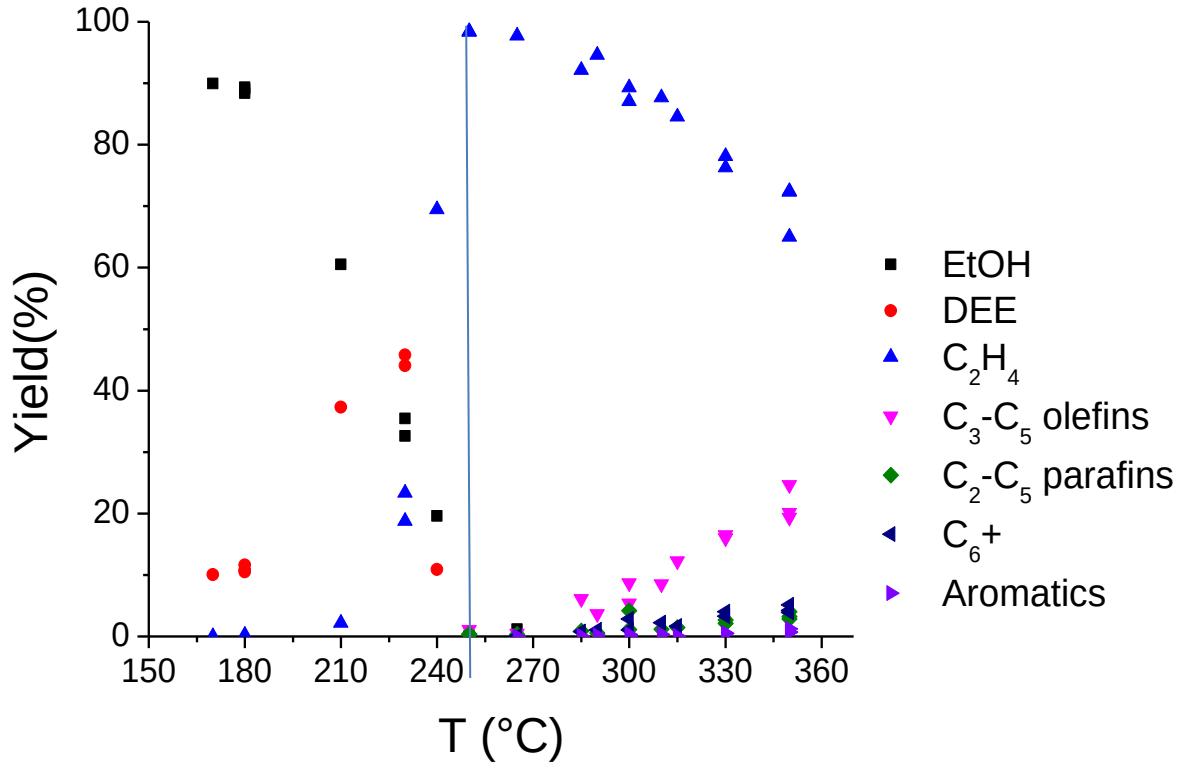

Figure 3-2 Temperature effect on product yield on HZSM-5 (SiO_2/Al_2O_3=30) W_{cat}/F^0=10 $kg_{cat}.s.mol_{EtOH}^{-1}$, p_{EtOH}=20kPa

3.3 Dehydration of ethanol

3.3.1 Spacetime

Ethanol conversion can be raised by increasing the reaction temperature, as shown in the previous paragraph, but conversion will also rise when the spacetime is increased at a constant temperature. The spacetime can be heightened by increasing the mass of the catalyst bed while keeping the reactant flow rate constant, or by decreasing the reactant flow rate at a constant catalyst mass. When studying selectivity as a function of the conversion, the conversion must be altered using the spacetime. Varying the temperature might change the favoured reaction pathway, thus muddling the conclusions drawn from the experiments.

In Figure 3-3 the results of experiments at 230°C on a HZSM-5 catalyst with a SiO_2/Al_2O_3 ratio of eighty are plotted. At this temperature, even the smallest spacetime implied during the experiments ($1{,}5 kg_{cat} \cdot s \cdot mol_{EtOH}^{-1}$) results in an ethanol conversion of about 20%. Diethyl ether is the sole reaction product up to a spacetime of $3 kg_{cat} \cdot s \cdot mol_{EtOH}^{-1}$. Above this value ethylene appears in the reaction product mixture. The ethylene yield rises continuously with rising spacetime, while the diethyl ether yield goes through a maximum at around $12{,}5 kg_{cat} \cdot s \cdot mol_{EtOH}^{-1}$ and becomes zero at spacetimes higher than $30 kg_{cat} \cdot s \cdot mol_{EtOH}^{-1}$. Translating these observations in terms of the selectivity of the reaction, increasing the spacetime – and thus the ethanol conversion – increases the selectivity towards ethylene, from 0% at low conversion to 100% at the highest values. It can be noted that at 230°C, only dehydration appears, even at the highest spacetimes. The selectivity towards ethylene reaches 100% at $30 kg_{cat} \cdot s \cdot mol_{EtOH}^{-1}$; no higher carbons are being formed yet.

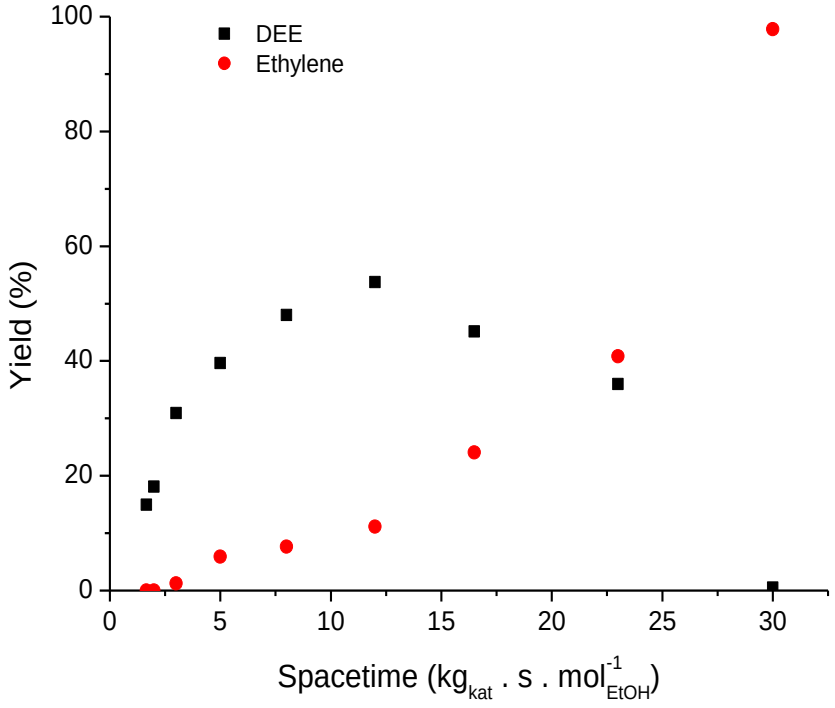

Figure 3-3 Yield of DEE and C_2H_4 on HZSM-5 (SiO_2/Al_2O_3 =80) (230°C, 20kPa EtOH)

3.3.2 Partial pressure of ethanol

The partial pressure of the reactant has an important effect on the reaction outcome. As shown in Figure 3-4, a higher partial pressure gives a higher ethanol conversion. Based on both thermodynamic and kinetic considerations, a higher reactant partial pressure will benefit the reaction from reactants to products. At a partial pressure of 14kPa, the conversion of ethanol starts to level off. When the catalyst surface is saturated, increasing the reactant partial pressure will no longer influence the concentration of active species, so at a specific set of reaction conditions, there is a maximum value to ethanol conversion.

As discussed in the paragraph on the spacetime, a higher ethanol conversion gives a higher selectivity towards ethylene (and lower selectivity towards DEE). Figure 3-4 shows the same trend.

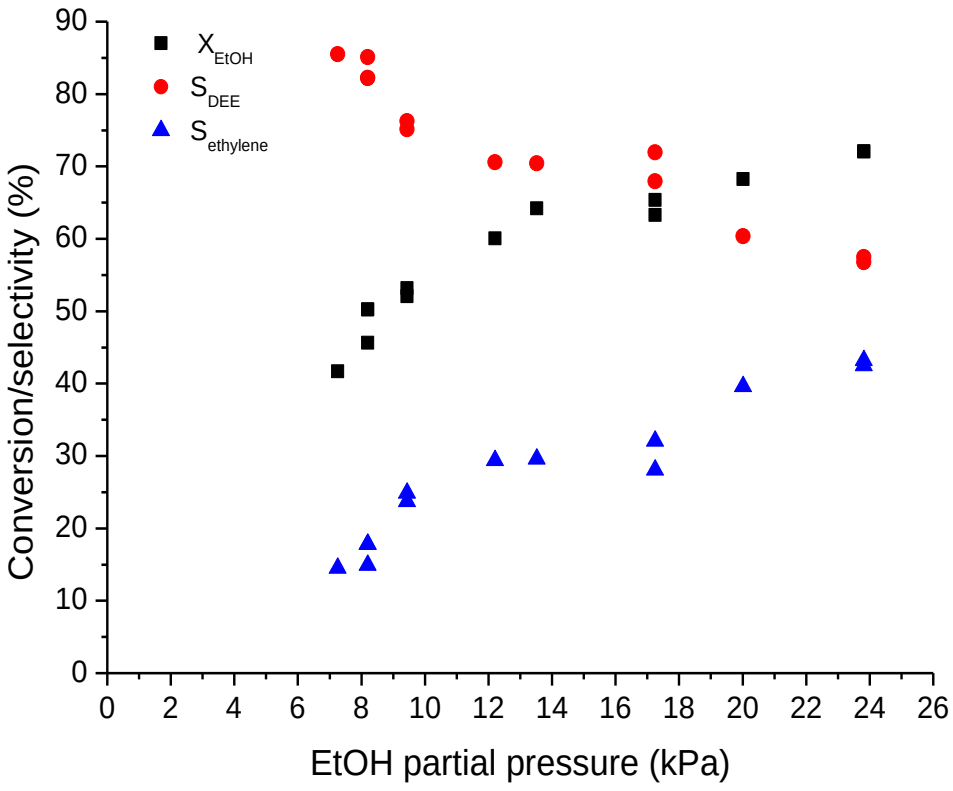

Figure 3-4 Effect of the ethanol partial pressure on the EtOH conversion and selectivity towards ethylene and DEE (W_{cat}/F^0=6,5 $kg_{cat}.s.mol_{EtOH}^{-1}$, T=230°C)

3.3.3 Water content of the feed mixture

Bioethanol produced by fermentation always contains a large amount of water. Even the most ethanol-tolerant yeasts and bacteria stop converting sugars to ethanol at ethanol concentrations above 20%. [9] Because water and ethanol form an azeotropic mixture, with 89,5mole% of ethanol, high purity ethanol can only be achieved via other separation techniques than classical distillation. Examples of these techniques are azeotropic distillation with benzene, molecular sieves or reverse osmosis. [9] A complex separation means a significant increase in process costs. For industrial application, it would be advantageous to use mixtures with low ethanol concentrations as reactor feed. Experiments with different ethanol/water mixtures as feed are performed in this context. To prevent condensation in cold spots, the amount of water is kept low compared to the fermentation mixture, but it is higher than the azeotropic composition. Experiments are designed to ensure ethanol spacetime and partial pressure are the same as for the experiments using pure ethanol.

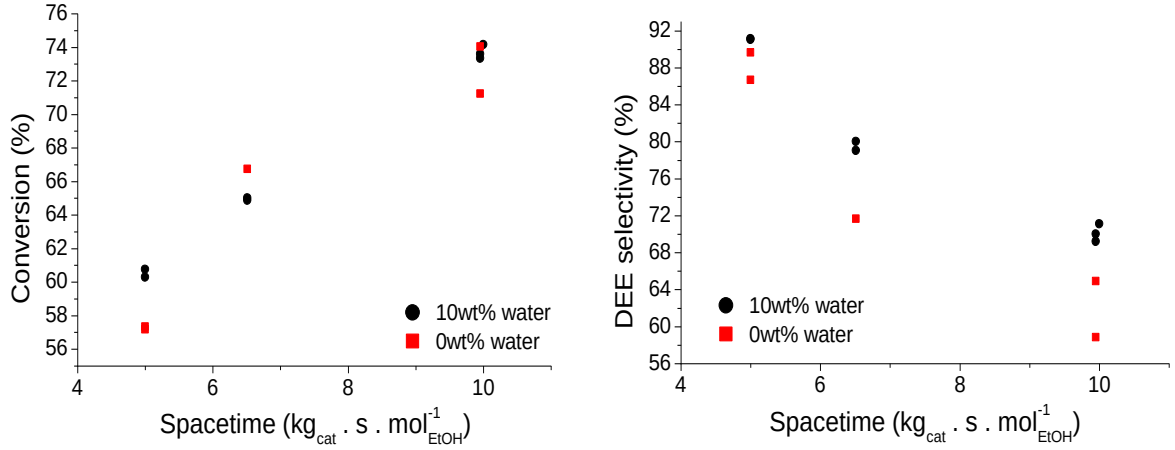

Figure 3-5 Conversion and selectivity towards DEE for pure EtOH feed and a 90/10wt% EtOH/water mixture (T=230°C, p_{EtOH}=20kPa)

Feeding a mixture with 10wt% water at 230°C does not influence the reaction outcome when compared to a pure ethanol feed. At this temperature, ethanol conversion is higher than 50%, meaning a significant amount of water is formed by the dehydration reaction. The additional water from the feed mixture has a small effect on the partial pressure of water. At 200°C, a small effect seems to be present, but no clear conclusions are possible. Further investigation is necessary.

3.3.4 DEE as feed component

To gain further insight in the reaction mechanism of ethanol dehydration, DEE is fed to the reactor. When constructing the dehydration reaction network, it is important to know whether DEE will react at those conditions.

A limitation of the experimental setup is observed when feeding DEE. The feed mixture must remain in the liquid phase until it is evaporated and mixed with the carrier gas in the evaporator. When a two-phase mixture is present before the evaporator, a pulsating flow results. The boiling point of DEE at ambient pressure is 34,6°C. Due to the tracing and heating around the feed piping, no good DEE experiments were possible.

Although this limitation makes quantitative conclusions regarding the reaction of diethyl ether on HZSM-5 impossible, a very important observation is made. When feeding DEE at conditions within the dehydration regime, both ethanol and ethylene are produced. Reactions of DEE resulting in ethanol and ethylene have to be considered in the reaction network for ethanol dehydration.

3.4 Conversion to higher hydrocarbons

3.4.1 Preliminary experiment

Preliminary experiments at high temperature are conducted. These experiments are used together with the calibration runs and previous work at the LCT [10] to identify the components in the product mixture. The product composition of this experiment at 350°C, 20kPa ethanol and a spacetime of 16.5 $kg_{cat}.s.mol_{EtOH}^{-1}$, is given in Figure 3-6. Under these reaction conditions, more than half of the product mixture still consists of ethylene. The second largest product lump is the light olefins (C_3-C_5) lump. Parafins, aromatics and heavy compounds are formed to a far lesser extent.

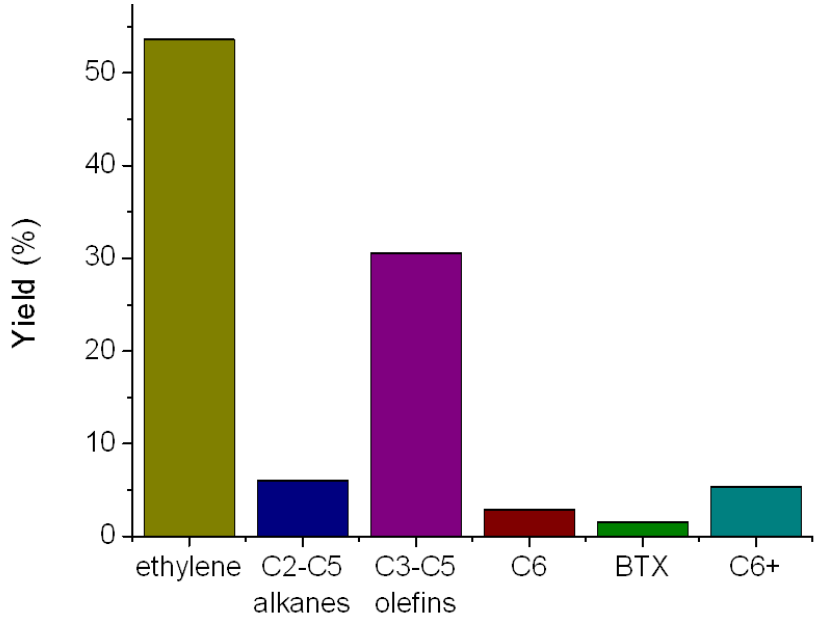

Figure 3-6 Product distribution of conversion to higher hydrocarbons on HZSM-5 (SiO_2/Al_2O_3=30) at: T=350°C, pp_{EtOH}=20kPa, W/F^0=16.5 $kg_{cat}.s.mol_{EtOH}^{-1}$

The significant formation of compounds with an odd carbon number is an important observation when constructing the reaction mechanism. These species cannot be formed directly from ethylene oligomerization, since this reaction only yields even carbon numbered molecules. Therefore, cracking of larger compounds or a hydrocarbon pool mechanism must be present to account for propene and the pentenes.

3.4.2 Stability of the catalyst

To investigate the catalyst stability, several experiments using the same reaction conditions are performed and plotted as a function of the time-on-stream. As long as these measurements form a line parallel to the x-axis, the catalyst is considered stable. As observed on Figure 3-7, the catalyst is stable for up to 12h.

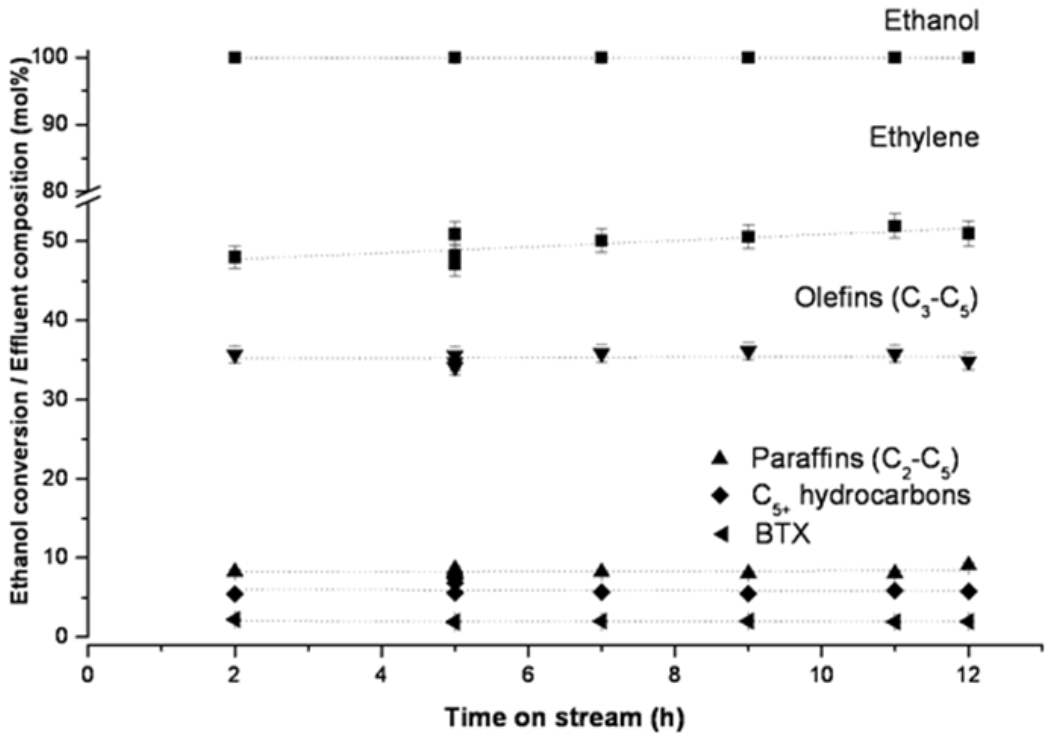

Figure 3-7 Catalyst performance as a function of time-on-stream

3.4.3 Spacetime

The effect of the spacetime is studied at several temperatures. The results are shown in Figure 3-8. This figure gives the selectivity towards ethylene. Since ethylene is the intermediate forming higher hydrocarbons, a decreasing ethylene selectivity is directly related to an increasing conversion to higher hydrocarbons.

As in the dehydration regime, a higher spacetime leads to higher conversion. This effect is very pronounced, looking at the curve for 350°C, at $10 kg_{cat}.s.mol_{EtOH}^{-1}$ the ethylene selectivity is higher than 70%, while at $16.6 kg_{cat}.s.mol_{EtOH}^{-1}$ it is about 50% .

At low spacetime, the effect of the temperature on the selectivity of ethylene is small. Nearly no further reaction occurs under these conditions. The time available for reaction appears to be smaller than the time scale on which the reactions proceed.

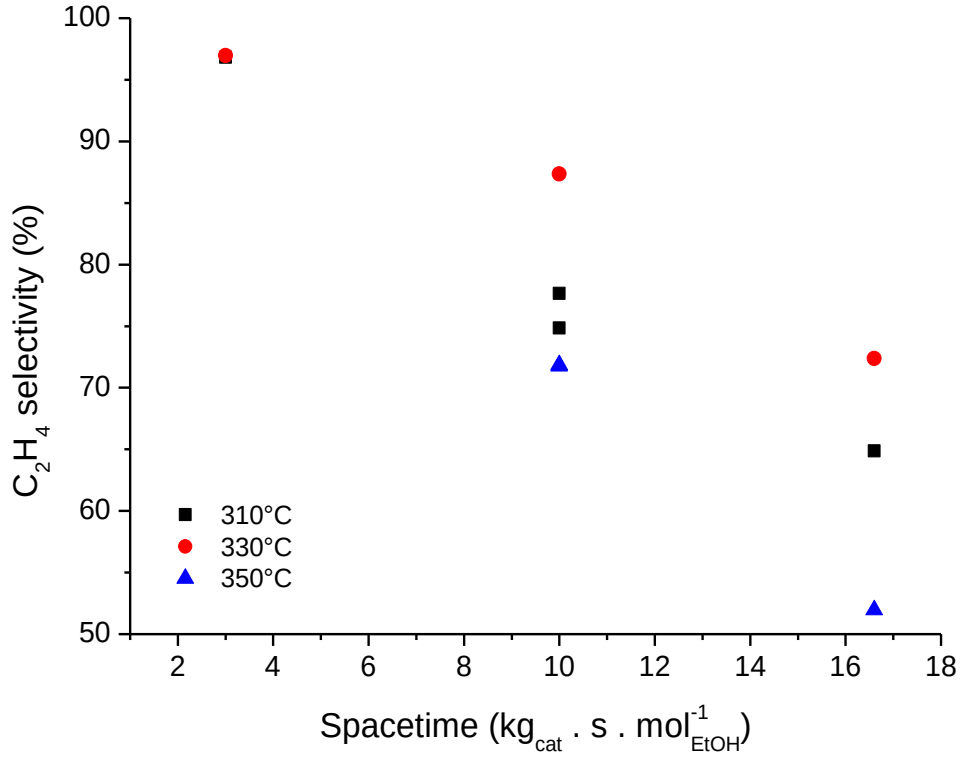

Figure 3-8 Conversion as function of spacetime and temperature for experiments on HZSM-5 (SiO_2/Al_2O_3=30) , pp_{EtOH}=20kPa

3.4.4 Partial pressure of ethanol

At higher temperatures, all ethanol is dehydrated towards ethylene and subsequently, ethylene converts into higher hydrocarbons (Figure 3-2). On Figure 3-9, the selectivity towards the different product lumps is plotted as a function of the ethanol partial pressure. This pressure is directly correlated with the partial pressure of ethylene upon dehydration, taking into account the production of one mole of water for every mole of ethylene.

Figure 3-9 shows a decreasing ethylene selectivity with a rising ethanol partial pressure. The same reasoning as for the dehydration reaction can be used to explain this: higher partial pressure favours the conversion from reactants to products. At high ethanol partial pressure (>30kPa) the selectivities towards the different product lumps remain constant. This is an indication that the catalyst surface is saturated. Further increasing the reactant concentration does not lead to more reaction, since ethanol cannot adsorb onto a free active site.

A slight decrease in the selectivity towards light olefins occurs at high ethanol partial pressure (>40kPa). The selectivity drops from 22% to 18%. Light olefins are intermediate species in the formation of the heavy hydrocarbons. Hence, increasing reaction leads to a decrease in selectivity towards these compounds. Apparently, there is not a specific product lump which is enlarged by the reaction of the light olefins.

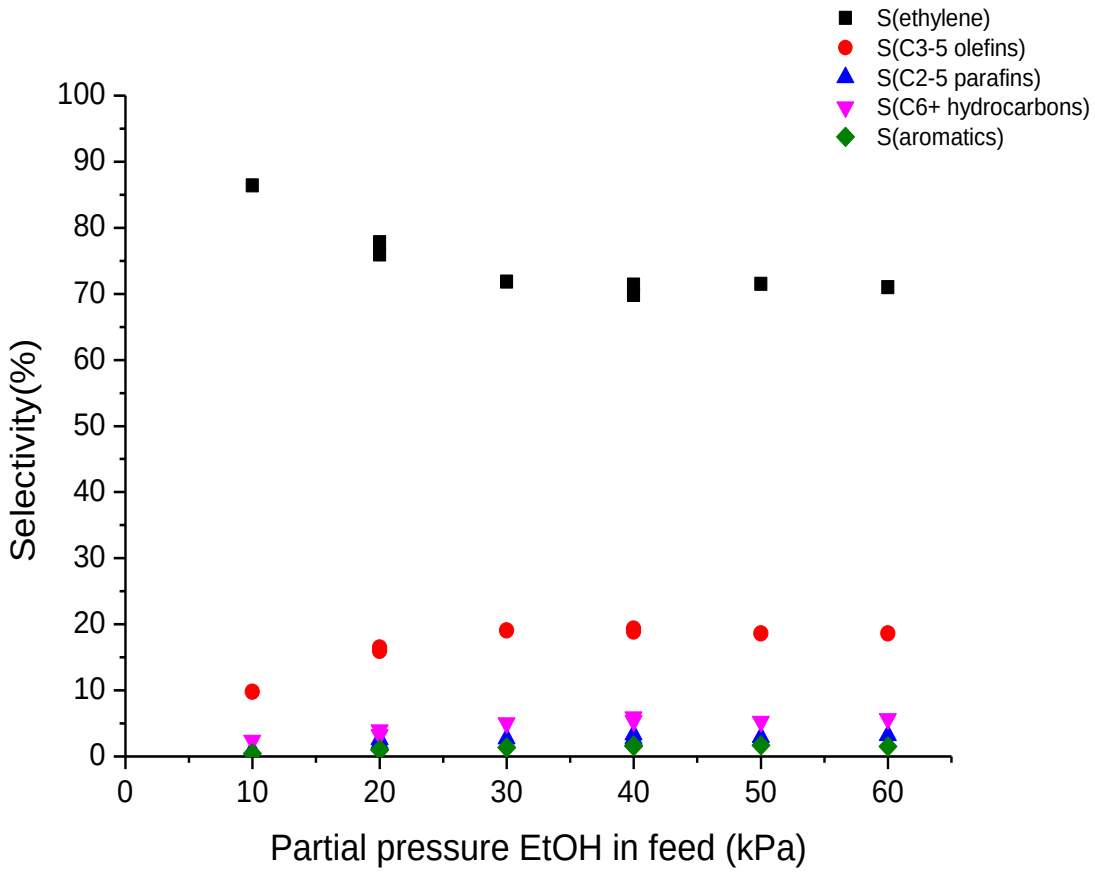

Figure 3-9 Effect of the partial pressure of EtOH in the feed mixture on the conversion and selectivities (W_{cat}/F^0=10 $kg_{cat}.s.mol_{EtOH}^{-1}$, T=330°C)

3.4.5 Ethylene conversion on HZSM-5

For the microkinetic modeling of the higher hydrocarbon formation, ethylene is considered to be the reactant. This assumption must be verified, hence some experiments with ethylene and ethylene-water mixtures are performed to compare the behaviour of these feeds to ethanol.

Figure 3-10 shows the ethylene conversion as a function of ethylene partial pressure for both pure ethylene and ethanol as feed. Compared to feeding ethanol, ethylene gives a much higher conversion at the same spacetime and partial pressure.

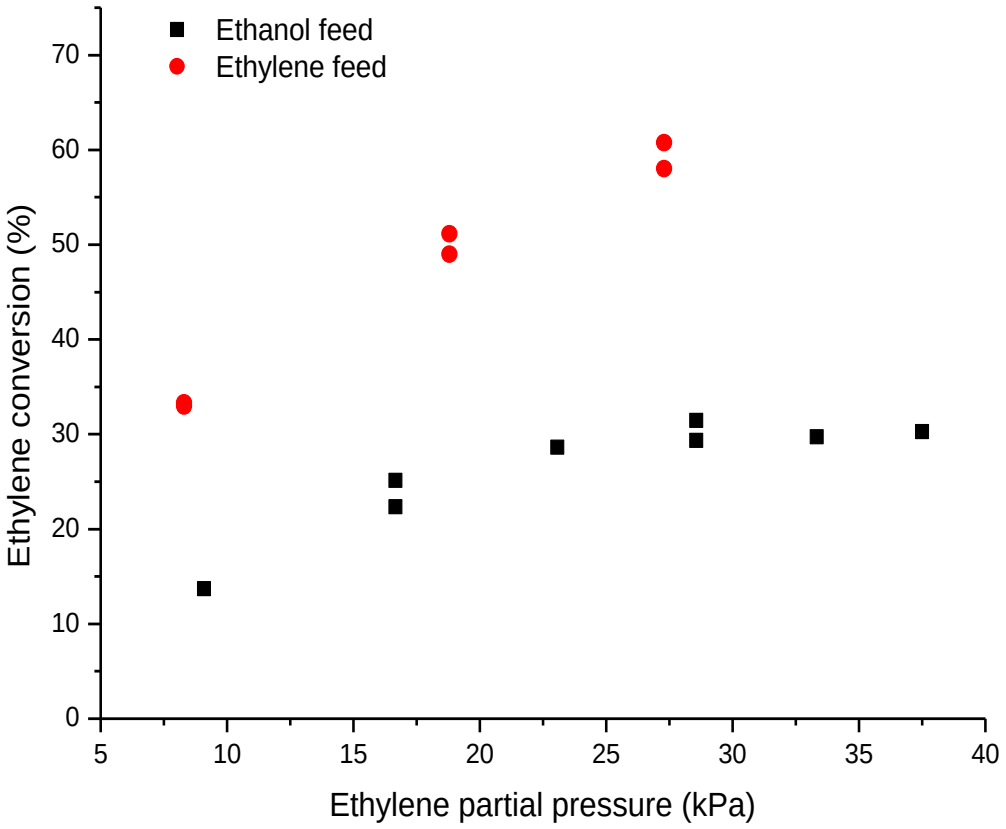

Figure 3-10 Comparison of the ethylene conversion for EtOH and ethylene feed on HZSM-5 (SiO_2/Al_2O_3=30) at W_{cat}/F^0=10 $kg_{cat}.s.mol_{EtOH}^{-1}$, T=330°C

To check whether the effect in Figure 3-10 is due to the presence of water from the dehydration reaction, an ethylene-water mixture is used as reactor feed. The composition of this mixture is equimolar in ethylene and water. The spacetime and ethylene partial pressure are the same as in the experiments with a pure ethylene feed.

If the difference between the two sets of experiments in Figure 3-10 is due to the presence of water from the dehydration reaction, these new experiments should give similar results as the ethanol experiments. If only spacetime and partial pressure of ethanol play a role, the results should be identical as those using pure ethylene.

Figure 3-11 shows water content has no effect on the ethylene conversion. Hence, water is not causing the difference in conversion between the experiments with ethanol and ethylene. This observation indicates the timescale for dehydration, although considerably smaller than the timescale of conversion to higher hydrocarbons, cannot be neglected and accounts for the reduced conversion when feeding ethanol.

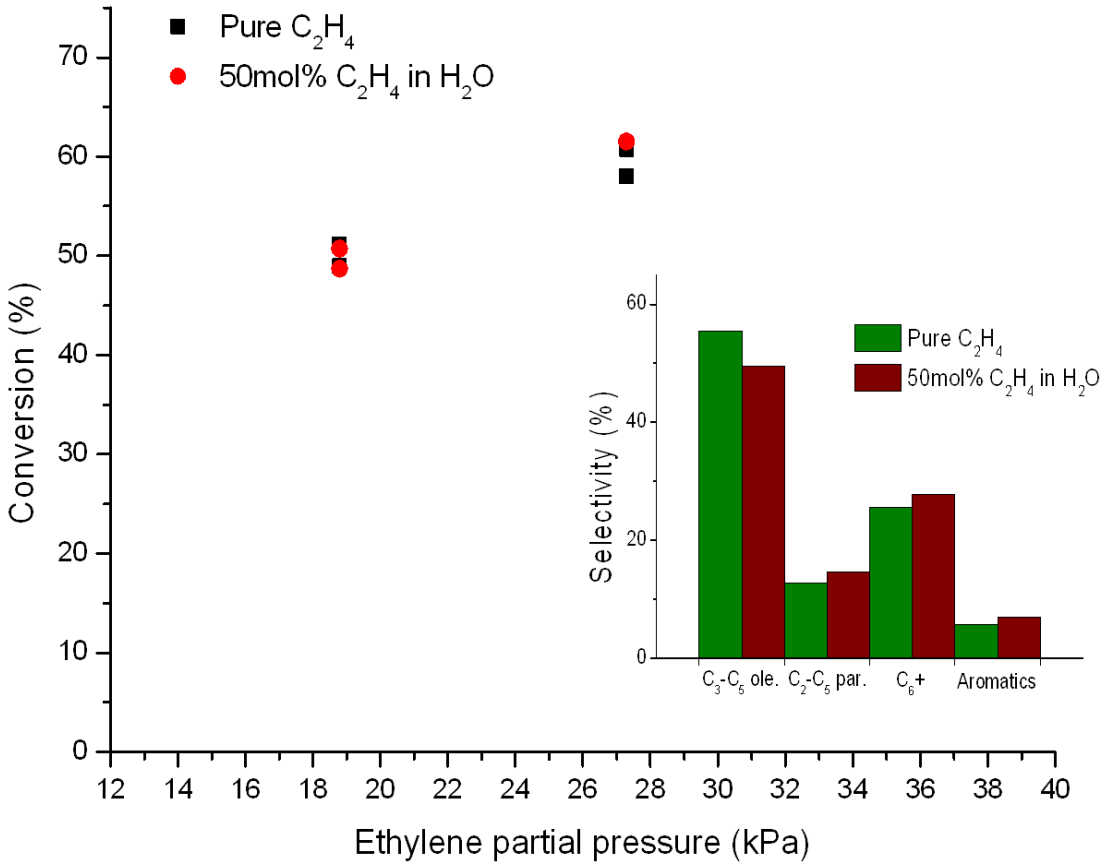

Figure 3-11 Effect of feeding a water/ethylene mixture on conversion and selectivity at 330°C, 27.3kPa and 10 $kg_{cat}.s.mol_{EtOH}^{-1}$

3.4.6 Product distributions

The evolution of the product distribution of the conversion of ethanol to hydrocarbons as a function of temperature has already been shown in Figure 3-2. Because of the low yield of most product lumps, no detailed information could be gathered from this figure, hence, a magnified view on the higher hydrocarbon lumps is given in Figure 3-12. The exact composition of this product mixture is very important. It is needed during the kinetic modeling of the process and it also defines how valuable the product stream is from an economical point of view. Mostly light olefins are being formed, light paraffins, heavy hydrocarbons and aromatics are formed to a far lesser extent.

Figure 3-13 shows the selectivity towards the different groups of the light olefins lump, being the most abundant product lump. The plot shows the C4 olefins are most abundantly formed, followed by propylene and the pentenes. Considering cracking reactions to be the main route for the production of odd carbon numbered light olefins, this observation makes sense. Butenes are formed via oligomerization of ethylene or cracking of C_8 components. Propylene can be formed via cracking of C_8, yielding a pentene molecule too. However, propylene is also formed by C_6 cracking, explaining the higher selectivity compared to pentene.

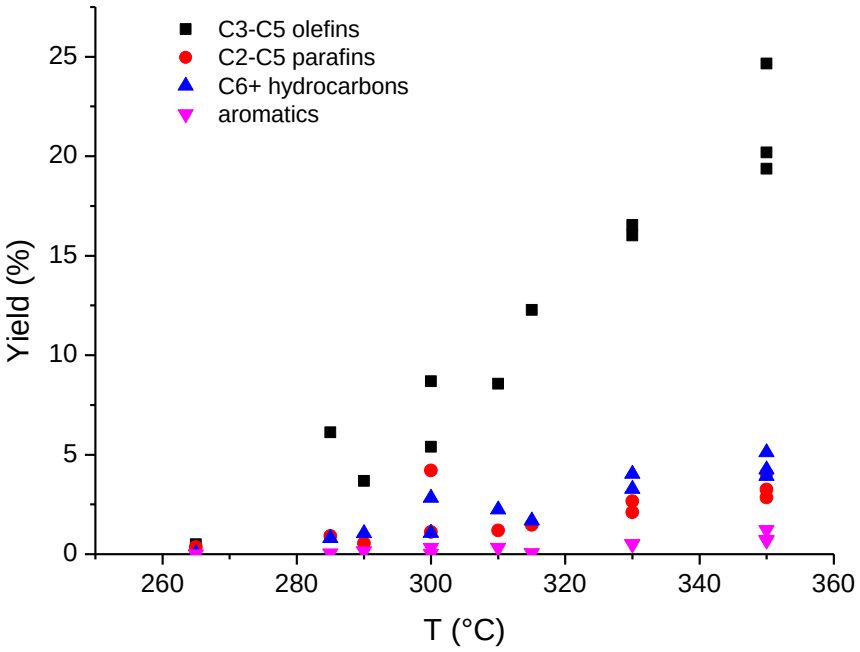

Figure 3-12 Yield of the different product lumps, experiment on HZSM-5 (SiO_2/Al_2O_3=30) W_{cat}/F^0=10 $kg_{cat}.s.mol_{EtOH}^{-1}$, p_{EtOH}=20kPa

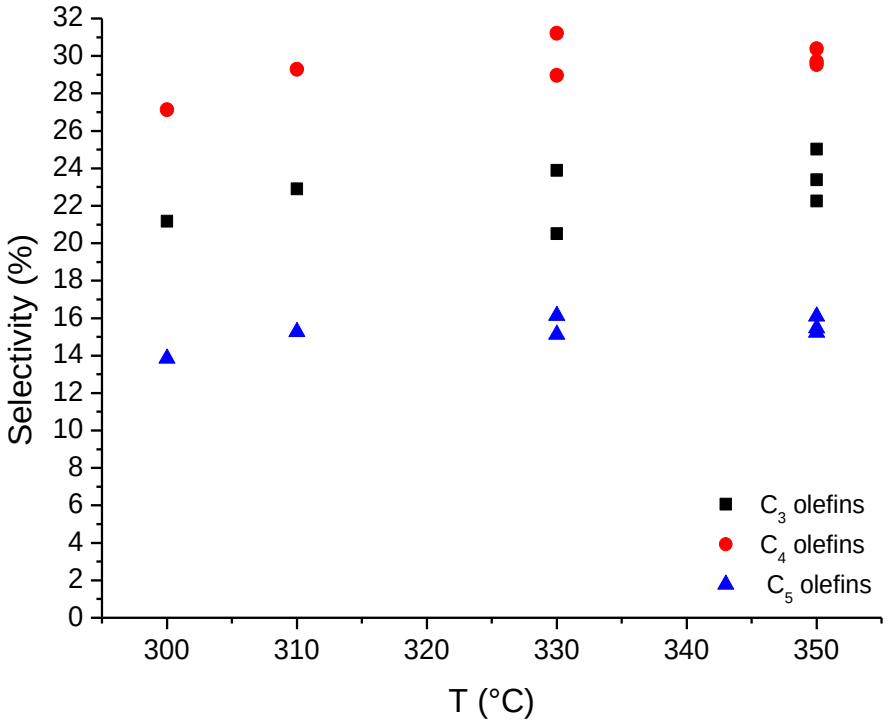

Figure 3-13 Light olefins: selectivity towards C3, C4 and C5 olefins, experiment on HZSM-5 (SiO_2/Al_2O_3=30) W_{cat}/F^0=10 $kg_{cat}.s.mol_{EtOH}^{-1}$, pp_{EtOH}=20kPa

Figure 3-14 gives the detailed composition of the butene product lump. Isobutene is the major product, comprising nearly half of the total butene mass flow, followed by trans-2-butene, cis-2-butene and 1-butene. With increasing temperature, the production of every component rises in an equal measure.

The high yield of isobutene is at first glance unexpected, since it cannot be formed directly from two ethylene molecules reacting, while the linear butenes can. The explanation to this phenomenon is given in the next paragraph, based on the observation that the C_4- and C_5-olefins are formed in equilibrium within their respective product lumps.

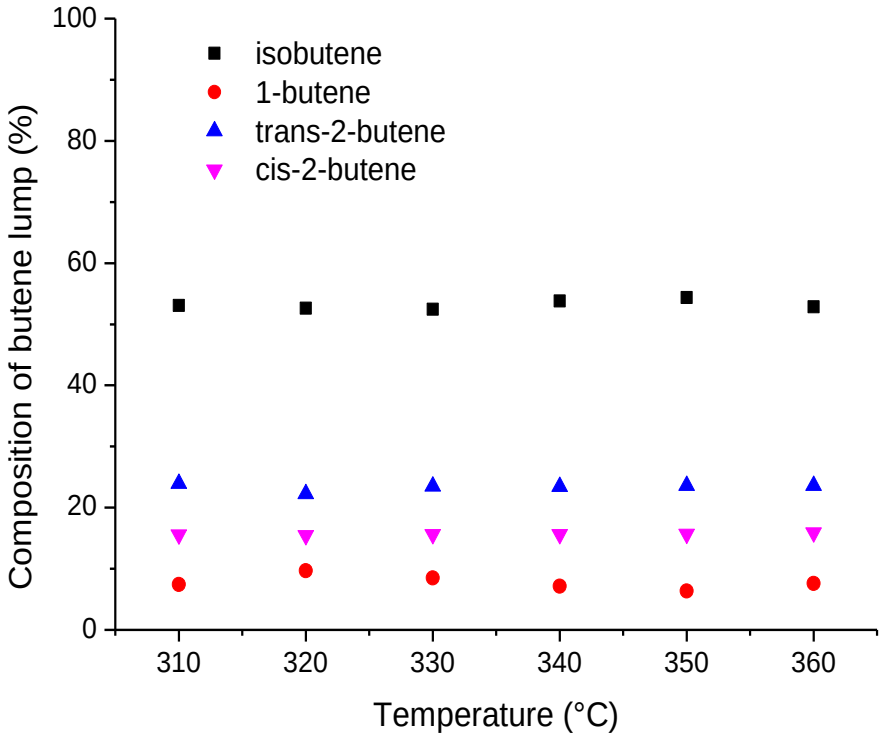

Figure 3-14 Composition of butene lump, W_{cat}/F^0=16.6 $kg_{cat}.s.mol_{EtOH}^{-1}$, p_{EtOH}=20kPa

3.4.6.1 Equilibrium compositions

Olefins with the same carbon number are formed in their thermodynamic equilibrium ratio. This is not valid for the total product mixture, which is far from its equilibrium composition.

Figure 3-15 gives a kind of parity plot with C_4 and C_5 olefins. As model, the thermodynamic equilibrium mixture under given reaction conditions is calculated in *Aspen* using the Peng-Robinsson product database. A Gibbs reactor is employed, which gives the equilibrium mixture of a group of selected compounds as output. From the output of the reactor, the mass fraction of every product is calculated. The massfraction of every component from the lump is experimentally determined via the chromatogram. The experimental observations and thermodynamic calculations are practically equal.

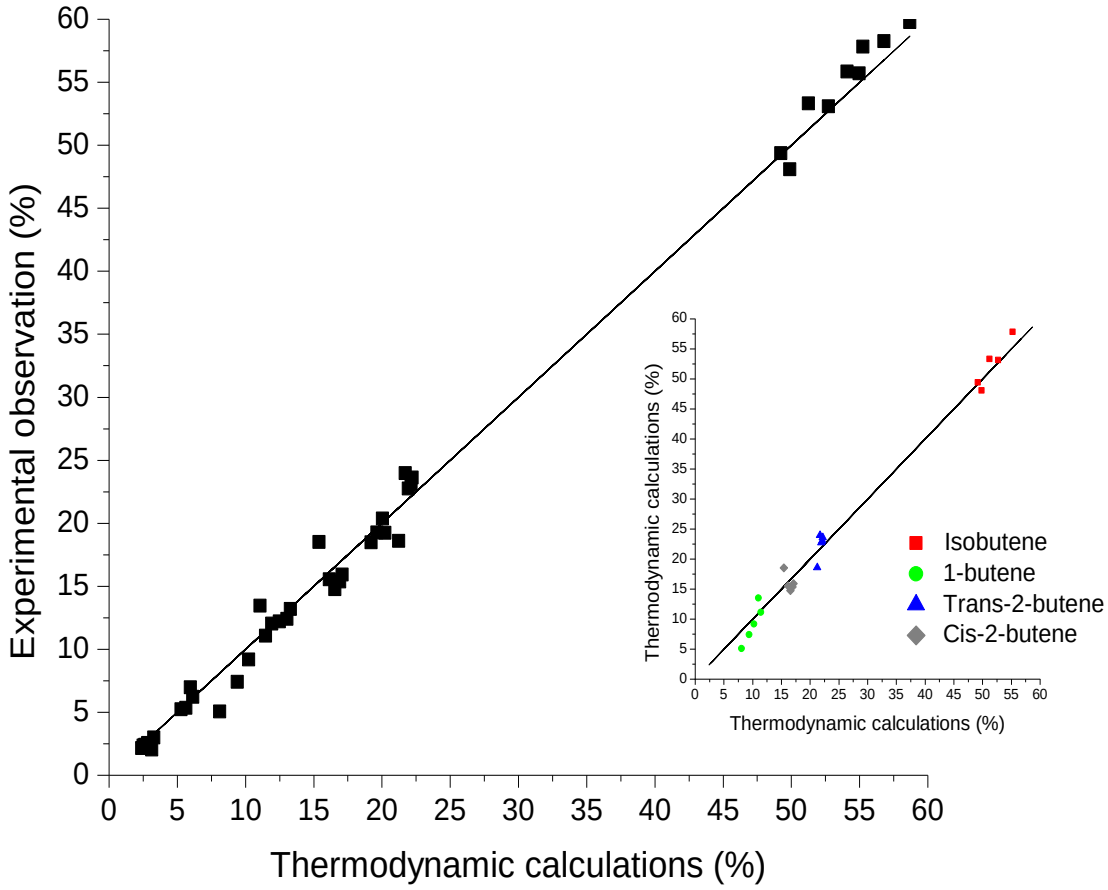

Figure 3-15 Parity plot of the experimental and thermodynamic equilibrium composition of the C_4 and C_5 olefins (T=278-360°C, W_{cat}/F^0=10 $kg_{cat}.s.mol_{EtOH}^{-1}$, pp_{EtOH}=20kPa) with detailed parity plot of composition the C_4 olefins lump

Double bond isomerization on acid catalysts is a well-known reaction. Hence, it comes as no surprise that e.g. 1-butene, and cis- and trans-2-butene are formed in equilibrium. More surprising is the formation of isobutene in equilibrium with the other butenes. Figure 3-15 also shows the detailed parity plot for the butenes, with the individual components indicated. Isobutene is formed in the largest quantities. This means a considerable amount of branching must take place, or else, isobutene is formed via cracking or a hydrocarbon pool mechanism.

The formation of butenes and pentenes in thermodynamic equilibrium, proves oligomerization and cracking – the reactions yielding the higher olefins – are reactions with a higher timescale than isomerization and branching. Thus, once formed, the C_4 and C_5 structures immediately change according to thermodynamic equilibrium conditions.

Figure 3-16 gives a representation of the thermodynamic equilibrium composition of the C_2-C_5 olefins, for temperatures ranging between 0 and 800°C. At low temperatures, the olefins with the highest carbon number are most stable. With increasing temperature, ethylene and propylene become more and more important. In the experimental range (at about 600K) the equilibrium concentration of C_5 and C_4 olefins is nearly the same and much larger than the equilibrium value for propylene and ethylene.

Looking back at Figure 3-13, it is observed that during the experiments the selectivity towards C_3 is larger than for C_5. This is a first indication the products are not formed in equilibrium when considering the whole mixture. A second proof can be found in the C_4/C_5 ratio. Experimentally, this ratio is equal to two, while thermodynamically, it is close to one.

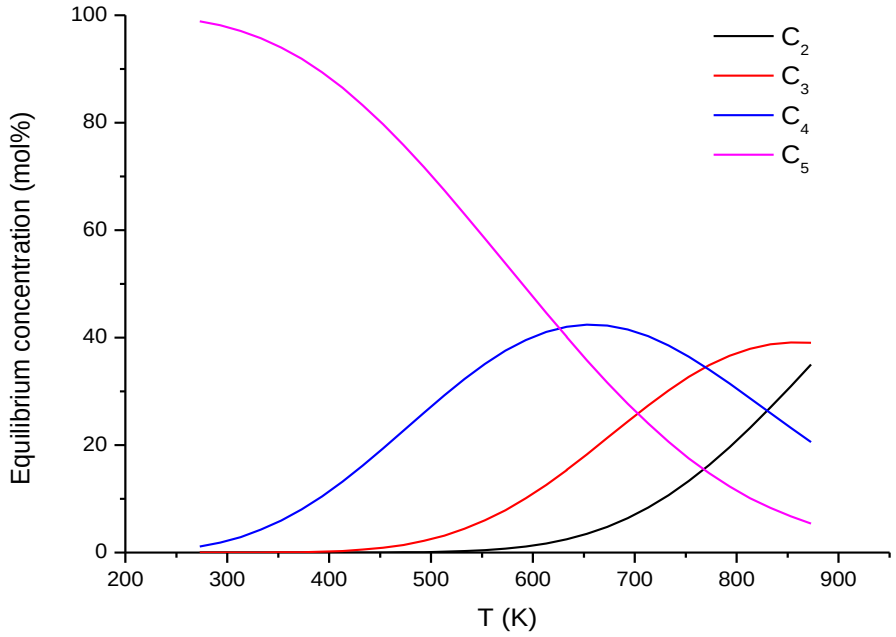

Figure 3-16 Equilibrium mixture for C_2 to C_5 olefins as calculated via Aspen (using Peng-Robinsson)

3.5 Catalyst comparison

3.5.1 Zeolite topology

Next to the concentration of acid sites, the zeolite topology is important for the catalytic conversion of ethanol to hydrocarbons. Experiments are performed on three types of zeolite: MFI, beta and mordenite. The SiO_2/Al_2O_3 ratios of these materials are 20 for mordenite, 25 for beta zeolite and 30 for the MFI zeolite . The experiments are performed in the dehydration regime, at 230°C and a spacetime of $6.5 kg_{cat}.s.mol_{EtOH}^{-1}$. Figure 3-17 depicts the results. The conversion on MFI is nearly three times larger than on mordenite, although the MFI zeolite has slightly less acid sites. Beta-zeolite has an intermediate conversion.

The selectivity is very different when using another zeolite topology and this is not the effect of a different conversion. Figure 3-17 shows that DEE selectivity on beta zeolite is higher than on mordenite, while it has a higher conversion. If the selectivity would show the same behavior as a function of conversion for all zeolite topologies, the DEE-selectivity on beta-

zeolite should be intermediate. Even more interesting is the curve of the DEE selectivity on mordenite. While the selectivity on MFI decreases with increasing partial pressure of ethanol, it increases when using mordenite.

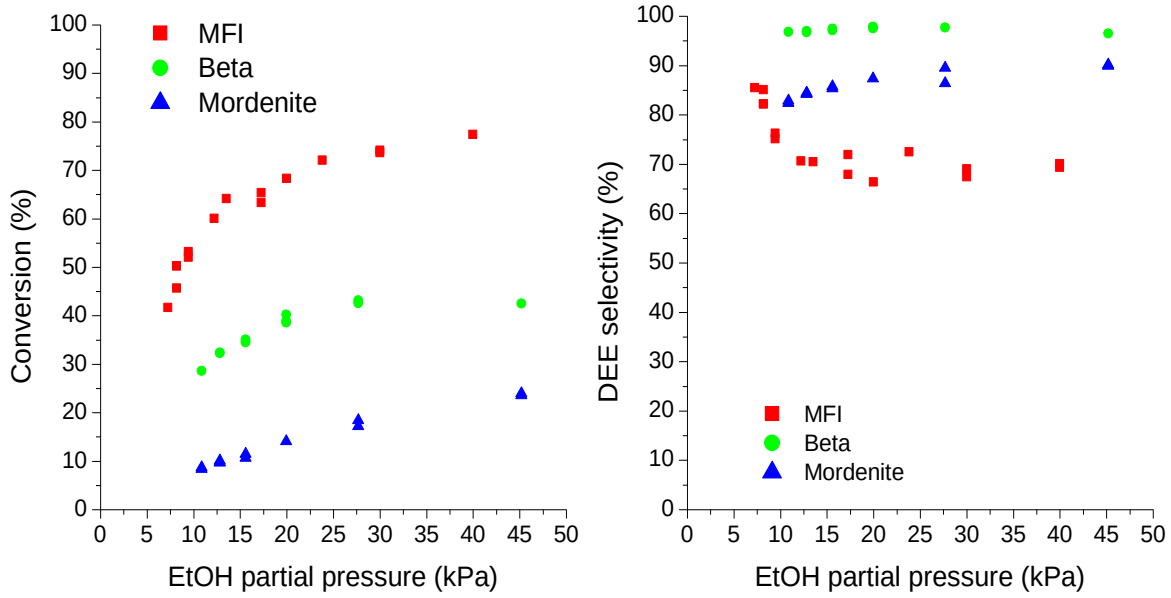

Figure 3-17 Conversion of EtOH and DEE selectivity on MFI, Beta-zeolite and mordenite at T=230°C and W_{cat}/F^0=6.5 $kg_{cat}.s.mol_{EtOH}^{-1}$

3.5.2 Catalyst modifications

Part of this thesis aims at investigating the effects of catalyst selection and post-synthesis modifications on the ethanol to hydrocarbons process. therefore, experiments are also conducted on HZSM-5 with an with an SiO_2/Al_2O_3 ratio of 80 and modified HZSM-5 catalysts (desilication and Al-ALD). These catalyst were provided by the Centre for Surface Chemistry and Catalysis (KU Leuven) and the Solid State Sciences of Ghent University.

Because of a fault during the ALD process, this catalyst showed a very low activity. This observation is a significant experimental result. A technique must be developed to selectively remove the extra-framework alumina deposits blocking the pores. A possible technique is HCl treatment. This information is of less relevance to the subject of this thesis, the ALD-catalyst will not be discussed any further.

Figure 3-18 shows the conversion of ethanol for three different catalyst: HZSM-5 (SiO_2/Al_2O_3=30 and 80) and the desilicated catalyst. It is clear the catalyst with the highest alumina content has the highest ethanol conversion. This can be explained by the higher number of acid sites in this catalyst. To investigate the effect of desilication, the experimental results of the parent material will be compared to the modified zeolite. Creating meso-pores eases mass transport in the pores and changes the shape selectivity of the material. When working under intrinsic conditions, no effect of transport phenomena on the reaction outcome

should be noted. Figure 3-18 shows the experimental results in the dehydration regime (T=230°C). No significant difference exists between the parent zeolite and the desilicated catalyst. The catalyst characterization did not show a large difference in the concentration of acid sites of these two materials, so when working intrinsically, this result is to be expected.

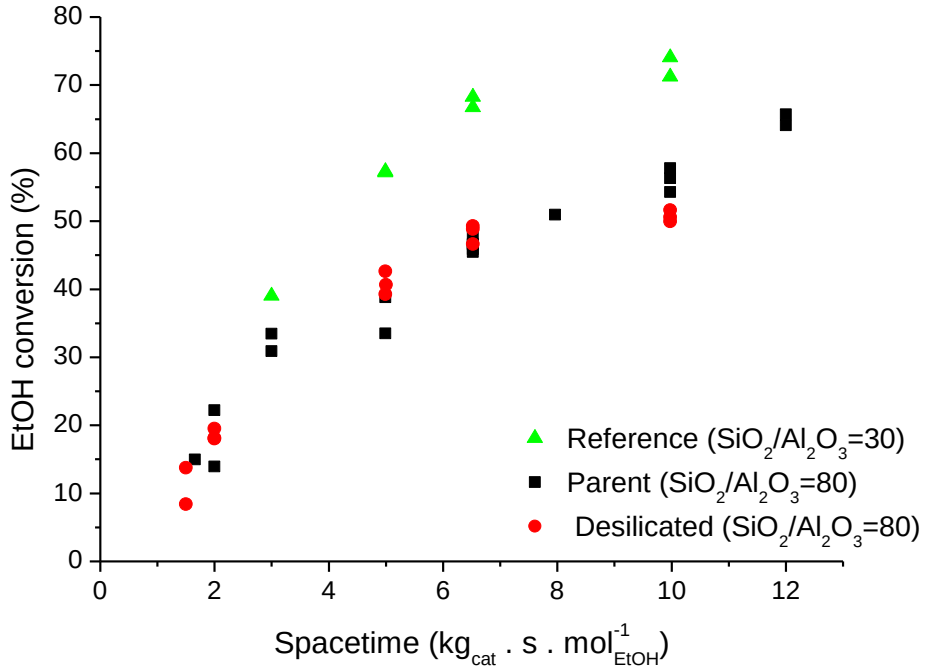

Figure 3-18 Conversion on the parent (SiO_2/Al_2O_3=80) and desilicated HZSM-5 (T=230°C, p_{EtOH}=20kPa)

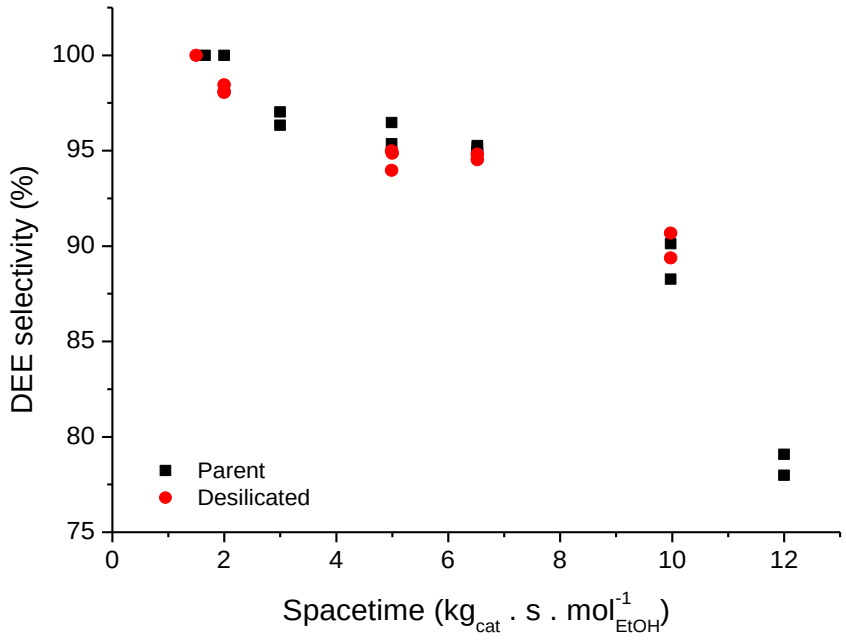

Figure 3-19 DEE selectivity on the parent (SiO_2/Al_2O_3=80) and desilicated HZSM-5 (T=230°C, pp=20kPa)

Because the shape selectivity of the material might be altered by creating meso-pores, there could be an effect of desilicating the zeolite on the product distribution in the higher hydrocarbons regime.

Experimentally, no effect is observed. Due to its small size, ethylene has no hindrance when diffusing in the zeolite framework. Hence, creating mesopores to facilitate mass transport does not influence the ethylene reactions, being the main reactions in this regime. Corma et al had the same observation with the oligomerization of propylene. [11]

The micro-pore volume is not changed drastically upon desilication. The main shape selectiveness of the ZSM-5 catalyst will still be present, even in the desilicated catalyst, so the effect on which higher hydrocarbons can be formed is similar in both catalysts.

3.5.3 Catalyst selection

To conclude this paragraph, Figure 3-20 shows the conversion of ethanol on all catalysts in the catalyst library. HZSM-5 converts ethanol to the largest extent, while H-mordenite yields the poorest results. For catalysts with the same zeolite structure, a higher Si/Al ratio gives a higher ethanol conversion.

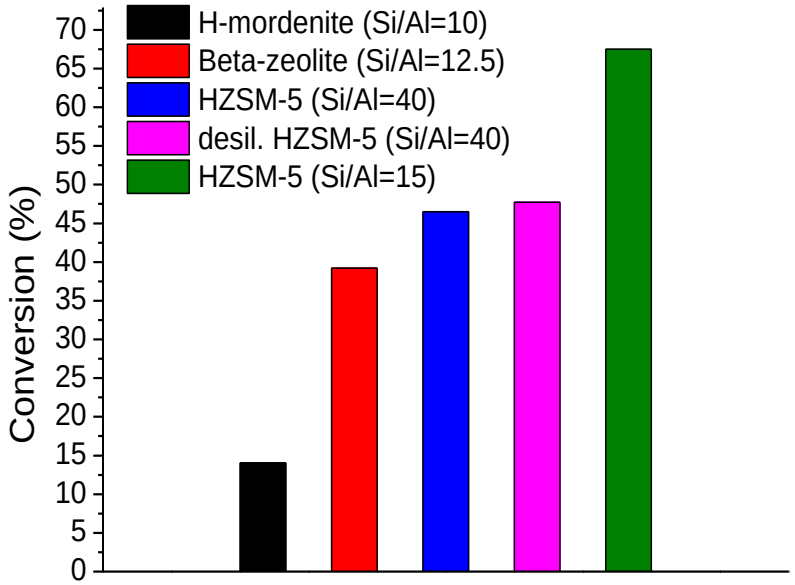

Figure 3-20 Comparison of the catalysts: EtOH conversion (230°C, 20kPa EtOH, 6,5kg$_{cat}$.s.mol$^{-1}_{EtOH}$)

3.6 Conclusion

Catalyst characterization shows the expected trends in the concentration of acid sites and zeolite structure. The only exception is the Al-ALD treated catalyst, where synthesis problems caused pore blocking by alumina species.

The kinetic dataset is constructed using the reference catalkyst, HZSM-5 with a SiO_2/Al_2O_3 ratio of 30. The experiments can be divided in two regimes. At temperatures around 250°C, all ethanol is converted to ethylene. If the temperature is raised further, the conversion to higher hydrocarbons starts.

Dehydration of ethanol gives two reaction products: diethyl-ether and ethylene. At low ethanol conversion, DEE is the main reaction product, while ethylene is the most abundant product when ethanol conversion approaches completion.

Adding water to the ethanol feed does not have an important influence on the reaction, however further investigation is still necessary to get a more detailed picture.

DEE cannot be used as feed component for quantitative experiments on the current reaction setup. A very important qualitative observation is made: DEE is converted into ethanol and ethylene under the reaction conditions used for the dehydration reaction.

The reference catalyst is stable for the conversion to higher hydrocarbons for 12h TOS.

Light olefins are the main product lump for the conversion of ethanol at temperatures between 300°C and 350°C, paraffin and aromatics production is negligible under these conditions.

Olefins with the same carbon number are formed in thermodynamic equilibrium. This does not hold true for the total product mixture, which is not in equilibrium. Formation of light olefins has a higher timescale than the isomerization reaction, explaining this observation.

Feeding ethylene yields a higher ethylene conversion than feeding ethanol. Adding water to the ethylene feed has no effect on the conversion. This indicates the timescale of ethanol dehydration is not negligible compared to the timescale of the formation of higher hydrocarbons.

When studying the different catalysts in the catalyst library, HZSM-5 proves to give the highest ethanol conversion. A higher Si/Al ratio gives less conversion. H-mordenite has the lowest conversion, although this catalyst has by far the highest concentration of acid sites.

3.7 Bibliography

1. Jacobsen, C.J.H., et al., *Zeolites by confined space synthesis – characterization of the acid sites in nanosized ZSM-5 by ammonia desorption and 27Al/29Si-MAS NMR spectroscopy.* Microporous and Mesoporous Materials, 2000. **39**(1–2): p. 393-401.
2. Rodríguez-González, L., et al., *The acid properties of H-ZSM-5 as studied by NH3-TPD and 27Al-MAS-NMR spectroscopy.* Applied Catalysis A: General, 2007. **328**(2): p. 174-182.
3. Madeira, F.F., et al., *Ethanol transformation over HFAU, HBEA and HMFI zeolites presenting similar Brønsted acidity.* Applied Catalysis A: General, 2009. **367**(1–2): p. 39-46.
4. Ogura, M., et al., *Alkali-treatment technique — new method for modification of structural and acid-catalytic properties of ZSM-5 zeolites.* Applied Catalysis A: General, 2001. **219**(1–2): p. 33-43.
5. Mao, R.L.V., et al., *ZSM-5 zeolite with enhanced acidic properties.* Applied Catalysis A: General, 1999. **185**(1): p. 41-52.
6. Gayubo, A.G., et al., *Selective production of olefins from bioethanol on HZSM-5 zeolite catalysts treated with NaOH.* Applied Catalysis B: Environmental, 2010. **97**(1–2): p. 299-306.
7. Gil, B., et al., *Desilication of ZSM-5 and ZSM-12 zeolites: Impact on textural, acidic and catalytic properties.* Catalysis Today, 2010. **152**(1–4): p. 24-32.
8. Stevens, S., *Transformation of bioethanol into hydrocarbons on modified ZSM-5*, in *Laboratory of Chemical Technology*. 2012, University of Ghent: Ghent. p. 98.
9. Kosaric, N., et al., *Ethanol*, in *Ullmann's Encyclopedia of Industrial Chemistry*. 2000, Wiley-VCH Verlag GmbH & Co. KGaA.
10. Van Borm, R., *Single-event microkinetics of hydrocarbon cracking on zeotype catalysts: effect of acidity and shape selectivity*, in *Faculty of Engineering and Architecture*. 2011, Ghent University: Ghent.
11. Corma, A., C. Martínez, and E. Doskocil, *Designing MFI-based catalysts with improved catalyst life for oligomerization to high-quality liquid fuels.* Journal of Catalysis, 2013. **300**(0): p. 183-196.

Chapter 4

Dehydration model

In this chapter, a kinetic model for the dehydration of ethanol over zeolites will be developed. The dehydration models are constructed manually and parameter estimation is performed via *AthenaVisualStudio*.

4.1 Dehydration reaction network

Based on literature [1-5] and experimental observations, a reaction network for the dehydration of ethanol over zeolites has been established. Figure 4-1 gives a depiction of this network. On this scheme, the light green area represents physisorption to the zeolite surfaces, while the dark green section represents adsorption to the acid sites.

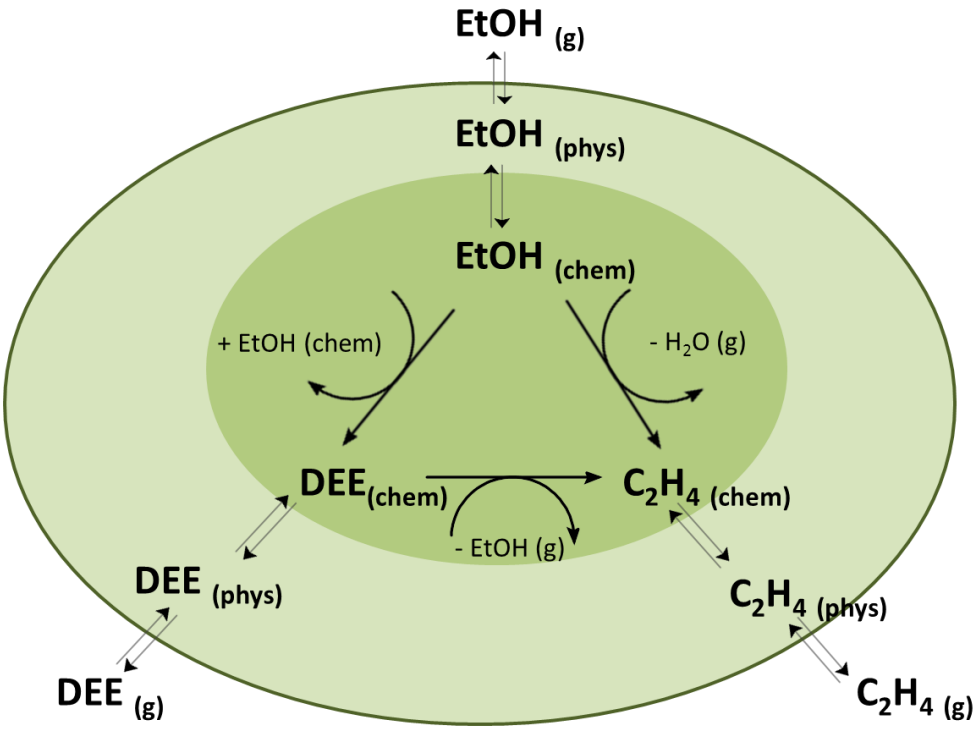

Figure 4-1 Schematic representation of the reaction network of ethanol dehydration on HZSM-5

4.2 Modelling of the dehydration reactions

All kinetic models that are implemented use a simplification of the network proposed in Figure 4-1. Physisorption and chemisorption will be considered as one single sorption step. Adsorption and desorption are also assumed to be in equilibrium in all models, according to the Langmuir sorption hypothesis.

In the most elusive mechanism found in literature, DEE formation goes over a dimer intermediate. [1] In this work, it is assumed that the dimer formation is sufficiently fast when two ethanol molecules are adsorbed on adjacent sites to consider the reaction of ethanol towards DEE as a one-step reaction.

4.2.1 The elementary reaction steps

The dehydration model can be split into two parts: the adsorption and desorption of reactants and reaction products and the actual surface reactions. The considered elementary reaction steps are given in Table 4-1.

Table 4-1 Elementary reaction steps for the dehydration mechanism

			LH1	LH2	ER
Adsorption	(1)	$EtOH_g + * \leftrightarrow EtOH^*$	x	x	x
	(2)	$DEE_g + * \leftrightarrow DEE^*$	x	x	x
	(3)	$C_2H_{4_g} + * \leftrightarrow {C_2H_4}^*$	x	x	x
	(4)	$H_2O_g + * \leftrightarrow H_2O^*$	x	x	x
Surface reactions	(5)	$EtOH^* \rightarrow {C_2H_4}^* + H_2O_g$	x	x	x
	(6)	$2EtOH^* \rightarrow DEE^* + H_2O^*$ LH	x	x	
	(7)	$EtOH^* + EtOH_g \rightarrow DEE^* + H_2O_g$ ER			x
	(8)	$DEE^* + * \rightarrow 2{C_2H_4}^* + H_2O_g$		x	
	(9)	$DEE^* \rightarrow EtOH^* + C_2H_{4_g}$	x		x
	(10)	$DEE^* \leftrightarrow {C_2H_4}^* + EtOH_g$			

For the occurring catalytic reactions, several mechanisms are possible. A first difference between the mechanisms is the type of surface-reaction: Langmuir-Hinschelwood (LH) or Eley-Rideal (ER). In literature, the reaction of DEE towards ethylene appears in several forms. While most authors state the reaction of one mole of DEE yields one mole of ethylene and one mole of ethanol [1-4], Kagyrmanova et al. [5] consider this reaction to give two moles of ethylene and one mole of water. The question remains whether the latter model is still based on elementary reactions. Both hypotheses are tested and are respectively labelled LH1 and LH2. The third model is based on a Eley-Rideal mechanism. In literature, only LH mechanisms are found.

4.2.2 Modelling results

The system of reaction rate equations and how these are calculated can be found in Appendix E. These equations are now used in *AthenaVisualStudio* to estimate the model parameters. The experimental dataset used for parameter estimation comprises 45 data points. The temperature ranges between 170°C and 250°C, the ethanol partial pressure lies between 10 and 40kPa and the spacetime goes from 5 to 16.6$kg_{cat}.s.mol_{EtOH}^{-1}$.

If less parameters have to be estimated by the software, these parameters can be estimated more easily. The adsorption coefficients for ethanol, ethylene and water on ZSM-5 zeolite are taken from literature. [6-9] The adsorption enthalpies that were used based on these literature sources are given in Table 4-2. No good data for DEE adsorption were found, so these parameters ($A_{DEE,ads}$ and $-\Delta H_{ads,DEE}$) are estimated. This reduces the number of parameter estimations from fourteen to eight. Table 4-3 gives the estimations and t-values for the parameters of the three models. The F-test for model significance and the R^2 value are also given.

Table 4-2 Fixed values for adsorption parameters

Parameter	Value
$-\Delta H_{ads,EtOH}$ (J/mol)	1.65E+05
$-\Delta H_{ads,Ethylene}$ (J/mol)	3.11E+04
$-\Delta H_{ads,water}$ (J/mol)	5.50E+04

From Table 4-3 it is clear the ER mechanism does not yield good parameter values. This is in accordance with the literature sources stating Langmuir-Hinschelwood to be the best model. The difference between the LH models in parameter values and statistical tests is not large.

The tabulated F-value is 3.84. Both LH1 and LH2 are significant models. Although the F-value of LH2 is larger than the value of LH1, the difference is not large enough to discriminate between these two models. The multiple correlation coefficient of both cases is very alike, indicating an equally good fit of the experiments to the model. R^2 doesn't give a conclusion on which model is best either.

Table 4-3 Parameter estimations for certain dehydration models

parameter	LH1		LH2		ER	
	Estimation	t-value	Estimation	t-value	Estimation	t-value
$A_{DEE,ads}$ (-)	1.87E-04	91.4	2.38E-04	5.75	8.87E+03	1.45
$A_{EtOH->C2H4}$ ($s^{-1} \cdot kg_{cat}^{-1}$)	6.50E+01	18.5	4.68E+01	13.1	6.36E-04	25.8
$A_{EtOH->DEE}$ ($s^{-1} \cdot kg_{cat}^{-1}$)	5.47E+02	28.2	5.20E+02	14.3	2.55E-02	2.00
$A_{DEE->C2H4}$ ($Pa^{-1}s^{-1} \cdot kg_{cat}^{-1}$)	1.22E+02	8.34	8.69E+01	6.47	2.99E-08	/
$-\Delta H_{ads,DEE}$ (J/mol)	7.92E+04	3.41	6.50E+04	2.65	1.31E+04	/
$E_{a,EtOH->C2H4}$ (J/mol)	1.82E+05	19.7	1.89E+05	13.9	1.57E+06	13.7
$E_{a,EtOH->DEE}$ (J/mol)	1.63E+05	32.5	1.59E+05	28.8	1.72E+05	5.96
$E_{a,DEE->C2H4}$ (J/mol)	1.08E+05	1.95	1.02E+05	4.36	7.84E+04	14.2
F	1126		1208		639	
F_{table}	3.84		3.84		3.84	
R^2	0.979		0.981		0.941	

The t-values of the individual parameters are examined to distinguish between the two models. For the parameter to be estimated significantly, the t-value should in this case be higher than 2,02. Only the LH1 activation energy of the reaction from DEE to ethylene does not suffice this criterion, but it is only slightly smaller than the boundary value.

Because the basic statistical tests do not allow discrimination between LH1 and LH2, the correlations between the different parameters are examined. If the correlations run counter the information comprised in the reaction mechanism, it can be an argument to select one of the models as the best.

In Appendix F, the correlation matrices for the estimated parameters of these two models are given. Such matrix is symmetric, with the elements on the main diagonal equal to 1 and each element belonging to the interval [-1,1]. A coefficient equal to 0 means no correlation exists between those two parameters, while 1 indicates a perfect linear relationship. Only absolute values higher than 0.95 are considered to indicate a correlation between two parameters.

The activation energy of the reaction from ethanol to ethylene for LH1 is uncorrelated to the other parameters. Especially the correlation to the reaction3 parameters is small. The third reaction yields ethanol as a product, so some correlation between the parameters of these two reactions was expected. Overall, most correlation coefficients for LH1 are lower than 0,7 in absolute value, so the correlation in this model is very limited. An exception are the adsorption parameters for DEE. Since adsorption plays a major role in the surface

concentration of the active species, varying the adsorption coefficient can have a great influence on the kinetics. This is reflected in these large correlation coefficients.

The adsorption parameters for LH2 have once again some correlation to some of the other parameters. The same reasoning as for LH1 can be used to explain this.

The reaction from DEE to ethylene has a small correlation to parameters of the first reaction, i.e. ethanol to ethylene. In case of LH2, this seem more legit than for LH1. Since DEE yields two ethylene molecules in this model, no direct link between the two reaction exists, so no important correlation is to be expected.

To analyse the results of the model estimation graphically, parity and residual plots of LH2 are constructed. In a parity plot, the model predicted and experimentally observed values of a certain quantity are plotted. The residual plots give the difference between model and experiment as a function of process conditions or model predictions. This allows the detection of trends in the modelling error, which could lead to better model formulations.

Figure 4-2 gives the parity plots of the three measured reactions products. These plots indicate the model performs well.

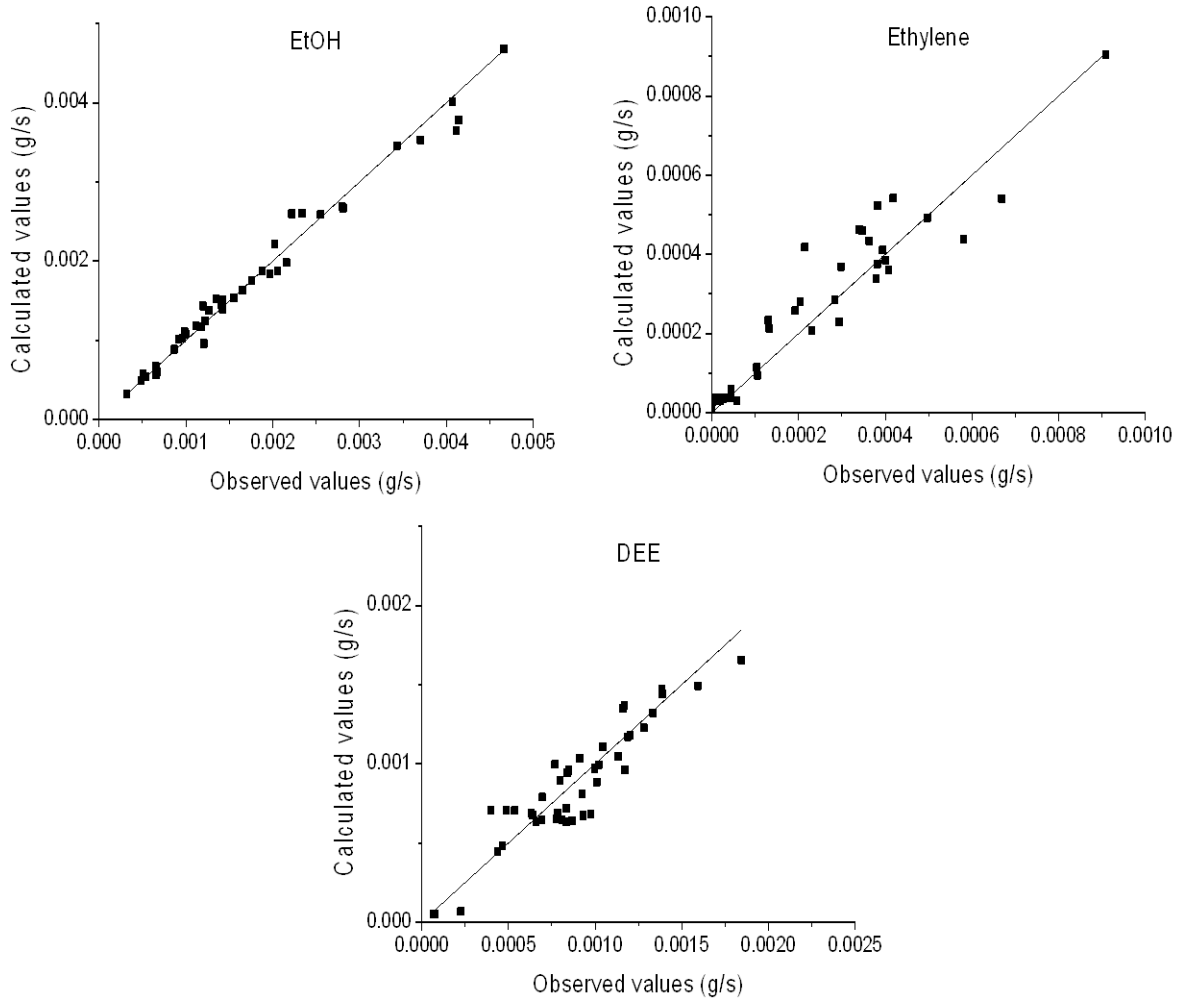

Figure 4-2 Parity plots of the EtOH, ethylene and DEE outlet flow rate (LH1)

Figure 4-3 represents the residuals as a function of ethanol feed – which is correlated to the spacetime – and as a function of temperature. No clear trend is visible in these plots. The residuals are equally distributed around zero, indicating the LH2 model can sufficiently predict these experimental results.

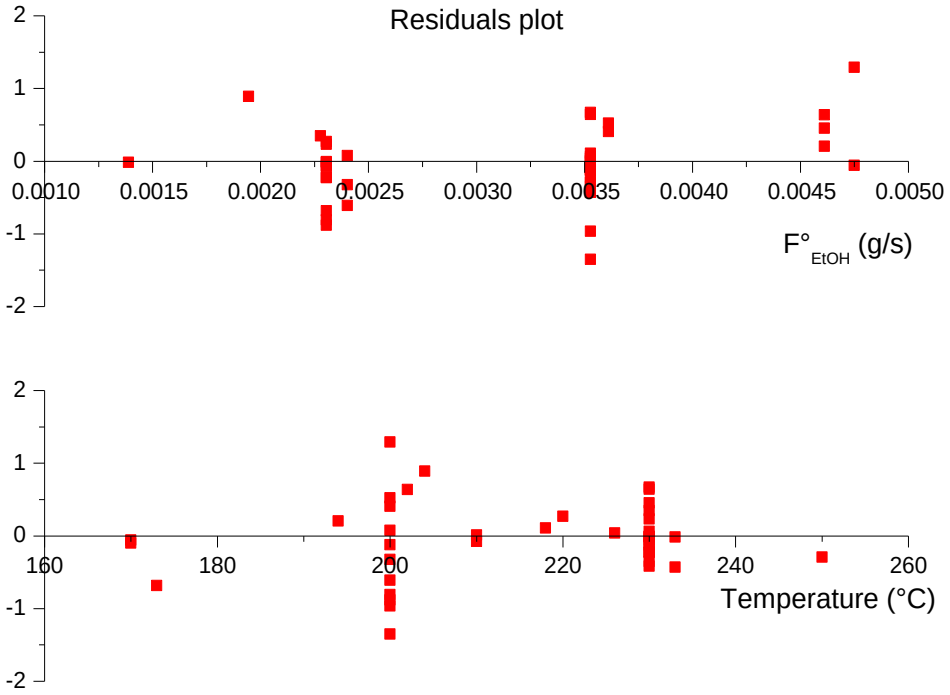

Figure 4-3 Residual plots as a function of temperature and EtOH feed (LH1)

4.2.3 Ab initio predictions

Next to the experimental approach used in this work, ab initio calculations represent a second methodology to obtain a micro-kinetic reaction model. At the LCT, the dehydration of ethanol is studied using both procedures.

Figure 4-4 has been provided by K. Alexopoulos, the calculations uses DFT to calculate the activation energies. The conversion is predicted very well, but the curves of the selectivity deviate from the experimental observations. According to the reaction mechanism, the reaction from ethanol to DEE is a bi-molecular reaction, while only one reactant is needed to form ethylene. Theoretically, it would be expected the DEE formation is more important at higher ethanol partial pressures, as is predicted by the ab initio calculations. Further investigation into this matter is necessary. [10]

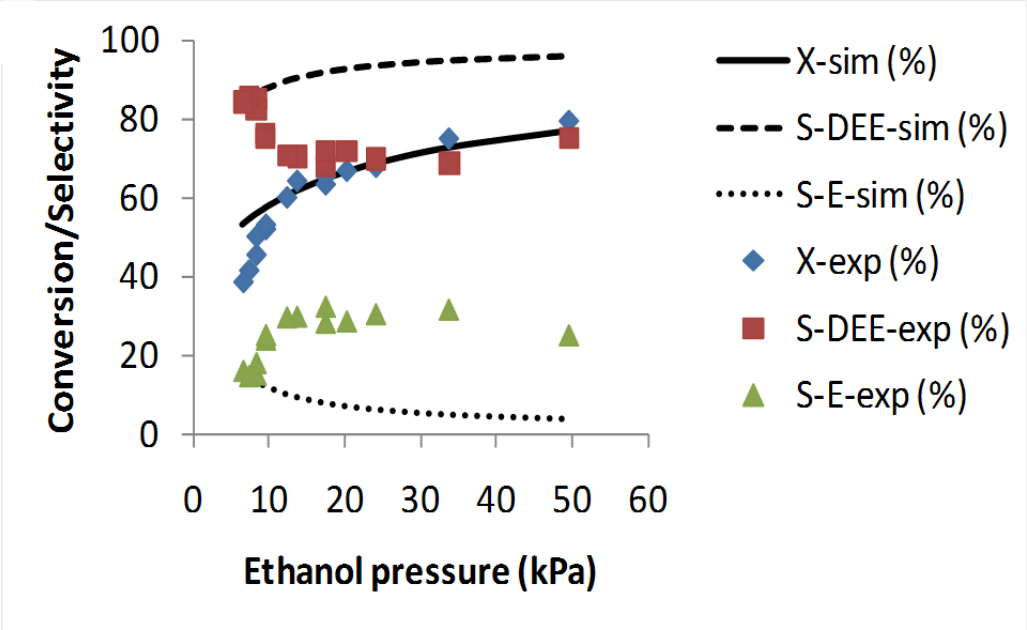

Figure 4-4 Ab initio simulated versus experimental results on HZSM-5 (SiO_2/Al_2O_3=30) (230°C, 6,5k_{cat}.s. mol_{EtOH}^{-1})

4.3 Conclusions

Several Dehydration mechanisms have been modeled and parameter estimations are performed using *AthenaVisualStudio*. The adsorption coefficients for ethanol, ethylene and water were taken from literature.

The Langmuir-Hinshelwood mechanism proved to yield the best results. No clear distinction between the two LH models is possible based on the parameters or statistical tests. The activation energies for the two LH models are very similar, deviating less than 10% from each other. The values are 182kJ/mol for the reaction from ethanol to ethylene, 163kJ/mol from ethanol to DEE and 108kJ/mol for the reaction from DEE to ethylene.

The good model performance is shown on Figure 4-5, where the calculated and measured outlet flow composition are given.

Comparison of the experimental results to the ab initio calculated model shows different trends in the selectivity towards ethylene and DEE. This observation indicates further investigation into the reaction mechanism is necessary.

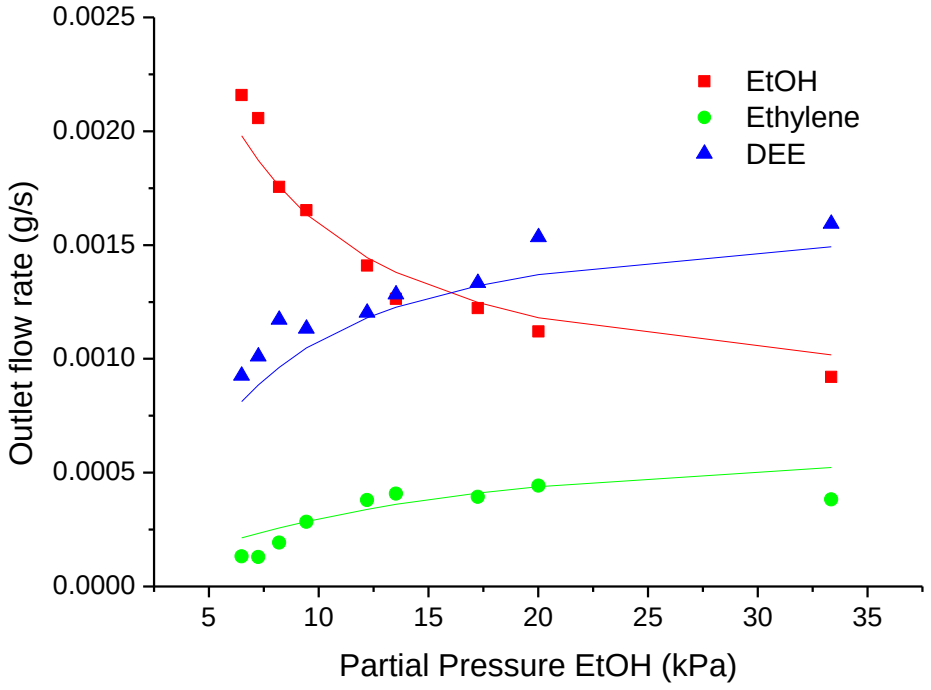

Figure 4-5 LH2-model calculation and experiments on HZSM-5 (SiO_2/Al_2O_3 =30) at 230°C and 6.5kg_{cat}.s.mol_{EtOH}^{-1} as a function of EtOH partial pressure

4.4 Bibliography

1. Chiang, H. and A. Bhan, *Catalytic consequences of hydroxyl group location on the rate and mechanism of parallel dehydration reactions of ethanol over acidic zeolites.* Journal of Catalysis, 2010. **271**(2): p. 251-261.
2. Chang, C.L., A.L. DeVera, and D.J. Miller, *A LUMPED KINETIC MODEL FOR DEHYDRATION OF ETHANOL TO HYDROCARBONS OVER HZSM-5.* Chemical Engineering Communications, 1990. **95**(1): p. 27-39.
3. Saito, Y. and H. Niiyama, *Reaction mechanism of ethanol dehydration on/in heteropoly compounds: Analysis of transient behavior based on pseudo-liquid catalysis model.* Journal of Catalysis, 1987. **106**(2): p. 329-336.
4. Golay, S., R. Doepper, and A. Renken, *In-situ characterisation of the surface intermediates for the ethanol dehydration reaction over γ-alumina under dynamic conditions.* Applied Catalysis A: General, 1998. **172**(1): p. 97-106.
5. Kagyrmanova, A.P., et al., *Catalytic dehydration of bioethanol to ethylene: Pilot-scale studies and process simulation.* Chem Eng J, 2011. **176-177**: p. 7-7.
6. Nguyen, C.M., M.-F. Reyniers, and G.B. Marin, *Theoretical study of the adsorption of C1-C4 primary alcohols in H-ZSM-5.* Physical Chemistry Chemical Physics, 2010. **12**(32): p. 9481-9493.
7. Myers, A.L., *Characterization of nanopores by standard enthalpy and entropy of adsorption of probe molecules.* Colloids and Surfaces A: Physicochemical and Engineering Aspects, 2004. **241**(1–3): p. 9-14.
8. Borges, P., et al., *Light olefin transformation over ZSM-5 zeolites: A kinetic model for olefin consumption.* Applied Catalysis A: General, 2007. **324**(0): p. 20-29.
9. Pope, C.G., *Water adsorption on ZSM-5 and its aluminum free analog, silicalite.* Journal of Colloid and Interface Science, 1987. **116**(1): p. 221-223.
10. Alexopoulos, K., B.L. K. Van der Borght, Editor 2013.

Chapter 5

Conversion of ethanol to higher hydrocarbons

5.1 Reaction network: generation and reduction

5.1.1 Active species

In literature, there is some debate concerning which kind of ion is the active species in the conversion of ethanol on zeolites. Both the ethyl carbenium and ethoxy ion are cited. [1-4]

A carbenium ion is a carbon species where an electron deficient carbon atom has three chemical bonds and is surrounded by six electrons. Carbenium ions have a plane structure. They are quite unstable and are known to be reactive intermediates to chemical reactions. The structure of the ethyl carbenium ion is given in Figure 5-1.

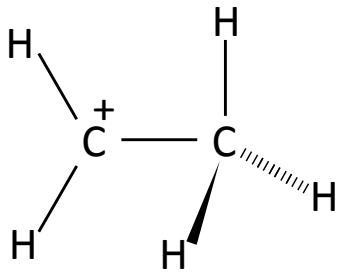

Figure 5-1 Ethyl carbenium ion

The ethoxy group is a far more stable chemical compound than a carbenium ion. It does not have an electron deficient carbon atom, but is constituted from an alkyl group bonded to an oxygen atom of the zeoltite structure. The ionic properties are caused by the electronegativity of oxygen.

To form an ethoxy ion in the zeolite framework, the alkene first forms a π-complex. Subsequent protonation of the alkene leads to the chemisorbed species: an alkoxy ion. The formation of such ion is represented in Figure 5-2. [5]

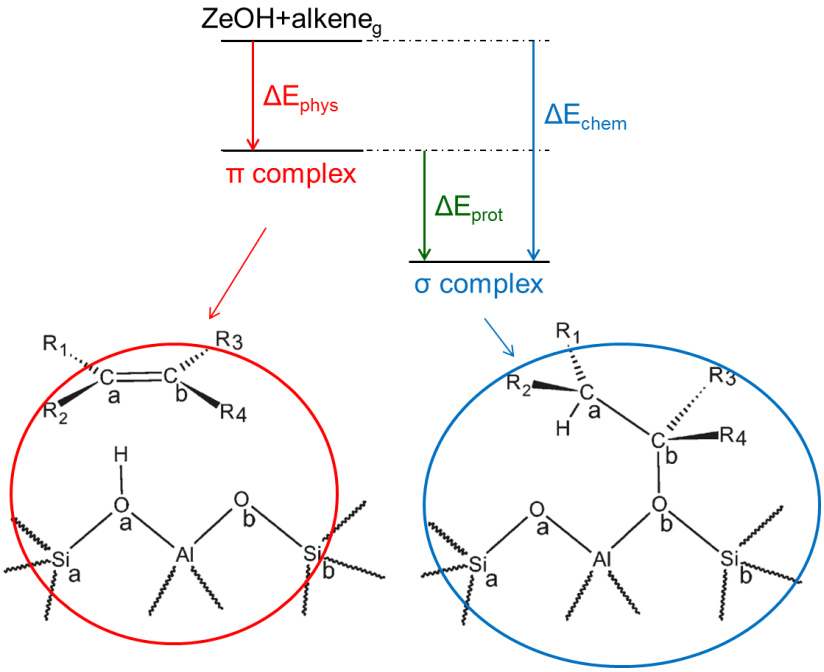

Figure 5-2 Formation of an alkoxy species [5]

Thermodynamic calculations indicate the ethoxy ion would be formed preferentially, but the question remains whether this rather stable cation would still be active for higher hydrocarbon formation. That is why in this work the ethyl carbenium ion is considered to be the active species. From a modelling point of view, the implementation of both types of cation into the reaction model is identical. However, when simulating the reaction or selecting initial values for parameter estimation, a choice must be made. The physical explanation of experimental observation and estimated parameter values also requires the knowledge of the correct active species.

5.1.2 Reaction network generation

Based on the experimental study, the full reaction network is generated via the in-house developed software ReNeGeP. The experimental observations are used to imply restrictions to the generating software. Without these stop criteria, the inclusion of oligomerization steps in the reaction network would lead to an infinite generation loop. This can be easily demonstrated by looking at the number of isomers for the olefins with four and six carbon atoms in the their chain. There are four butene isomers, while hexane already has 17. Without restrictions, the network size would go out of control.

Experimentally, the longest chain hydrocarbons that are identified are C_9 compounds. These are formed to a very limited extent. Hence, the first limitation on the generated reaction network is a maximal chain length of nine carbon atoms. No other constraints are introduced into the program.

The reactions that are allowed to proceed are given in Table 5-1. Based on this information, the extensive reaction network is generated by ReNeGeP. The number of each type of reaction and compounds included in this reaction network are given in Table 5-2 and Table 5-3 respectively.

Table 5-1 Reactions introduced into the extensive reaction network (with examples)

Protonation	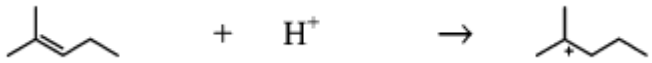
Deprotonation	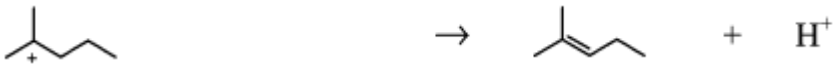
Hydride shift	
Methyl shift	
PCP branching	
Oligomerization	
β-scission	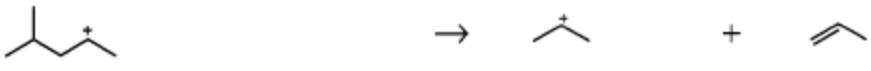
Hydride abstraction/donation	
Cyclization	
Aromatization	

Normally, primary carbenium ions are not allowed in the reaction network by the program. So the code had to be adapted to include the ethyl carbenium ion. Without this modification, no components could be formed, since the ethyl carbenium ion is the starting point of the entire network. The only reaction where this ion is added is the oligomerization, since primary carbenium ions are less stable than secondary and tertiary ions and thus much less likely to form via e.g. β-scission reactions.

When examining Table 5-2, the number of oligomerizations and β-scissions seem to be contradicting. Since these are complementary reactions, their numbers are expected to be equal. However, there are more oligomerizations included in the network than there are β-scissions, due to the inclusion of the oligomerization reaction of the ethyl carbenium ion in the network. This ion cannot be formed via β-scission, because based on stability considerations it is not allowed for this reaction. The number of oligomerization reactions of the ethyl carbenium ion is 20, exactly the difference between oligomerization and β-scission in the reaction network.

Table 5-2 Number of each type of elementary reaction included in the reaction network

Elementary Reaction type	*Number*
Protonation /deprotonation	149
Hydride shift	389
Hydride abstraction	146
Methyl shift	62
PCP branching	304
Oligomerization	41
β-scission	21
Aromatization	18
Hydride donation	347
Cyclization	30

Table 5-3 Types of components and their respective number as included in the network

Component	*Number*
Parafins	33
Naphtenes	21
Aromatics	6
Olefins	104
Carbenium ions (parafinic/cyclic/olefinic)	80 / 75 / 192

Experimentally, the fraction of aromatics and paraffins in the product mixture is quite low. The combined selectivity of these two lumps always remains below 10%. The extensive reaction network is simplified by neglecting paraffin and aromtics production.

Next to the aromatics, cyclopentene is the only cyclic product that is identified. Cyclisation reactions can be excluded from the network based on this observation.

The new reaction network, using these constraints, is given in Table 5-4 and Table 5-5. It is this reduced network that will be implemented in the modelling software.

Table 5-4 Number of each type of elementary reaction included in the reaction network

Elementary Reaction type	*Number*	*Included in network*
Protonation /deprotonation	149	Yes
Hydride shift	389	Via thermodynamic equilibrium calculations
Methyl shift	62	
PCP branching	304	
Oligomerization	41	Yes
β-scission	21	Yes

Table 5-5 Types of components and their respective number as included in the network

Component	*Number*
Olefins	104
Carbenium ions	80

5.2 Single Event Methodology

The description of the single event methodology in this paragraph is based on articles by Froment, Park et al. and Guillaume et al. [6-8]

The reaction network is constructed using the methodology described in the paragraph on network generation. The employed computer algorithm leads to a huge set of elementary reactions, belonging to a limited number of reaction types. Single event microkinetic modeling aims at estimating the kinetic parameters of all the elementary step, using a very limited set of parameter estimations. To achieve this, a number of assumptions must be made.

Since these ions are less stable than the secondary or tertiary ions, this assumption is reasonable. The exceptions to this rule are situations where only a primary ion can be formed

(e.g. ethyl carbenium ion) and the primary butyl ion, since reaction products formed from these ions are observed in the product mixture.

It is assumed that the rate coefficients are independent of the number of carbon atoms in the molecule and of the carbenium ion structure. Hence, they are defined completely by the type of carbenium ion participating in the reaction (secondary, tertiary, etc.).

However, when a reaction coefficient would only be dependent on the type of carbenium ion, the total structure of the ion plays no role whatsoever in the reaction rate. Intuitively, it seems the structure of the reactant should have some influence. As an example, the methyl-shift from 2-methyl-3 pentylcarbenium ion towards 3-methyl-2 pentylcarbenium ion is given. [6]

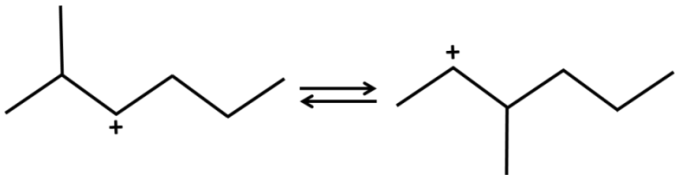

Figure 5-3 Methyl-shift from 2-methyl-3 pentylcarbenium ion towards 3-methyl-2 pentylcarbenium ion

From the figure, it is clear two methyl-groups can shift when the reaction proceeds from left to right, but only one group can shift when the reaction proceeds in the opposite direction. This examples shows clearly that defining the ions purely based on their type is insufficient. This is where the single event theory is introduced.

The single event concept must be viewed in the context of the transition state theory. The rate coefficient for the conversion of a reagent into a product, passing through an activated complex, is written as follows:

$$k' = \frac{k_B T}{h} \cdot \exp(\frac{\Delta S^{0\neq}}{R}) \cdot \exp(\frac{-\Delta H^{0\neq}}{RT})$$

In this equation, h is the Plank constant and k_B the Boltzman constant. Three terms contribute to the standard entropy of a component, namely: the vibrational, translational and rotational part. The rotational contribution may be selected as the representative part for the structure. This contribution has an intrinsic part (S^0) and a part due to the symmetry number of the compound (σ). The formula for the rotational entropy is as follows:

$$S^0 = S^0 - R \ln(\sigma)$$

Next, a global symmetry number is defined, which takes into account the chirality of the component with n chiral centres:

$$\sigma_{gl} = \frac{\sigma}{2^n}$$

By introducing these concepts, the rate coefficient for an elementary step can be rewritten:

$$k' = \frac{k_B T}{h} \cdot \left(\frac{\sigma_{gl,reagent}}{\sigma_{gl,\neq}}\right) \cdot \exp\left(\frac{\Delta S^{0\neq}}{R}\right) \cdot \exp\left(\frac{-\Delta H^{0\neq}}{RT}\right)$$

Or, by defining the number of single events (n_e) as the ration of the global symmetry number of the reagent and the transition state:

$$k' = \frac{k_B T}{h} \cdot n_e \cdot \exp\left(\frac{\Delta S^{0\neq}}{R}\right) \cdot \exp\left(\frac{-\Delta H^{0\neq}}{RT}\right) = n_e \cdot k$$

Where k is the rate coefficient of a single event.

To determine the number of single events of a certain elementary reaction step, the configuration of the transition state must be known. This configuration can be calculated via quantum mechanical packages. These packages calculate data for gas phase components. In the case of ethanol conversion over zeolites, the molecules are adsorbed on the zeolite surface. Since the effect of the zeolite on the trasition state is the same as on the reactant, the division of the symmetry numbers of the components in the gas phase will yield the same result as this calculation performed with the symmetry number of the adsorbed species. By separating the number of single events from the single event rate coefficient, the effect of the structure on the entropy is taken into account, however, the effect of the structure on the enthalpy of formation of the activated complex is neglected.

Up to now, the number of parameters to be estimated has already been reduced drastically, since only the single event parameters remain to be estimated, instead of a rate coefficient for every component in the reaction mixture. To further reduce the set of parameters, some extra assumptions and constraints are introduced.

Thermodynamic constraints can be calculated using the thermodynamic properties of the compounds. Since thermodynamic properties are known for a wide range of molecules and can be calculated by quantum mechanical packages, this further reduces the number of estimations needed. Possible examples are equilibrium coefficients for adsorption [8], deprotonation for components with the same C-number [6], etc. The thermodynamic properties are calculated using Bensons group theory. [9]

In this model the reaction rate for each component is calculated individually. The parameter estimation is done by grouping the outlet flow rates by carbon number. This is done because of analytical limitations. The implementation of this methodology is done using in-house developed software.

5.3 The Single-event microkinetic model

5.3.1 Thermodynamic properties

Thermodynamic properties allow for e.g. calculating equilibrium coefficients. Because these properties can be calculated before the model simulation or parameter estimations, it introduces an important reduction in computational effort. The thermodynamic properties of most compounds are well known. Also, several methods have been established to calculate the properties of a specific species. In this work, the Benson group theory [9] is employed to determine the thermodynamic data of the compounds that were returned by ReNeGeP. Once again, in-house developed software is available to perform these computations. The resulting database of thermodynamic properties is used as input in the modelling software later on.

5.3.2 The SEMK model

In constructing the rate equations for the single-event micro-kinetic model for higher hydrocarbon formation, a similar approach is used as with the dehydration model. The only data on the reaction compounds that is experimentally accessible with the setup are bulk concentrations or partial pressures. For the reaction rate equation, the surface concentration of the active species must be known.

The concentration of a specific compound on the catalyst surface will be calculated via a Langmuir isotherm. It is assumed only one molecule can bind to an adsorption site and the occupation of adjacent sites does not influence the coverage of a site. The equation is constructed for equilibrium circumstances:

$$C_{phys,i} = \frac{K_i p_i}{1 + \quad_j K_j p_j}$$

$$K = A \cdot e^{-\frac{\Delta H}{RT}}$$

With $C_{phys,i}$ the concentration of physisorbed component i, K_i the adsorption equilibrium coefficient of component i and p_i its partial pressure.

The adsorption enthalpy is considered to be constant for all olefins with the same carbon-number. Per carbon-number, an adsorption enthalpy is calculated, based on ethylene as reference component. The difference in adsorption enthalpy between two adjacent carbon-numbers is assumed to be a constant value:

$$\Delta_{ads}H_i = \Delta_{ads}H_{i-1} + \Delta\ \Delta H$$
$$\Delta_{ads}H_{2+n} = \Delta_{ads}H_{ethylene} + n \cdot \Delta\ \Delta H$$

Going from an adsorbed species to an active species happens via protonation of the olefin. This reaction yields a carbenium ion, which can then react with e.g. an olefin in an oligomerization reaction. This reaction is considered to be in equilibrium.

Experimentally, it is observed the olefins with a certain carbon-number are formed in thermodynamic equilibrium. This observations justifies a simplification to the model. The only reactions that must be added are those changing the carbon-number or the nature of the compounds. Isomerizations can be calculated afterwards via thermodynamic data. The reactions that are introduced into the model are:

- ✓ Protonation and deprotonation
- ✓ Alkylation
- ✓ β-scission

The activation energy of these elementary reactions is considered to be dependent on the type of carbenium ion (primary, secondary or tertiary) and independent of the chain length. This assumption limits the number of model parameters drastically. This assumption might not hold true for the protonation reaction. The protonation enthalpy of small olefins is dependent on both type and chain length. Adaptation of the code to include chain length dependency might be necessary. In literature, both aproximations are found (Table 5-6).

Table 5-6 Protonation ethalpies in literature

Process	Protonated species	$E_a/\Delta H$ (kJ/mol)
Catalytic cracking [10] (activation energy)	Primary	/
	Secondary	96,7
	Tertiary	80,5
MTO [12] (protonation enthalpy)	Ethene	-11
	Porpene	-42
	Butene	-53
	Pentene	-61
	Hexene	-67
	Heptene	-70

Deprotonation and β-scission are calculated via thermodynamic constraints from their respective complementary reactions: protonation and alkylation.

5.3.3 Simulation of the ETH process

Before the SEMK model parameters are estimated, a simulation is run using literature values for the activation energies and adsorption and protonation enthalpies. Since no micro-kinetic model on this process exist yet, the parameter values are taken from articles concerning catalytic cracking and the MTO-process. [2, 10-12] The goal of the simulation is twofold:

checking if the model is plausible and finding good initial estimates to use during the parameter estimation. Due to the single-event approach, the number of parameters has been reduced to 13.

Table 5-7 gives the SEMK model parameters and their values. However, with the given parameters, simulation does not result in any significant higher hydrocarbon formation. The reason for this deviation can maybe be explained by a wrong assumption in the reaction mechanism or a phenomenon which is not taken into account.

Table 5-7 Parameters SEMK model used for simulation

Parameter	Value (J/mol)
ΔH_{chem}	-179,6E+03
$\Delta H_{prot,prim}$	-100,55E+03
$\Delta H_{prot,sec}$	-100,55E+03
$\Delta H_{prot,tert}$	-130,8E+03
ΔH_{phys}	130,99E+03
$\Delta(\Delta H_{phys})$	32,9E+03
$E_{a,alk,pp}$	90,0E+03
$E_{a,alk,ps}$	70,0E+03
$E_{a,alk,pt}$	70,0E+03
$E_{a,alk,ss}$	29,4E+03
$E_{a,alk,st}$	55,4E+03
$E_{a,alk,ts}$	90,0E+03
$E_{a,alk,tt}$	61,4E+03

5.4 Conclusion

Based on the experimental data, the reaction network for the conversion of ethanol to higher hydrocarbons has been constructed using ReNeGeP. This network has been simplified based on the observation that very few paraffins and aromatics are formed during the experiments.

The reaction network is employed to construct a single-event micro-kinetic network. Due to the experimental observation that olefins with equal carbon-numbers are formed in thermodynamic equilibrium, only protonation, deprotonation, alkylation and β-scission reactions have to be modelled.

With the literature values, no significant higher hydrocarbon production was calculated.

5.5 Bibliography

1. Chiang, H. and A. Bhan, *Catalytic consequences of hydroxyl group location on the rate and mechanism of parallel dehydration reactions of ethanol over acidic zeolites.* Journal of Catalysis, 2010. **271**(2): p. 251-261.
2. Nguyen, C.M., M.-F. Reyniers, and G.B. Marin, *Theoretical study of the adsorption of C1-C4 primary alcohols in H-ZSM-5.* Physical Chemistry Chemical Physics, 2010. **12**(32): p. 9481-9493.
3. Costa, E., et al., *Ethanol to gasoline process: effect of variables, mechanism, and kinetics.* Industrial & Engineering Chemistry Process Design and Development, 1985. **24**(2): p. 239-244.
4. Ermakov, R.V. and V.A. Plakhotnik, *Conversion of lower alcohols into C2–C4 olefins over acid-base catalysts.* Petroleum Chemistry, 2008. **48**(1): p. 1-5.
5. Nguyen, C.M., et al., *Physisorption and Chemisorption of Linear Alkenes in Zeolites: A Combined QM-Pot(MP2//B3LYP:GULP)–Statistical Thermodynamics Study.* The Journal of Physical Chemistry C, 2011. **115**(48): p. 23831-23847.
6. Froment, G.F., *Kinetic modeling of acid-catalyzed oil refining processes.* Catalysis Today, 1999. **52**(2–3): p. 153-163.
7. Park, T.Y. and G.F. Froment, *Kinetic modeling of the methanol to olefins process. 2. Experimental results, model discrimination, and parameter estimation.* Industrial & Engineering Chemistry Research, 2001. **40**(20): p. 4187-4196.
8. Guillaume, D., K. Surla, and P. Galtier, *From single events theory to molecular kinetics—application to industrial process modelling.* Chemical Engineering Science, 2003. **58**(21): p. 4861-4869.
9. Benson, S.W. and J.H. Buss, *Additivity Rules for the Estimation of Molecular Properties. Thermodynamic Properties.* The Journal of Chemical Physics, 1958. **29**(3): p. 546-572.
10. Van Borm, R., M.-F. Reyniers, and G.B. Marin, *Catalytic cracking of alkanes on FAU: Single-event microkinetic modeling including acidity descriptors.* AIChE Journal, 2012. **58**(7): p. 2202-2215.
11. Van Borm, R., *Single-event microkinetics of hydrocarbon cracking on zeotype catalysts: effect of acidity and shape selectivity*, in *Faculty of Engineering and Architecture*. 2011, Ghent University: Ghent.
12. Kumar, P., et al., *Single-Event Microkinetics for Methanol to Olefins on H-ZSM-5.* Industrial & Engineering Chemistry Research, 2012. **52**(4): p. 1491-1507.

Chapter 6

Conclusions & Future work

Several catalyst have been synthesized and characterized. The catalyst library used during this master thesis consist of: HZSM-5 (SiO_2/Al_2O_3=30 and 80), desilicated HZSM-5 (SiO_2/Al_2O_3=80), H-mordenite (SiO_2/Al_2O_3=20) and β-zeolite (SiO_2/Al_2O_3=25). The number of acid sites, surface area and micro- and meso-pore volume of these materials are determined. All results follow the expected trends. The ethanol conversions over several zeolitic catalysts are compared. The highest ethanol conversion is observed on the MFI-zeolite with a SiO_2/Al_2O_3 ratio of 30, H-mordenite has the lowest conversion. Desilication of the HZSM-5 catalyst has no effect on the dehydration reaction.

An experimental dataset is constructed using HZSM-5 (SiO_2/Al_2O_3=30). The experiments show a clear division into two regimes: the dehydration of ethanol and further conversion to higher hydrocarbons. Full ethanol conversion with nearly 100% selectivity towards ethylene is reached at temperatures around 250°C.

The dehydration experiments are performed in a temperature range between 170°C and 250°C. At very low ethanol conversion, DEE is the sole reaction product. Increasing conversion causes a decrease in DEE selectivity and an increasing ethylene selectivity.

The kinetic database on the reference catalyst (HZSM-5 with SiO_2/Al_2O_3=30) has been finished. Datasets on other catalysts are not yet extensive. Some experimental work remains on HZSM-5 with different SiO_2/Al_2O_3 ratios and desilicated an Al-ALD treated zeolite.

In the higher hydrocarbons regime, light olefins are the most abundant reaction products. The butylene-lump has the highest yield, followed by propylene and pentene. At temperatures up to 350°C, formation of paraffins and aromatics remains rather small.

Using thermodynamic calculations in *Aspen*, it is observed that the olefins with the same carbon number are formed in thermodynamic equilibrium. The total reaction product mixture is not formed in equilibrium quantities. This observation indicates the isomerization reactions between the different olefins have a smaller time-scale than the formation of these olefins.

Ethylene is used as reactor feed too. Compared to ethanol experiments with the same ethylene partial pressure (after dehydration) and spacetime, feeding ethylene has a higher conversion. The selectivity as function of conversion is similar for both sets of experiments. Adding the same amount of water to the ethylene feed as would be formed during dehydration of ethanol, does not change the reaction outcome. When feeding ethanol, part of the catalyst bed is used for dehydration of ethanol. The “true spacetime” ethylene experiences for the formation of higher hydrocarbons will only be a fraction of the calculated value. Since the difference in

conversion is significant, the timescale of ethanol dehydration cannot be neglected compared to the timescale of higher hydrocarbon formation at the employed reaction conditions.

The experiments performed with a water/ethanol mixture as feed, showed interesting results. No conclusions could be drawn from the current dataset however. Since bio-ethanol produced by fermentation consist for the major part of water, the effect of water content is an important aspect of the reaction. A detailed investigation is appropriate.

Due to the limitations of the setup, the DEE-experiments did not yield quantitative results. Valuable qualitative information on the dehydration reaction network could still be gained from them. Using the new experimental setup that will be available soon, these experiments should be reconsidered. In the context of reaction network clarification, co-feeding ethanol and ethylene in the two reaction regimes has to be considered too.

To get a detailed overview of the composition of the reaction product mixture, the liquid fraction can be analysed using e.g. GCxGC. Valuable information can be obtained, e.g. on the C_6+ hydrocarbons, which now remain largely unidentified.

Several micro-kinetic models for ethanol dehydration are constructed. The best fit to the experiments is obtained with a Langmuir-Hinshelwood type of reaction. Statistical test show a good significance for both the model and the individual parameter values. The micro-kinetic model for ethanol dehydration can be extended to include catalyst descriptors. This has not yet been validated due to the limited experimental dataset on other catalyst than HZSM-5 with a SiO_2/Al_2O_3 ratio of 30.

Via in-house developed reaction network generation software, the extensive reaction network for the conversion of ethanol to hydrocarbons is determined. Ethylene is considered to be the reactant for this reaction, based on the experimental observation that ethanol is dehydrated completely to ethylene before the conversion to higher hydrocarbons begins. The maximal carbon number for the generated hydrocarbons is set to be 9. To simplify the network, extra assumptions are made. Cyclisation, aromatization and hydride abstraction/donation are neglected. This simplified reaction network is used for the micro-kinetic modelling.

The single-event methodology is employed to create the micro-kinetic model for higher hydrocarbon production. This methodology limits the total number of model parameters by making use of the transition state theory. The reaction families considered in the model are: (de)protonation, alkylation and β-scission the outcome of the other reactions is determined via thermodynamic equilibrium calculations.

Physisorption is modelled dependent on the chain length of the hydrocarbon. All reactions, including protonation (=chemisorption), are dependent on the character of the reactant (primary, secondary or tertiary), neglecting the effect of the chain length.

Parameter estimation for the simplified SEMK model for higher hydrocarbon production has to be performed. The model should be extended to include paraffin and aromatics formation.

The two models should be merged, to yield one micro-kinetic model for both dehydration and further conversion to higher hydrocarbons.

Appendix A

NH_3-TPD TCD calibration

To calibrate the TCD detector for the NH_3-TPD experiments, five runs with a well-known mixture of 4mol% NH_3 in helium are performed. The average peak area of these five experiments is then correlated to the corresponding amount of NH_3. The results of these calibration experiments are given in Table A-1.

Table A-1 Results of the TCD calibration experiments

Peak number	T at maximum (°C)	Area (a.u.)	Peak Height
1	24	0.0295	0.33886
2	24	0.03245	0.35604
3	24	0.03128	0.36178
4	23.7	0.0296	0.3659
5	23.9	0.03146	0.36873

Via the ideal gas law, the amount of NH_3 can be calculated:

$$n_{NH_3} = \frac{p_{NH_3} \cdot V}{R \cdot T} = 6{,}28 \cdot 10^{-6} mol$$

With:

p_{NH_3} the ammonia partial pressure equal to 0,04bar

V the volume equal to 5ml

T the temperature equal to 110°C

Dividing the amount of ammonia by the average surface area gives the calibration factor :

$$CF_{NH_3} = \frac{n_{NH_3}}{A_{av}} = 2{,}04 \cdot 10^{-4}\, mol \;\; (a.u.)$$

Appendix B

Calibration curves mass flow controllers

The experimental setup has several mass flow controllers, used to regulate the different product flows through the system. Exact measurements of the product flow rates is crucial for the experimental data gathering, so these valves are calibrated prior to the data gathering.

There are four control valves in the setup that will be used during the experiments. Three of these control gas flows: the inert gas (helium or nitrogen), the internal standard (methane) and ethylene used as reactant in some experiments. The liquid flows are controlled by a coriolis mass flow controller. The amount of liquid is checked via a mass balance.

The setpoint of the gas valves is their opening in percentages. To construct a calibration curve, several percentage-volumetric flow pair are measured over a broad range of setpoints, using a flow meter. Visually, it is checked the valve has linear behavior as a function of volumetric flow in its operating range. A linear correlation for this range is determined. These calibration curves and the linear correlations are given in Figure B-1 to Figure B-4

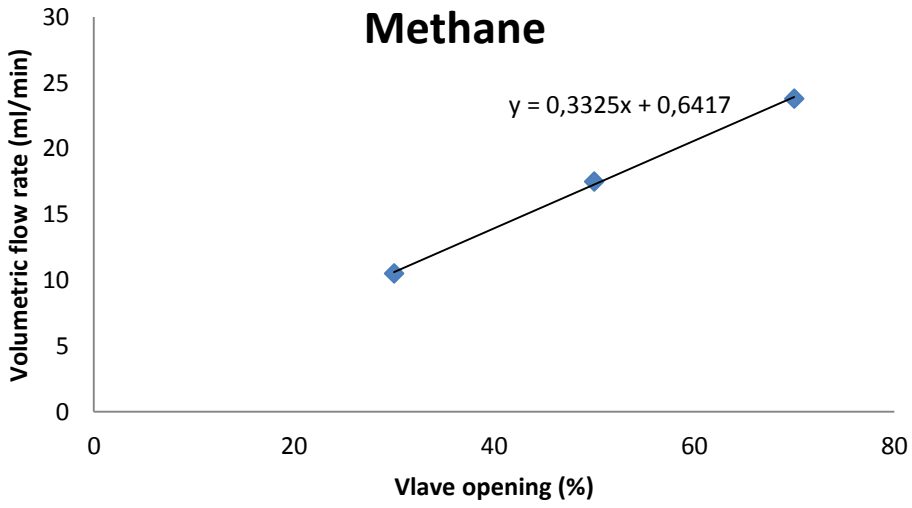

Figure B-1 Calibration curve for the internal standard

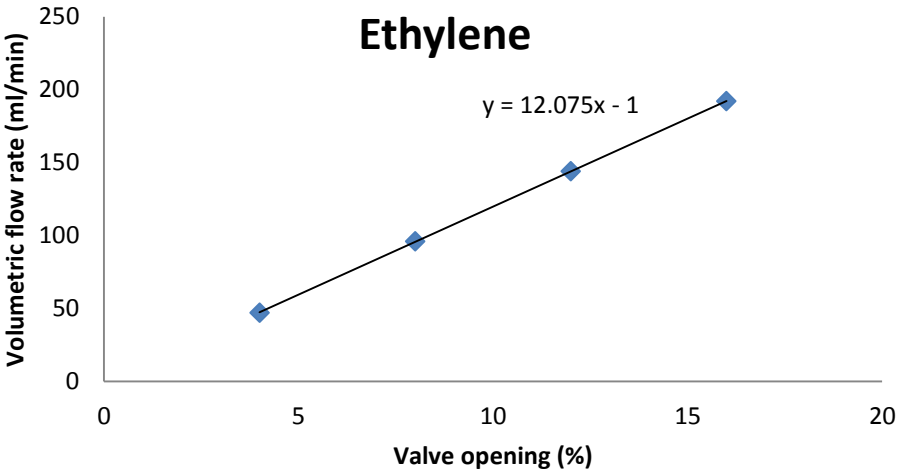

Figure B-2 Calibration curve for ethylene

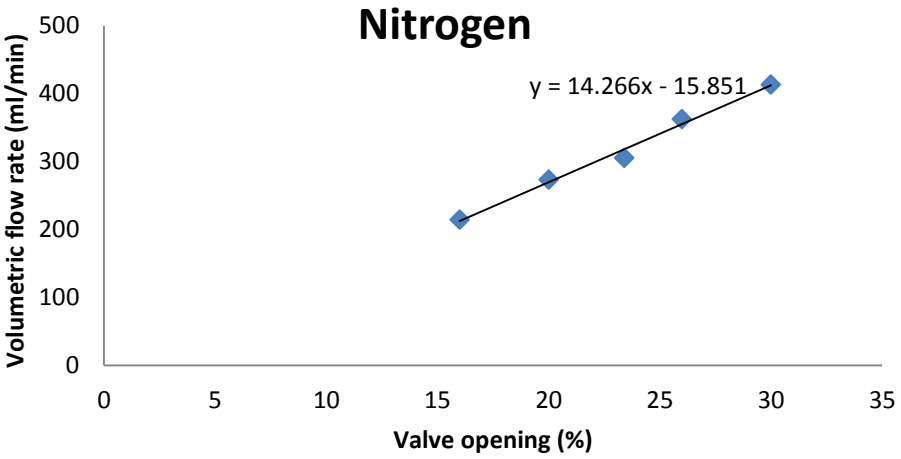

Figure B-3 Calibration curve for nitrogen

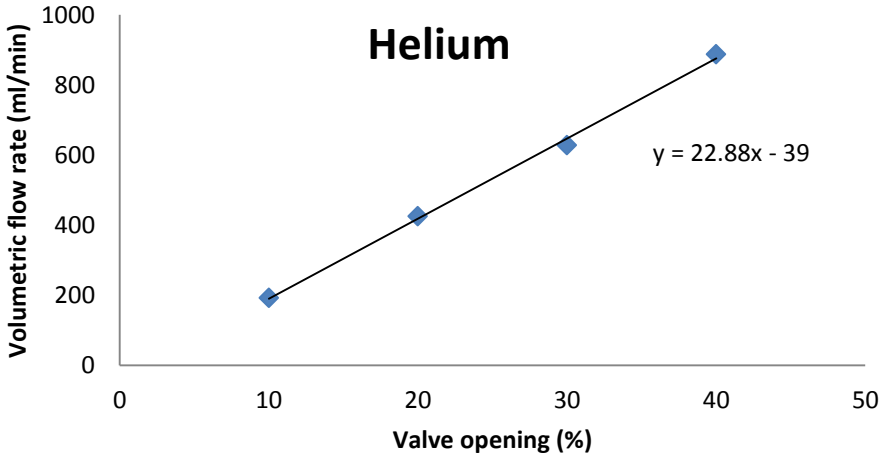

Figure B-4 Calibration curve for helium

Appendix C

Dietz response factors for GC analysis

The response factors used during the experimental data gathering are based on an article by Dietz et al. [1] These factors are determined for use of a FID detector. Employing the response factors, a corrected area is calculated:

$$A_{cor,i} = \frac{A_i}{CF_i}$$

By means of normalization, the weight percentage of each compound can then be calculated.

For most hydrocarbons, the response factor is close to 1. Whenever information on the exact factor is absent, 1 will hence be used as default value. The response factors for the identified peaks are listed in Table C-1.

Table C-1 Response factors for GC analysis

Component	CF	Component	CF
methane	0.97	trans-4-methyl-2-pentene	1
ethylene	1.02	3-methylpentane	1.04
ethane	0.97	1-hexene + 2-methyl-1-pentene	1
ethanol	0.46	n-hexane	1.03
propylene	1	t-&-c-3-hexene	1
propane	0.98	t-2-hexene	1
isobutane	1.03	2-methyl-2-pentene	1
isobutene	1	cis-3-methyl-2-pentene	1
1-butene	1	3-methyl-cyclopentene	1
n-butane	1.09	cis-2-hexene	1
trans-2-butene	1	trans-3-methyl-2-pentene	1
cis-2-butene	1	2.4-dimethylpentane	1.02
Diethyl ether	0.55	3,4-dimethyl-1-pentene	1

3-methyl-1-butene	1	benzene	1.12
isopentane	1.05	trans-2-heptene (5)	1
1-pentene	1	n-heptane	1
2-methyl-1-butene	1	cis-3-heptene	1
n-pentane	1.04	toluene	1.07
trans-2-pentene	1	1-octene	1.03
cis-2-pentene	1	ethylbenzene	1.03
2-methyl-2-butene	1	p-&-m-&xylene	1.02
cyclopentene	1	o-xylene	1.02
3 & 4-methyl-1-pentene	1	1-methyl-3-ethylbenzene	1.01
2,3-dimethyl-butane	1.03	1-methyl-4-ethylbenzene	1
cis-4-methyl-2-pentene	1	1,2,4-trimethylbenzene	0.97
2-methyl-pentane	1.05		

Bibliography

1. Dietz, W.A., *Response Factors for Gas Chromatographic Analyses.* Journal of Chromatographic Science, 1967. **5**(2): p. 68-71.

Appendix D

GC-chromatogram with identified peaks

In this appendix, the chromatogram of an experiment in the conversion to higher hydrocarbons regime is given. The catalyst is the reference catalyst (HZSM-5, SiO_2/Al_2O_3=30) and ethylene is used as feed component. The ethylene conversion in this experiment is 51,1%.

On the chromatogram, some peaks are identified. For C_6+ compounds, identification is difficult due to the huge amount of rather small and often overlapping peaks. From these peaks, only the benzene-toluene-xylene (BTX) aromatics and some C_9 aromatics and a few linear hydrocarbons are identified.

The conditions for this experiment are given is Table D-1.

Table D-1 Experimental conditions

Ethylene partial pressure	20kPa
Temperature	330°C
Spacetime	$10kg_{cat}.s.mol^{-1}_{ethylene}$

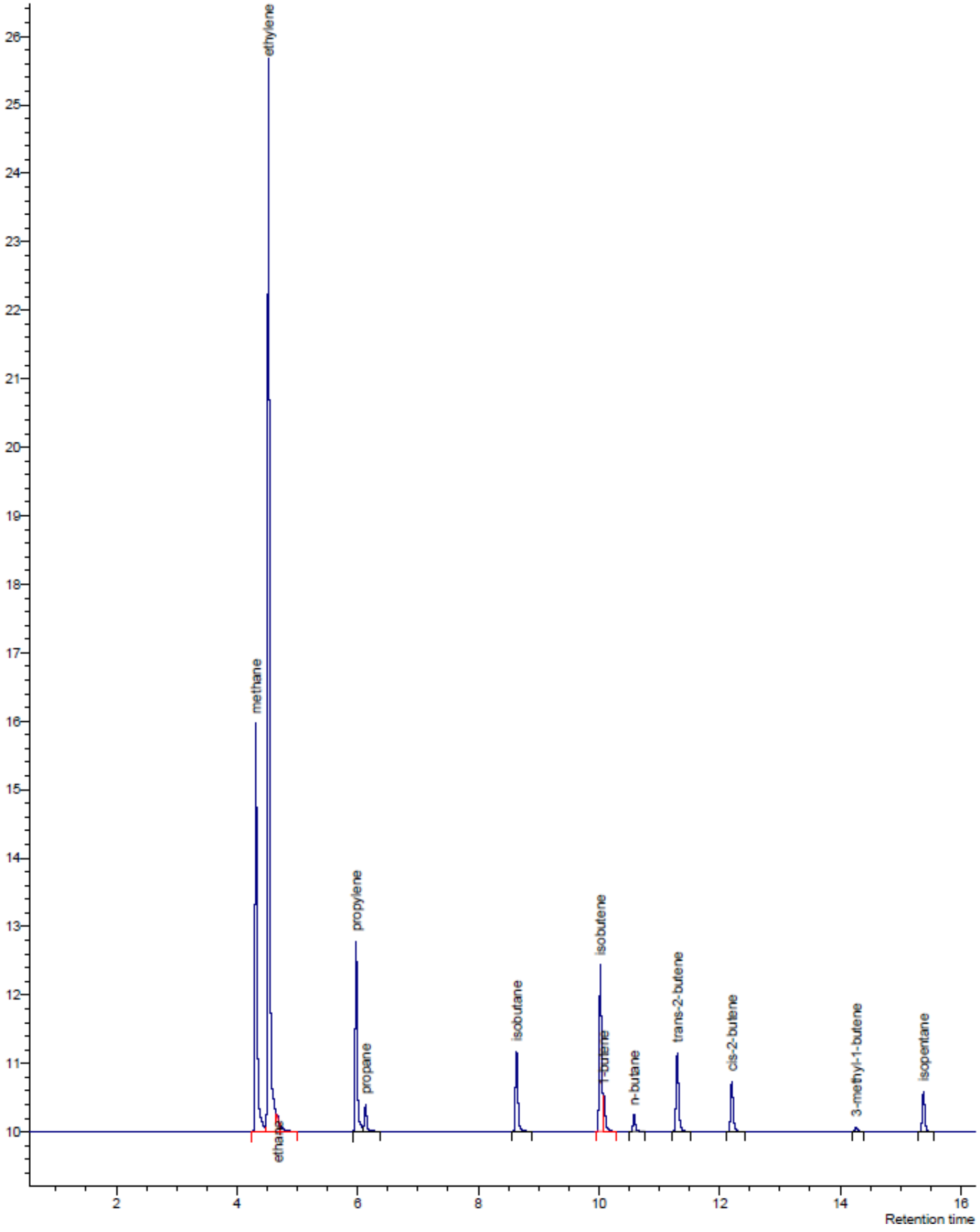
ethylene
methane
propylene
propane
isobutane
isobutene
1-butene
n-butane
trans-2-butene
cis-2-butene
3-methyl-1-butene
isopentane
ethane
Retention time

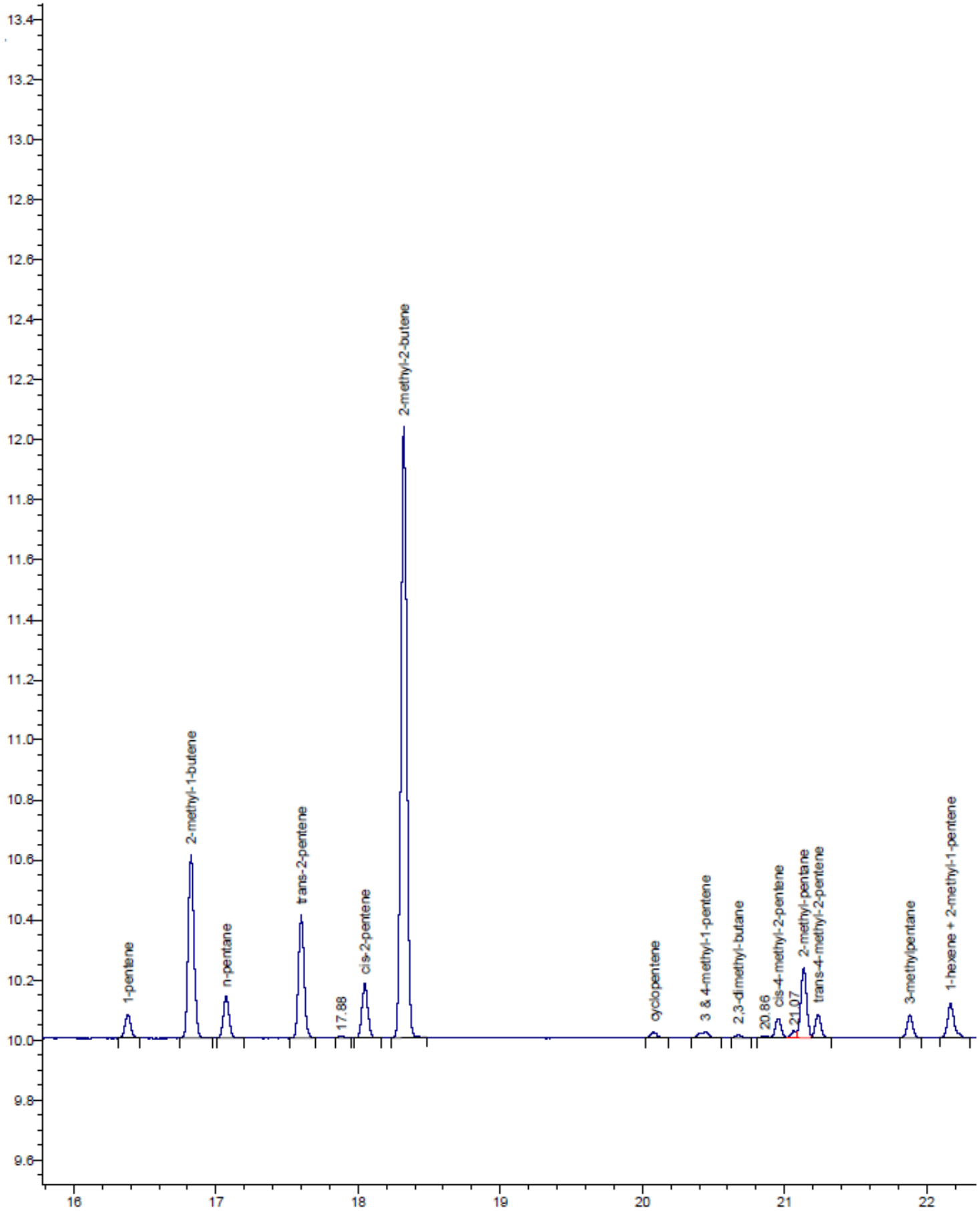
1-pentene
2-methyl-1-butene
n-pentane
trans-2-pentene
17.88
cis-2-pentene
2-methyl-2-butene
cyclopentene
3 & 4-methyl-1-pentene
2,3-dimethyl-butane
20.86
cis-4-methyl-2-pentene
21.07
2-methyl-pentane
trans-4-methyl-2-pentene
3-methylpentane
1-hexene + 2-methyl-1-pentene

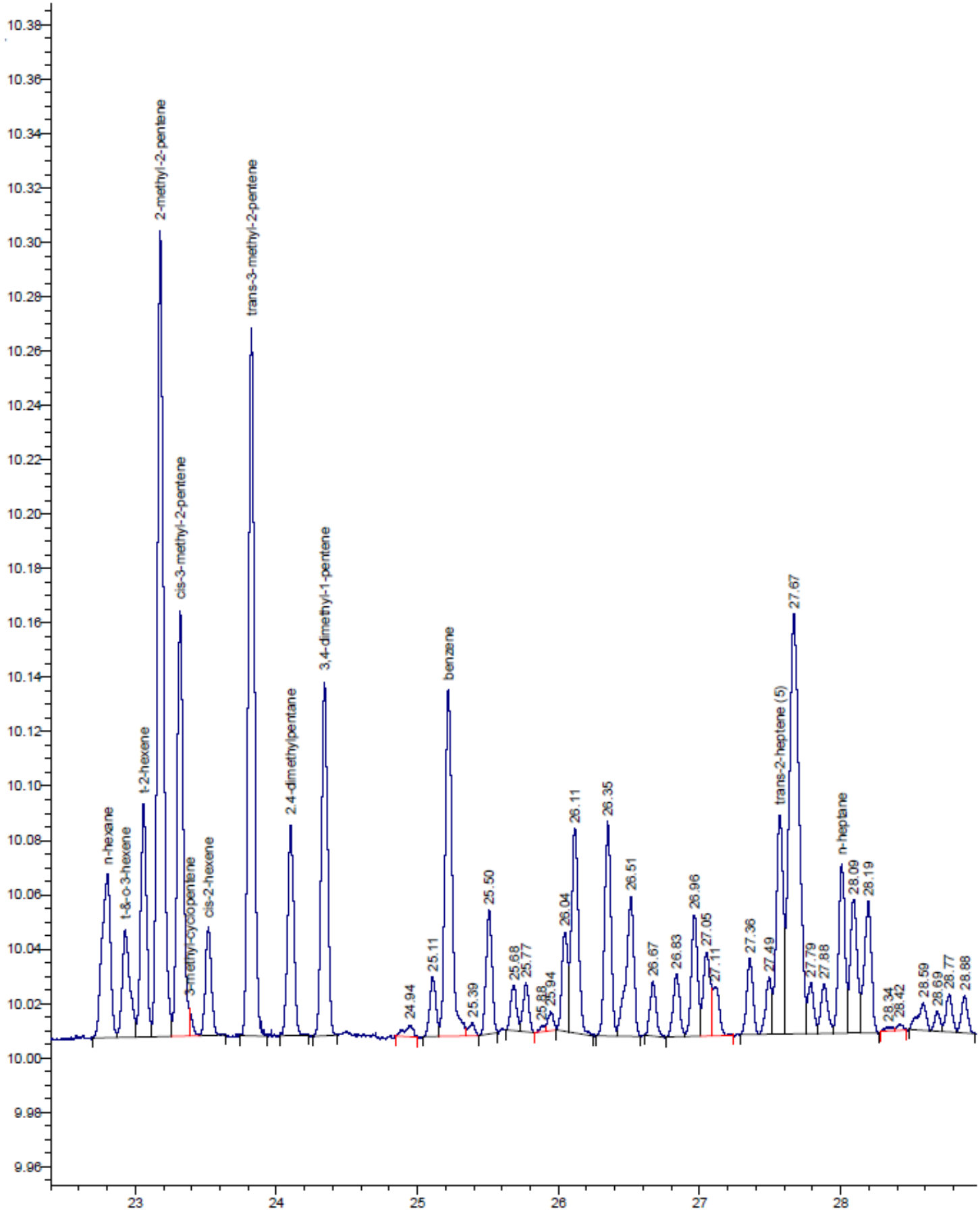
n-hexane
t-&-o-3-hexene
t-2-hexene
2-methyl-2-pentene
3-methyl-cyclopentene
cis-3-methyl-2-pentene
cis-2-hexene
trans-3-methyl-2-pentene
2,4-dimethylpentane
3,4-dimethyl-1-pentene
benzene
trans-2-heptene (5)
n-heptane
24.94
25.11
25.39
25.50
25.68
25.77
25.88
25.94
26.04
26.11
26.35
26.51
26.67
26.83
26.96
27.05
27.11
27.36
27.49
27.67
27.79
27.88
28.09
28.19
28.34
28.42
28.59
28.69
28.77
28.88
10.38
10.36
10.34
10.32
10.30
10.28
10.26
10.24
10.22
10.20
10.18
10.16
10.14
10.12
10.10
10.08
10.06
10.04
10.02
10.00
9.98
9.96
23
24
25
26
27
28

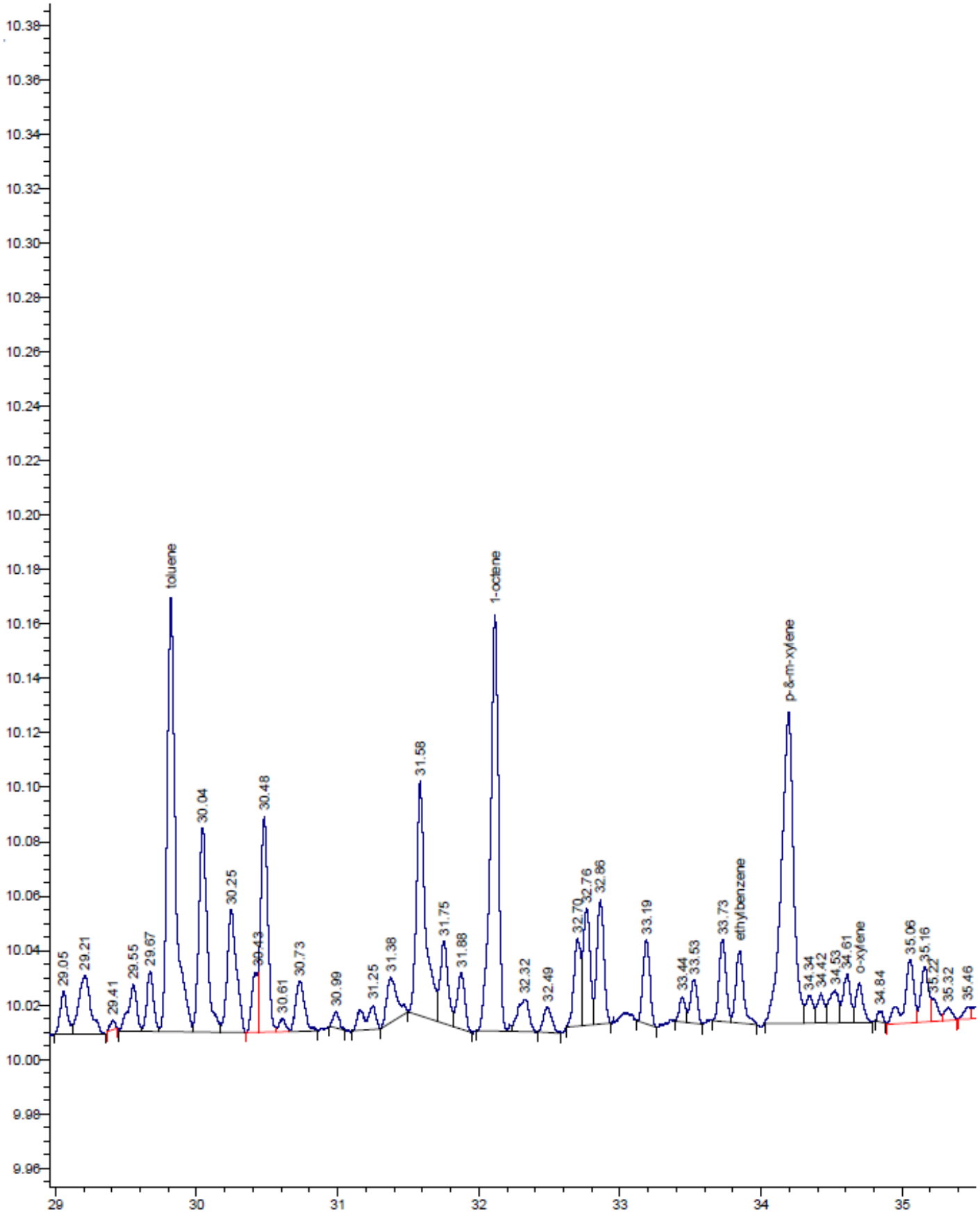
10.38
10.36
10.34
10.32
10.30
10.28
10.26
10.24
10.22
10.20
10.18
10.16
10.14
10.12
10.10
10.08
10.06
10.04
10.02
10.00
9.98
9.96
29
30
31
32
33
34
35
29.05
29.21
29.41
29.55
29.67
toluene
30.04
30.25
30.43
30.48
30.61
30.73
30.99
31.25
31.38
31.58
31.75
31.88
1-octene
32.32
32.49
32.70
32.76
32.86
33.19
33.44
33.53
33.73
ethylbenzene
p-&-m-xylene
34.34
34.42
34.53
34.61
o-xylene
34.84
35.06
35.16
35.22
35.32
35.46

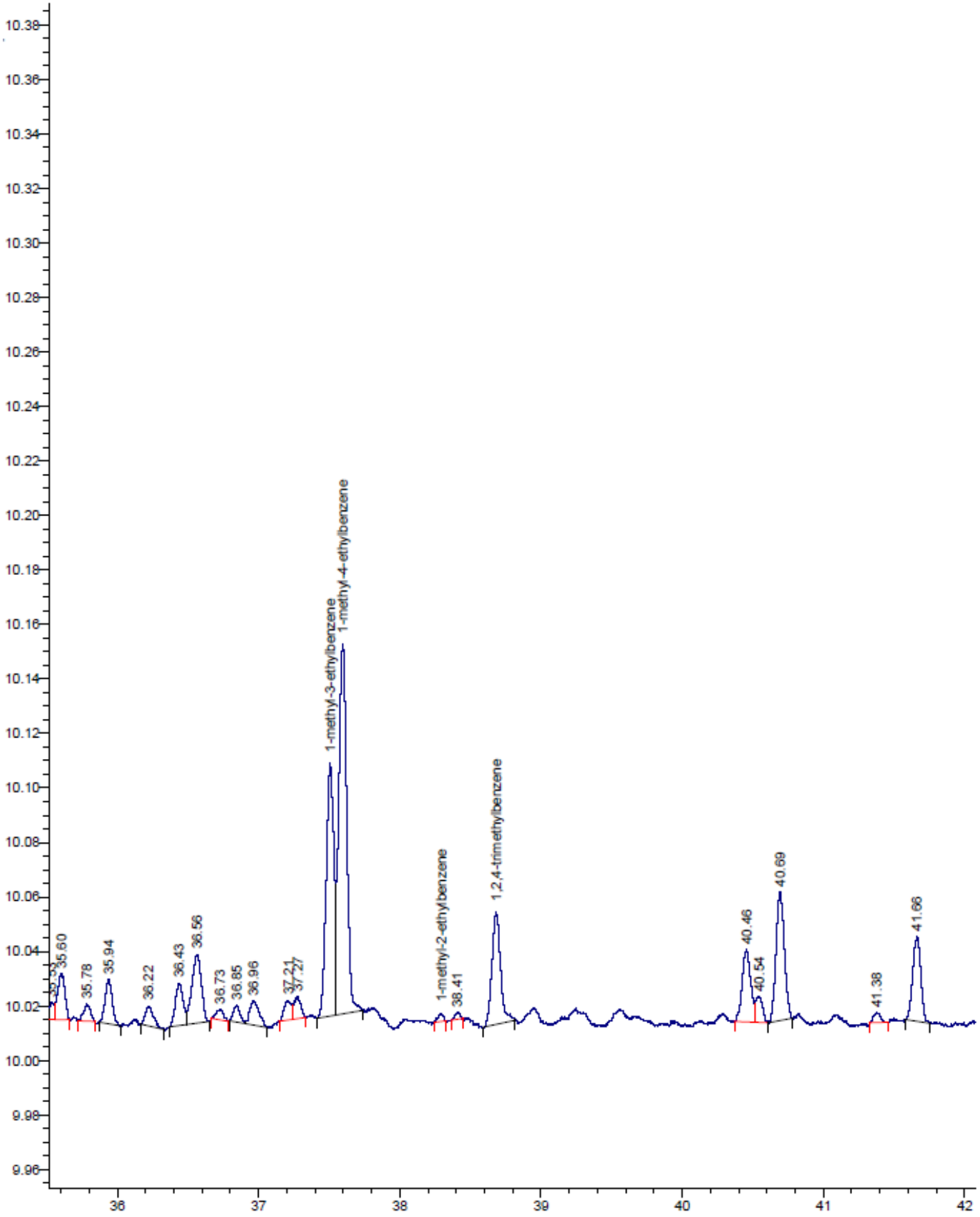
10.38
10.36
10.34
10.32
10.30
10.28
10.26
10.24
10.22
10.20
10.18
10.16
10.14
10.12
10.10
10.08
10.06
10.04
10.02
10.00
9.98
9.96
36
37
38
39
40
41
42
35.60
35.78
35.94
36.22
36.43
36.56
36.73
36.85
36.96
37.21
37.27
1-methyl-3-ethylbenzene
1-methyl-4-ethylbenzene
1-methyl-2-ethylbenzene
38.41
1,2,4-trimethylbenzene
40.46
40.54
40.69
41.38
41.66

Appendix E

Dehydration reaction rate equations

In this appendix, the reaction rate equations for the dehydration model are constructed. For an elementary reaction step, the law of mass action can be applied to get the rate equation:

$$r_{el.step} = k_{el.step} \cdot \prod_{i=0}^{N} C_i^{\nu_i}$$

With:

$k_{el.step}$: rate coefficient of the elementary step (units dependent on the reaction)

N: number of reactants

C_i: Surface concentration of component i (mol.g^{-1})

ν_i: the stoichiometric coefficient of component i

The reaction rate coefficient $k_{el.\ step}$ is calculated via the Arrhenius equation:

$$k_{el.step} = A_{el.step} \cdot \exp(-\frac{E_a}{RT})$$

With:

$A_{el.step}$: the pre-exponential factor (units dependent on the reaction)

E_a: activation energy for the elementary reaction (J/mol)

R: the universal gasconstant (8.314 J.K^{-1}.mol^{-1})

T: temperature (K)

To limit the correlation between the activation energy and pre-exponential factor while estimating their values, re-parameterization is employed:

$$k_{el.step} = k_{el.step}^{T_{av}} \cdot \exp(-\frac{E_a}{R}(\frac{1}{T} - \frac{1}{T_{av}}))$$

Where the coefficients are related to the coefficient at the average temperature T_{av} of the experimental database used for parameter estimation.

Table E-1 Reaction network for dehydration

Adsorption	(1)	$EtOH_g + * \leftrightarrow EtOH^*$	
	(2)	$DEE_g + * \leftrightarrow DEE^*$	
	(3)	$C_2H_{4_g} + * \leftrightarrow C_2H_4{}^*$	
	(4)	$H_2O_g + * \leftrightarrow H_2O^*$	
Surface reactions	(5)	$EtOH^* \rightarrow C_2H_4{}^* + H_2O_g$	
	(6)	$2EtOH^* \rightarrow DEE^* + H_2O^*$	LH
	(7)	$EtOH^* + EtOH_g \rightarrow DEE^* + H_2O_g$	ER
	(8)	$DEE^* + * \rightarrow 2C_2H_4{}^* + H_2O_g$	
	(9)	$DEE^* \rightarrow EtOH^* + C_2H_{4_g}$	
	(10)	$DEE^* \leftrightarrow C_2H_4{}^* + EtOH_g$	

Based on the reactions given in Table E-1 the reaction rate equation for each reaction can now be generated.

Since the Langmuir hypothesizes are used to described the adsorption and desorption of the reactants and products to the catalyst surfaces, these steps are considered to be in equilibrium. Only the adsorption/desorption equilibrium coefficients are calculated:

$$K_{EtOH,ads} = K_{EtOH,ads}^{T_{av}} \cdot \exp(-\Delta H_{EtOH,ads}(\frac{1}{T} - \frac{1}{T_{av}}))$$

$$K_{DEE,ads} = K_{DEE,ads}^{T_{av}} \cdot \exp(-\Delta H_{DEE,ads}(\frac{1}{T} - \frac{1}{T_{av}}))$$

$$K_{C_2H_4,ads} = K_{C_2H_4,ads}^{T_{av}} \cdot \exp(-\Delta H_{C_2H_4,ads}(\frac{1}{T} - \frac{1}{T_{av}}))$$

$$K_{H_2O,ads} = K_{H_2O,ads}^{T_{av}} \cdot \exp(-\Delta H_{H_2O,ads}(\frac{1}{T} - \frac{1}{T_{av}}))$$

The elementary step rate equitation needs the reactant surface concentration as input. Since this value cannot be accessed experimentally, the equation has to be written as a function of observable experimental outputs. C_i has to be written as a function of known variables. To achieve this, the site balance is used. The normalized form of this balance will be used:

$$\sum_{i=1}^{N} \theta_i = 1$$

Where θ_i is the fraction of adsorption sites occupied by component i.

For this particular case, the site balance is:

$$\theta_{EtOH} + \theta_{DEE} + \theta_{C_2H_4} + \theta_{H_2O} + \theta_* = 1$$

θ_* denotes the fraction of free adsorption sites.

Adsorption and desorption are considered to be in equilibrium:

$$\theta_i = K_i \cdot p_i \cdot \theta_*$$

$$\leftrightarrow K_{EtOH} \cdot p_{EtOH} \cdot \theta_* + K_{DEE} \cdot p_{DEE} \cdot \theta_* + K_{C_2H_4} \cdot p_{C_2H_4} \cdot \theta_* + K_{H_2O} \cdot p_{H_2O} \cdot \theta_* + \theta_* = 1$$

$$\leftrightarrow \theta_* = \frac{1}{1 + K_{EtOH} \cdot p_{EtOH} + K_{DEE} \cdot p_{DEE} + K_{C_2H_4} \cdot p_{C_2H_4} + K_{H_2O} \cdot p_{H_2O}}$$

Using the expression for θ_*, the fraction of adsorption sites occupied by every compound can be calculated. This yields the reaction rate equation for the surface reactions:

$$r_{(5)} = k_{(5)} \cdot \frac{K_{EtOH} \cdot p_{EtOH}}{1 + K_{EtOH} \cdot p_{EtOH} + K_{DEE} \cdot p_{DEE} + K_{C_2H_4} \cdot p_{C_2H_4} + K_{H_2O} \cdot p_{H_2O}}$$

$$r_{(6)} = k_{(6)} \cdot \left(\frac{K_{EtOH} \cdot p_{EtOH}}{1 + K_{EtOH} \cdot p_{EtOH} + K_{DEE} \cdot p_{DEE} + K_{C_2H_4} \cdot p_{C_2H_4} + K_{H_2O} \cdot p_{H_2O}}\right)^2$$

$$r_{(7)} = k_{(7)} \cdot \frac{(K_{EtOH} \cdot p_{EtOH})^2}{1 + K_{EtOH} \cdot p_{EtOH} + K_{DEE} \cdot p_{DEE} + K_{C_2H_4} \cdot p_{C_2H_4} + K_{H_2O} \cdot p_{H_2O}}$$

$$r_{(8)} = k_{(8)} \cdot \frac{K_{DEE} \cdot p_{DEE}}{(1 + K_{EtOH} \cdot p_{EtOH} + K_{DEE} \cdot p_{DEE} + K_{C_2H_4} \cdot p_{C_2H_4} + K_{H_2O} \cdot p_{H_2O})^2}$$

$$r_{(9)} = k_{(9)} \cdot \frac{K_{DEE} \cdot p_{DEE}}{1 + K_{EtOH} \cdot p_{EtOH} + K_{DEE} \cdot p_{DEE} + K_{C_2H_4} \cdot p_{C_2H_4} + K_{H_2O} \cdot p_{H_2O}}$$

The reaction rate equation of (10) is identical to $r_{(9)}$.

Appendix F

Correlation matrices

Table F-1 correlation matrix for the LH1 model

	A_{DEEads}	$A_{EtOH->C2H4}$	$A_{EtOH->DEE}$	$A_{DEE->C2H4}$	$\Delta H_{ads,DEE}$	$E_{a,EtOH->C2H4}$	$E_{a,EtOH->DEE}$	$E_{a,DEE->C2H4}$
A_{DEEads}	1	0,896	0,494	-0,866	-0,766	0,285	0,8	-0,627
$A_{EtOH->C2H4}$	0,896	1	0,654	-0,684	-0,339	-0,077	0,569	-0,386
$A_{EtOH->DEE}$	0,494	0,654	1	-0,236	-0,686	0,275	0,893	-0,649
$A_{DEE->C2H4}$	-0,866	-0,684	-0,236	1	0,722	-0,265	-0,639	0,43
$\Delta H_{ads,DEE}$	-0,766	-0,339	-0,686	0,722	1	-0,535	-0,788	0,046
$E_{a,EtOH->C2H4}$	0,285	-0,077	0,275	-0,265	-0,535	1	0,404	-0,04
$E_{a,EtOH->DEE}$	0,8	0,569	0,893	-0,639	-0,788	0,404	1	-0,418
$E_{a,DEE->C2H4}$	-0,627	-0,386	-0,649	0,43	0,046	-0,04	-0,418	1

Table F-2 correlation matrix for the LH2 model

	A_{DEEads}	$A_{EtOH->C2H4}$	$A_{EtOH->DEE}$	$A_{DEE->C2H4}$	$\Delta H_{ads,DEE}$	$E_{a,EtOH->C2H4}$	$E_{a,EtOH->DEE}$	$E_{a,DEE->C2H4}$
A_{DEEads}	1	0,434	0,92	-0,872	-0,367	0,742	0,182	-0,431
$A_{EtOH->C2H4}$	0,92	1	0,498	-0,495	-0,13	0,394	-0,224	-0,095
$A_{EtOH->DEE}$	0,434	0,498	1	-0,827	-0,298	0,795	0,191	-0,39
$A_{DEE->C2H4}$	-0,87	-0,495	-0,827	1	0,308	-0,664	-0,105	0,21
$\Delta H_{ads,DEE}$	-0,367	-0,13	-0,298	0,308	1	-0,707	-0,138	0,852
$E_{a,EtOH->C2H4}$	0,742	0,394	0,795	-0,664	-0,707	1	0,222	-0,126
$E_{a,EtOH->DEE}$	0,182	-0,224	0,191	-0,105	-0,138	0,222	1	-0,703
$E_{a,DEE->C2H4}$	-0,431	-0,095	-0,39	0,21	0,852	-0,126	-0,703	1

Appendix G

Table of contents of lab-journal

Table G-1 Table of contents lab-journal